AFRL-SR-BL-TR-98-

0101

# REPORT DOCUMENTATION PAGE



| 1. AGENCY USE ONLY (Leave blank) | 2. REPORT DATE | 3. REPORT TYPE AND DATES COVERED |
|---|---|---|
| | 9 Dec 97 | FINAL 01 Jun 93 to 31 May 97 |

**4. TITLE AND SUBTITLE**
Development of LES Methodology for the Analysis of High-Reynolds Number 2-D and 3-D Dynamic Stall Phenomenon

**5. FUNDING NUMBERS**
AFOSR
F49620-93-1-0393
2307/A3

**6. AUTHOR(S)**

K. Ghia and U. Ghia

**7. PERFORMING ORGANIZATION NAME(S) AND ADDRESS(ES)**

University of Cincinnati
Department of Aerospace Engineering and Engineering Mechanics
Department of Mechanical, Industrial, and Nuclear Engineering

**8. PERFORMING ORGANIZATION REPORT NUMBER**
AFL Report No.
97-12-86

**9. SPONSORING / MONITORING AGENCY NAME(S) AND ADDRESS(ES)**

Air Force Office of Scientific Research
Aerospace Sciences
Building 410
Bolling Air Force Base, DC 20332-6648

NA

**10. SPONSORING / MONITORING AGENCY REPORT NUMBER**

**11. SUPPLEMENTARY NOTES**

**12a. DISTRIBUTION / AVAILABILITY STATEMENT**

Distribution of this report is unlimited.

**12b. DISTRIBUTION CODE**

DTIC QUALITY INSPECTED 2

**13. ABSTRACT** ***(Maximum 200 Words)***

The major objective of the AASERT Grant was to improve the analysis tools as well as assure the level of accuracy and efficiency that can be realized in the study of physics of the dynamic stall and related unsteady phenomena, through the development of the LES/DNS methodology. One M.S. and three Ph.D students were supported partially on this grant. The work carried out consisted of study of external unsteady flow using vorticity-Stream function formulation, analysis of boundary-layer receptivity and transition using DNS methodology with spectral technique and, finally, compressibility effects in maneuvering body flows. Significant accomplishment is made in Object Oriented Numerics and high performance computing.

19980129 070

| 14. SUBJECT TERMS | | | | 15. NUMBER OF PAGES |
|---|---|---|---|---|
| Unsteady Flow | Unsteady Flow | (ω-ψ) Formulation | Maneuvering Wing | 87 |
| Stability | Receptivity.. | Plane & Curved | Compressibility effects | 16. PRICE CODE |
| Transition | 2-D & 3-D Flows | Channel Flow | Navier-Stokes Eqs. | |
| | Direct Numerical Simulation | | Spectral Technique | |

| 17. SECURITY CLASSIFICATION OF REPORT | 18. SECURITY CLASSIFICATION OF THIS PAGE | 19. SECURITY CLASSIFICATION OF ABSTRACT | 20. LIMITATION OF ABSTRACT |
|---|---|---|---|
| | | | |

# DEVELOPMENT OF LES METHODOLOGY FOR THE ANALYSIS OF HIGH-REYNOLDS NUMBER 2-D AND 3-D DYNAMIC STALL PHENOMENON

**K.N. GHIA***
Department of Aerospace Engineering and Engineering Mechanics

**U. GHIA***
Department of Mechanical and Industrial Engineering

University of Cincinnati
Cincinnati, Ohio

This research was supported by the Air Force Office of Scientific Research, Bolling Air Force Base, under AFOSR Grant No. F49620-93-1-0393, with Major Daniel B. Fant as Technical Monitor.



* Professor.

# Contents

# SECTION 1

## OBJECTIVES

An analytical-numerical study was pursued by the present investigators under AFOSR Grant No. F 49620-92-J-0292 between May 1992 and December 1995. The primary objectives were: (i) to characterize the unsteady separation in terms of vortex dynamics that leads to dynamic stall of an airfoil and a rectangular wing in constant pitch-rate motion; (ii) to identify the physical mechanism responsible for moment stall, and formulate an active-control strategy to manage stall. For this program, one additional graduate student's effort was made possible through the AASERT Grant No. F 49620-93-1-0398, between June 1, 1993 and May 31, 1996. This grant was extended, at no cost, for one additional year, to May 31, 1997. For this AASERT grant, the major objective was to improve the analysis tools as well as assure the level of accuracy and efficiency that can be realized in the study of physics of the dynamic-stall and related unsteady phenomena through the development of the LES/DNS methodology.

The effort on the AASERT project was started with Ms. Susan Beltz who studied unsteady flows using a vorticity-based formulation. She examined, in detail, the surface and outflow boundary condition for the unsteady formulations, and wrote a Master's Thesis in August 1994. Due to an exciting offer from a high-tech software company, run by my previous students who had worked on the AFOSR project, Susan Beltz decided to temporarily bifurcate from pursuing a doctoral degree program. Keith Blodgett a doctoral student, was appointed on this project in place of Susan Beltz. Keith worked on a spectral technique in generalized coordinates, also using a vorticity-based formulation, to study the problem of receptivity and completed his Doctoral Dissertation in May 1995. Subsequently, Chris Noll and Brad Duncan, both doctoral students, were partially supported on this project. They will complete their doctoral dissertations by March 1998. Brad Duncan has been using direct

numerical simulation methodology and a spectral technique, in the area of early stages of transition, before the nonlinear breakdown occurs. On the other hand, Chris Noll has been studying the effect of compressibility on the flow past maneuvering bodies. The last two studies are heavily involved in the new paradigm of Object-Oriented Programming (OOP). Chris Noll has been improving the OOP, and has created an Object Oriented Numerics (OON) that not only facilitates large-scale programming requiring complex software, but also has been able to retain high code efficiency.

Through GPA, both Chris Noll and Brad Duncan have been able to develop software that uses all the available tools of high-performance computing, and have also developed parallel versions of this software for more than one high-performance platform.

Each of these four studies are briefly described next.

# SECTION 2

## DESCRIPTION OF SIGNIFICANT ACCOMPLISHMENTS

All of the areas of research pursued and the progress, as well as specific achievements, made in these studies during the four-year grant period are briefly summarized in this section.

Since the technical discussion pertaining to progress made for some individual objectives is quite long, the details are relegated to the corresponding reports and papers included in the appendices of this report.

### 2A. Improving the Outflow Boundary Condition for Vorticity-Based Formulation -Susan Beltz, M.S. Student

A vorticity-stream function circulation $(\omega,\psi,\Gamma_\infty)$ formulation was developed based upon our earlier work, which focused on the accurate implementation of the far-field boundary condition to provide a unique formulation. Although the study considered unsteady incompressible viscous flows past Joukowski airfoils, the ability of the formulation, which used generalized orthogonal coordinates, to incorporate any sequence of conformal mappings enables a range of flow configurations to be studied. The uniqueness in the formulation has been realized through the incorporation of viscous circulation $\Gamma_\infty$ into the formulation. The resulting system of governing equations was solved numerically using the Block Gaussian Elimination (BGE) procedure to solve the integral form of the curl equation, and the Alternating Direction Implicit (ADI) technique of Douglas and Gunn to solve the vorticity-transport equation, with an integrative procedure used to ensure pressure continuity along the airfoil surface. Due to a lack of available data pertaining to Joukowski airfoils, the validation study was performed using the circular cylinder geometry, for which there exist a wealth of available experimental and numerical data. Specifically, validation was performed on the cylinder geometry using early-time

results for two different values of the Reynolds Re number. Based on measurements of the length and width of the symmetric eddies which form at the rear of the cylinder, a comparison was made with the available experimental data. Additionally, the grid independence of the solutions obtained was analyzed using the Grid Convergence Index (GCI). It was found that, for the case of Re=9500, a grid size of (705x91) is adequate, based on the GCI. Thus, the present analysis was validated and is available for application to a class of unsteady two-dimensional incompressible flows. The results of this study are discussed in detail by Beltz and K Ghia (1995).

## 2B. A Spectral Multidomain Method for Studying Receptivity

**- Keith Blodgett,Ph.D. Student**

A spectral method in generalized curvilinear coordinates was developed for investigating the early stages of transition to turbulence on complex geometries. The earliest stage of transition is receptivity, the process by which small disturbances, originating in the free stream penetrate the boundary layer and excite the boundary-layer instabilities. A spectral method was chosen over other numerical methods because of its higher accuracy and negligible phase errors, both of which are deemed important in the **simulation of receptivity problems**. The spatial directions were discretized with a spectral collocation method using the Gauss-Lobatto points, with a choice of either Chebyshev or Legendre polynomials. A semi-implicit finite-difference scheme was utilized for the temporal discretization, with the linear terms being treated implicitly and the nonlinear terms treated explicitly. The resulting algebraic system of equations was solved iteratively sing a preconditioned truncated conjugate residual method. Several issues were addressed, including the choice of formulation of the governing equations, the accurate implementation of the no-slip boundary condition, the choice of preconditioner, and the solution method. A multidomain method was also incorporated in to the spectral method to aid in the resolution of the disparate length scales of the problem. In effect, it decomposes the problem into a set of sub-problems, which are related through interface conditions. Two interface conditions

were tested and evaluated for the two types of equations solved in this study, namely, transport and Poisson equations. For those geometries examined that require an outflow boundary, a buffer domain technique was developed for the vorticity-stream-function formulation that allows disturbances and vortex structures to exit out of the domain of interest without reflection.

The spectral method was first tested using the shear-driven cavity, both standard and regularized, to validate the method, ascertain its accuracy, and address the issues mentioned above. Results for various Reynolds numbers and grid discretization were presented along with favorable comparisons between the two formulations tried in this study and with other numerical results. The multidomain method was also examined as to its performance with the shear-driven cavity problem. In particular, the proper choice of interface conditions was investigated for the two types of equations being used. Next, the simulation of the linear-stability problem on a flat plate boundary layer was examined to test the accuracy of the interface conditions with respect to the passage of small amplitude waves. This problem provides validation for the spectral multidomain method for use in studying receptivity, and also introduced additional complexities such as grid stretching, and far-fieldfield and outflow boundary conditions. The spectral technique in generalized coordinates is given by Blodgelt, K.Ghia and Street(1994).

The present method was tested to insure that the base flow, the Blasius boundary-layer solution, was maintained in the absence of disturbances. Two cases of linear stability were simulated. The results were compared with other DNS results and linear stability theory. Grid studies were performed and the results were checked to insure that they are linear. Two additional geometries were examined that make use of the generalized curvilinear coordinates and for which leading-edge receptivity is investigated: **the parabola, and the flat plate with an elliptic leading edge.** Base-flow results were obtained and excellent comparisons were observed between the present parabola results and those of Davis (1972). Good qualitative comparisons were obtained between the results from the present method and the

finite-difference results of Lin et al (1992). A receptivity study was attempted on the parabola geometry, but the problem, when discretized, proved to be ill-conditioned. This led to unacceptable errors and numerical instabilities. However, receptivity to plane acoustic waves was successfully simulated for the flat plate with and elliptic leading-edge geometry. Favorable comparisons with the results of Lin et al. were obtained for two values of the leading-edge aspect ratio and two values of the forcing frequency. In all of the receptivity results, the Tollmien-Schlichting wave was seen to appear downstream of the ellipse-plate juncture. Some preliminary results on receptivity were discussed by Blodgett, K.Ghia, U.Ghia and Streett(1994).

The next two studies by Duncan and Noll are currently still being investigated and they will now be discussed.

## 2C Direct Numerical Simulation of Transition and Turbulence In Complex Geometry Internal Flows - Bradley Duncan, Ph.D student

### *Purpose*

The simulation of transition to turbulence as well as fully developed turbulence is key to producing accurate, predictive simulations of high Reynolds-number flows. Correct simulation of turbulent unsteady flows over aerospace vehicles requires that fine-scale boundary layer turbulence is correctly computed, so that the large-scale effects of boundary layer separation and resulting unsteadiness will also be accurate. In the discipline of direct numerical simulation (DNS) of flows governed by the incompressible Navier-Stokes equations, all of the fundamental scales of transitional and turbulent phenomena are computed in the simulation. The issues that are then faced are primarily computational, i.e., the computation is intensive and complex. The addition of geometric complexity exacerbates the computational difficulties. In order to eventually attain the capability to perform simulations of turbulent unsteady flow over a three-dimensional wing, the purpose of the current study is to work toward DNS methodology for complex geometries.

The present work is focused on resolving computational and numerical analysis issues in DNS of transition and turbulence in flows with some geometric complexity, but within the domain of application of traditional spectral methods. Spectral methods are useful for creating benchmark results with which other less accurate but more flexible numerical approaches can be validated. Large eddy simulation(LES) sub-grid-scale models are also developed using spectral methods, then applied to other approaches. The goal of the current project is to develop a general DNS approach for spectrally-accurate simulation in complex geometries, that is, geometries with arbitrary (but smooth) coordinate transformations.

The current application of the approach is to DNS of instability and transition in periodic channel flows. The work has focused on the development of the computational analysis, and has been successfully tested on a curved channel geometry. The final objective of the current work is to obtain benchmark results of transition to turbulence in the more complicated geometry of channel flow with distributed, periodic, surface roughness. These benchmark results will be of interest to the transition community as it investigates the receptivity of channel flow to surface roughness and the corresponding route to turbulence.

## *Progress*

The study is currently underway. Significant progress had been made in DNS of instability and transition in periodic channel flows. The work has focused on the development of the computational analysis, and has been successfully tested on a curved channel geometry, a two-dimensional channel with large-amplitude waviness, and a three-dimensional channel with small-amplitude waviness. Key milestones have been achieved in the present study in the specific areas of algorithm development, programming methodology, and code validation. DNS results have been obtained for several cases.

### *Algorithm development*

The development of spectral methods for complex geometry has been challenging, and has mandated new strategies than have been used in previous studies with traditional spectral methods. In order to improve numerical stability and robustness, two fully-coupled schemes were developed for the study. Both schemes avoid the commonly-used time-splitting method for decoupling velocity and pressure. Instead, the velocity and pressure systems are solved within a multi-level iteration scheme, and the fully-coupled linear algebra system is converged. The two variants on the fully-coupled scheme are obtained by using either a fully-implicit second-order time-discretization or a semi-implicit second-order time-discretization in which the convective terms are treated with an explicit Adams-Bashforth discretization. The fully-implicit scheme employs Newton's method as the outer iteration level, and for each iteration, a linearized system is solved. For the semi-implicit scheme, iteration is not required at the outer level. For both methods, the linear system is solved using preconditioned GMRES iteration. Preconditioning is performed using an approximate lower-upper (LU) factorization of the equations which decouples the velocity and pressure solution procedures. The velocity and pressure solutions are also obtained using preconditioned iterative methods. The pressure system uses a fast Poisson solver technique obtained by a transformation into wavenumber space. The DNS strategy has been significantly refined in the last six months, and has been successfully implemented into an efficient solution procedure for DNS of complex geometry channel flows.

### *Programming methodology*

In any numerical simulation code development effort, successful design and implementation of the details of the programming approach are critical to the success of the project. Currently, research is underway in the Computational Fluid Dynamics Research Laboratory to develop object-oriented numerics (OON) technology which allows the rapid prototyping and development of complex CFD applications. The fundamental idea of OON is the re-use of numerical algorithms that are universal in

nature and are expressed in mathematical language. In the OON approach, these algorithms also must be implemented in an optimized manner such that computing performance meets or exceeds that obtained with a conventional non-object-oriented approach. While this effort is in its early stages, the current development of DNS of channel flows is an experimental case study for the application of OON technology. The code has been developed in a completely object-oriented framework, with interchangeable components each representing a single abstraction of the CFD problem. This allows much needed experimentation with different numerical approaches at both the macro- and micro-levels of the code structure. Individual DNS "applications", or codes, can be developed rapidly from the existing components in order to try a new approach. Within the last six months, this effort has been successful in allowing testing of various numerical approaches, and in selection of an efficient solution procedure for DNS of complex geometry channel flows.

### *Code validation*

During each stage of development of the current DNS code, detailed numerical validations have been performed. First, analytically-prescribed solutions have been used, along with a forcing term in the equations, to test the convergence of the residual and computed solution with increasing spatial and temporal resolution. This approach will continue to be used as grids for new geometries are examined and as changes to the algorithms are introduced, in order to insure that accuracy has not been compromised. Second, validation cases involving the evolution of linear waves in plane and curved channel flows have been used to examine the accuracy of the solution. The growth rate and frequency of oscillation of these waves compare well with the linear stability values, and allow detailed study of the effects of spatial and temporal resolution and wave amplitudes. Finally, long-time computations of two-dimensional saturated states in plane and curved channel flow have demonstrated that the nonlinear evolution of waves is computed correctly. Saturated states have been computed for Tollmien-Schlicting (TS) waves and Dean vortices in channels with different Reynolds number and curvature. Most of the validation stages were

performed early in the study; however, the validations are repeated as new code developments are applied. Also, the computational time required to compute two-dimensional saturated states has recently been greatly reduced due to algorithm improvements, and results have been obtained, for Dean vortex flows, which compare well to other published results.

### *Results*

Though the code is not yet in "production" mode, recently, three-dimensional results have been obtained which demonstrate the code's potential for calculation of transition and turbulence. Starting with a two-dimensional saturated TS wave plus a small streamwise vortex disturbance, the evolution of a highly three-dimensional flow containing a single lambda vortex was obtained in a curved channel flow. Subsequent coarse grid results show the breakdown of large scale structure of the flow into a broadband small-scale structure indicative of turbulence. The lambda vortex structure compares well with expected results, and the subsequent breakdown to turbulence demonstrate correct behavior of the simulated results, though the small-scale structures are not fully resolved. Figure 3 shows the lambda-vortex at a time of $t$=75. Streamlines are shown lifting off from the bottom wall and wrapping around the vortex (the head of the vortex is on the domain boundary). On the wall and the inflow and side domain boundaries, contours of the magnitude of vorticity are shown. The wall vorticity shows the angular structure of the lambda vortex, and the spanwise non-uniformity can be seen in the inflow plane. The side domain boundary predominantly shows the characteristic TS wave which is undergoing three-dimensional breakdown.

Two-dimensional wavy-channel results are shown in Figure 4 as contours of the x-component of velocity, the pressure, and the vorticity magnitude. The results are shown at and early time of $t$=6.5, and were started with an initial condition obtained by projecting a fully-saturated TS wave onto a divergence-free solution space. The large-scale waviness adds a vortex shedding event to the dynamics of the two-dimensional instability, as can be seen in the vorticity plot.

Dean vortex solutions were obtained for two-dimensional flow through the channel cross-section. At a Reynolds number of $Re$=250, this two-dimensional flow in unstable to streamwise disturbances. A low-amplitude surface waviness was used to excite this instability, and, in Figure 5 results are shown at $t$=1, where a streamwise variation in the Dean vortex rolls can be seen.

### *Presentations*

The code development research as well as some validation and demonstration results have been recently discussed by Duncan and Ghia(1997a,1997b) at two conferences, the First AFOSR International Conference on DNS/LES at Louisiana Tech University in August, 1997, and at the American Physical Society Division of Fluid Dynamics meeting in San Francisco in November.

### Proposed Work

The future goal of this study are to obtain benchmark results for three-dimensional instability of flows in curved channels with wall waviness. Both TS-wave and Dean-vortex simulations are currently being performed, and the final results will be presented at conferences, submitted for publication, and will be the culmination of Brad Duncan's Ph.D. research.

## 2 D Development of Object Oriented Software For The Study Of Compressibility Effects on Dynamic Stall- Chris Noll, Ph.D student

### *Dynamic Stall*

One of the goals for this study was to construct a simulation tool for studying the compressibility effects on the dynamic stall of an airfoil. Compressibility effects, such as shocks, already become prevalent at free stream Mach numbers as low as 0.2.

Because of the unsteady flow induced by the maneuvering body, local Mach numbers can exceed unity in this case. Compressibility effects have the effect that they lessen the advantages of a maneuver. As the Mach number increases, the maximum lift coefficient $C_l$ decreases. and, the dynamic stall occurs at lower angles of attack. From the experimental studies of Chandrasekhara Carr and Wilder(1993 ), this was attributed to two effects. At lower free stream Mach number (from 0.2 to 0.4), a shock forms above the airfoil surface triggering leading-edge separation, normally associated with incompressible dynamic stall at high Re. At higher free-stream Mach numbers (above 0.4), the formation of numerous small shocklets is thought to increase the local vorticity production hastening the dynamic stall event.

Through initial simulation studies, several difficulties were encountered. Since the simulation software developed is time-accurate, it was not possible to impulsively start the airfoil from rest. When this was done, a shock would form enveloping the airfoil and then rapidly move out from the airfoil as time progressed. This feature caused many numerical problems as the code was not yet designed to handle moving shocks. A scheme was devised to accelerate the body from rest. This was beneficial because the modifications to the fluid dynamics equations to allow for a moving grid were necessary in order to compute the pitching airfoil case.

Another difficulty that was introduced as a result was with the traditional definitions of Mach number and Reynolds number. Since the body is initially starting from rest and remains moving at a slow motion over the first characteristic time, the Mach number and Reynolds numbers of the flow begin at zero and slowly move toward their final values progressing through the flow regimes in between.

Finally, after the airfoil was kept at a steady speed for approximately 30 characteristic time, it was pitched up. Oscillations developed in the flow wherever flow features (such as the wake) passed through regions where the grid was clustered. This problem is still unresolved, but it is believed that it is due to the absence of artificial dissipation in the model equations. The model uses a non-traditional staggered continuity equation. This is being done in order to remove the extra

boundary condition on pressure, namely that the pressure gradient normal to the body surface is zero, as this condition does not hold when the flow separates from the surface.

Streamlines and velocity vectors, colored by local Mach number, appear in the figure below. This is an initial result for a coarse-grid case and has the oscillation problem discussed above. These initial results were presented by Noll and K Ghia (1996). More recently a different approach has been taken to eliminate the pressure boundary condition. The result of this work and a complete discussion of the approach will appear in Noll (1998).

### *Partial Differential Equation Model*

The governing equations that are being solved have been derived from the first principles of conservation of mass, momentum and energy. A time-dependent transformation is used to allow for the motion of the body. The Newtonian form of the viscous stress tensor is being used along with Sutherland's law for viscosity. Stokes' hypothesis is used for the second coefficient of viscosity and the assumption of constant Prandtl number is used to obtain the conductivity. In addition, the equation of state for a perfect gas is used.

**Governing Equations**

$$\frac{1}{J}\left(J\rho\right)_\tau + div\left(\rho\vec{U}\right) = 0$$

$$\frac{1}{J}\left(J\rho\vec{V}\right)_\tau + div\left[\rho\vec{V}\vec{U} + \left(p - \lambda div\vec{V}\right)\bar{\bar{I}} - \mu def\vec{V}\right] = 0$$

$$\frac{1}{J}\left(J\rho e_0\right)_\tau + div\left[\rho e_0\vec{U} + \left(p - \lambda div\vec{V}\right)\vec{V} - \mu\vec{V}\cdot def\vec{V} - kgradT\right] = 0$$

$$J = x_\xi y_\eta - x_\eta y_\xi$$

where $\vec{U} = \vec{V} - \vec{W}$ and $\vec{W}$ is the grid velocity.

The boundary conditions that are being used include free-stream flow far from the body and the standard no-slip and constant temperature condition on the body. Much care has been given, not to introduce the commonly used, but inaccurate, normal pressure gradient equal to zero condition.

### *Numerics*

The governing partial differential equations were discretized using central differences for all spatial derivatives and a second-order trapezoidal integration method for the time derivative. This discretized system has been solved using an O-grid topology and care has been given to ensure that the proper fluid dynamics equations have been solved on the branch cut.

The resulting non-linear algebraic system is solved through an approximate Newton's method. The coefficient matrix is loaded and frozen in time, so that it can be factored only once for a given number of time steps. When convergence becomes difficult, due to the inaccuracies thus introduced into the Jacobian matrix, it is re-computed and re-factored at that time. It was found that the same Jacobian matrix could be used over the course of several characteristic time of the computation. This was true during the constant angle-of-attack phase of a computation. The Jacobian matrix had to be re-computed more often during the pitch-up phase.

The linear system resulting from the use of Newton's method was solved with an approximate factorization method similar to Douglas and Gunn's ADI method. Several of these iterations were used for each pseudo-Newton iteration until the solution converged to machine-zero for each time step.

### *Object-Oriented programming*

An object-oriented approach was taken to develop the CFD software. This approach was chosen because of the flexibility that it gives. This was deemed necessary because many numerical methods were to be tested and rapid development

of the software needed to solve the equations was essential to allow for the variety of methods to be tested. The main use for object-oriented programming was in the solution of the equations. A linear algebra class library was developed to provide facilities for building and solving multi-dimensional matrices of either a dense or structured form. The member functions made extensive use of BLAS subroutines to get optimum performance for a given hardware platform. A discussion of this work was presented by Noll et al. (1996) and Brandes-Duncan et al. (1996).

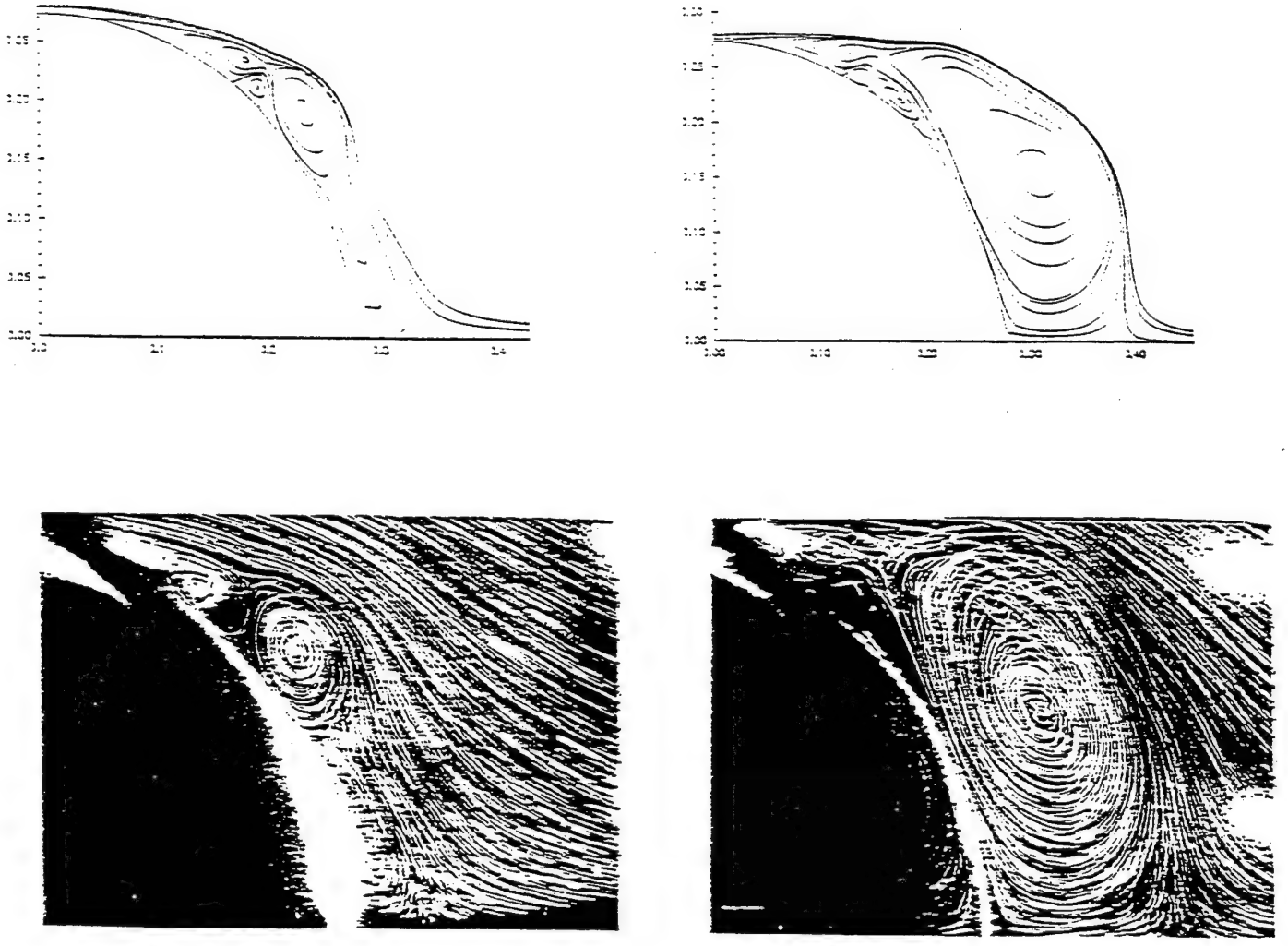

(a) (b)

**Figure 1** Comparison of numerical results with experimental data of Bouard and Coutanceau: $Re_D = 9500$, grid size (705 x 91).
(a) $t_D = 1.0$ and (b) $t_D = 1.5$.

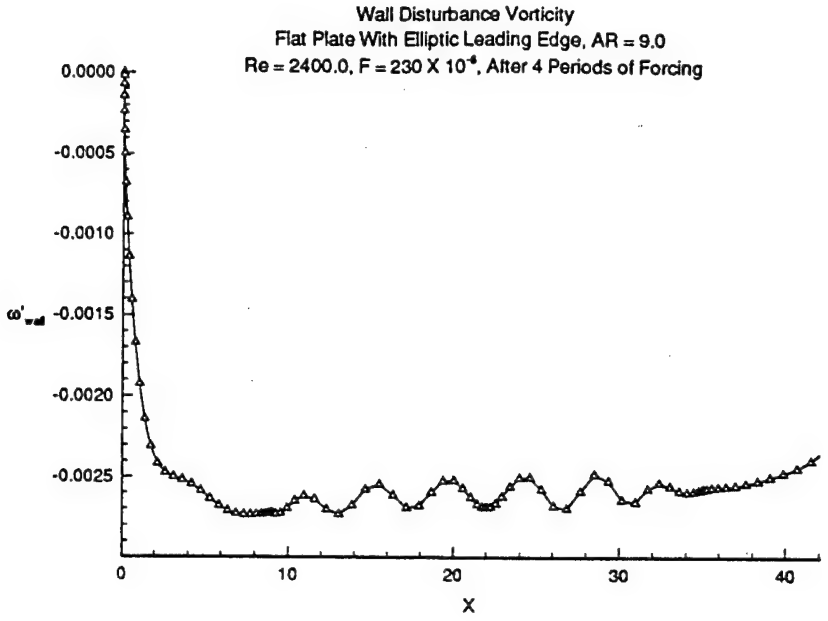


**Figure 2a** Instantaneous Disturbance Vorticity Along the Surface, $Re = 2400$, AR = 9, F = 230 x $10^{-6}$.

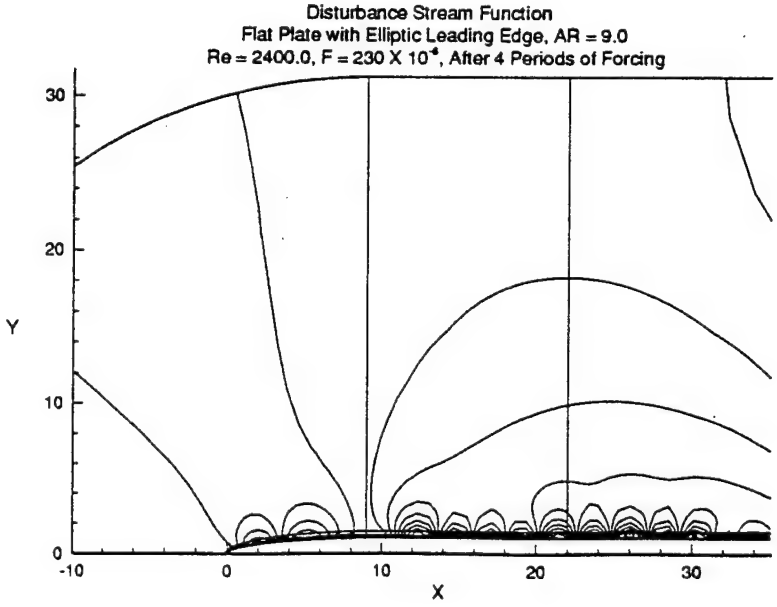


**Figure 2b** Instantaneous Stream Function Contour Plot, $Re = 2400$, AR = 9, F = 230 x $10^{-6}$.

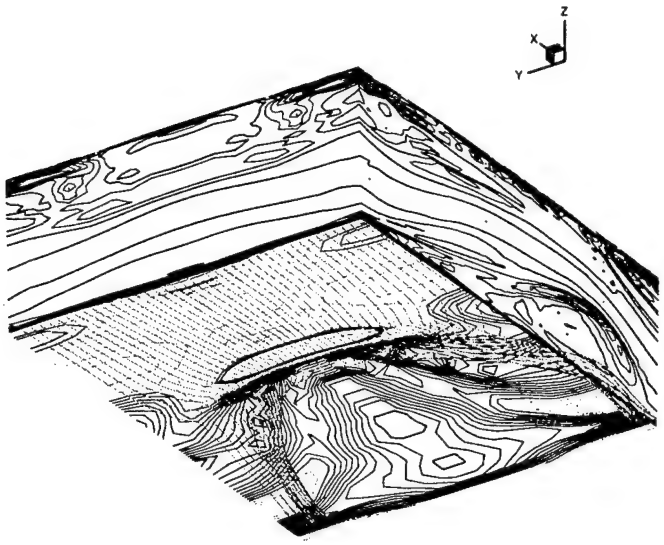


**Figure 3.** Integrated streamlines starting near the lower-wall of a curved channel, and vorticity magnitude contours on the lower wall, inflow plane, and side plane. Flow is from upper left to lower right. The parameters for the simulation are Re=5000, radius of curvature ($R_C$)=100, $\alpha$=100, $\beta$=1.25, grid resolution=32x32x64, $\Delta t$=0.01, $t$=75.

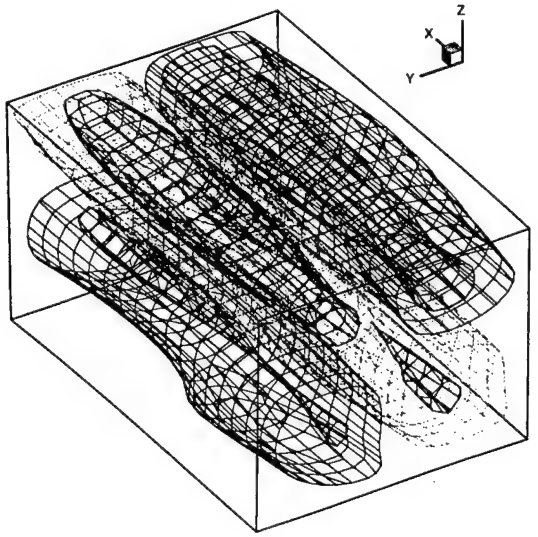


**Figure 4.** Contours of y-component of velocity for a twisting Dean vortex developing in a curved channel with small amplitude ($a$=0.01) surface waviness. The flow is from upper left to lower right. The parameters of the simulation are Re=250, $R_C$=79, $\alpha$=135, $\beta$=2.5, $\Delta t$=0.01, $t$=1, grid resolution=16x16x32.

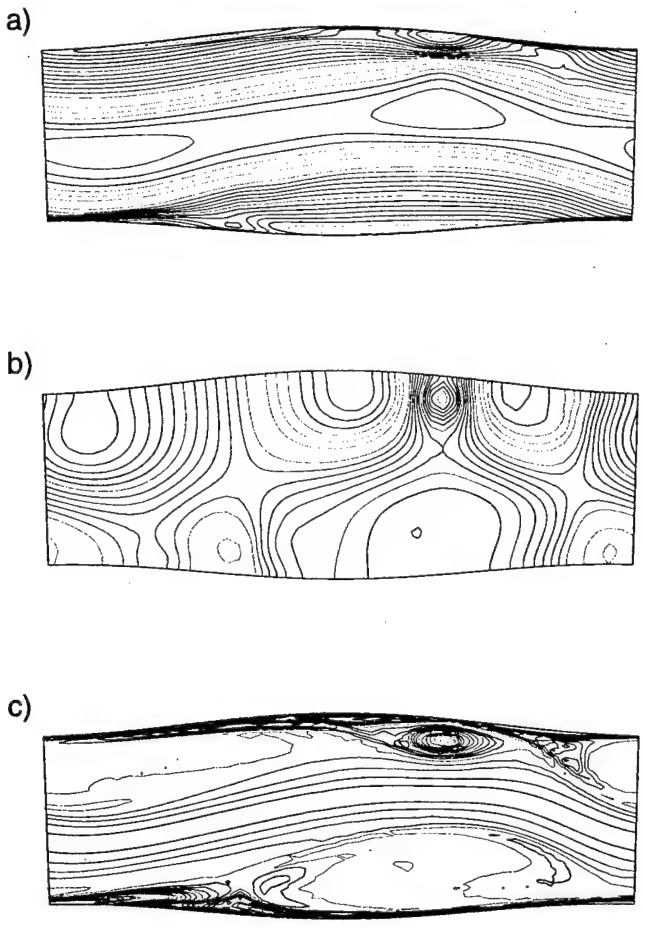


**Figure 5.** Contours of a) x-component of velocity, b) pressure, and c) vorticty magnitude, all for a TS wave developing in a wavy channel. Flow is from left to right. The amplitude of the channel wall is $a$=0.1, and the parameters of the simulation are Re=5000, $R_C$=100, $\alpha$=100, $\Delta t$=0.01, $t$=6.5, grid resolution = 48x64.

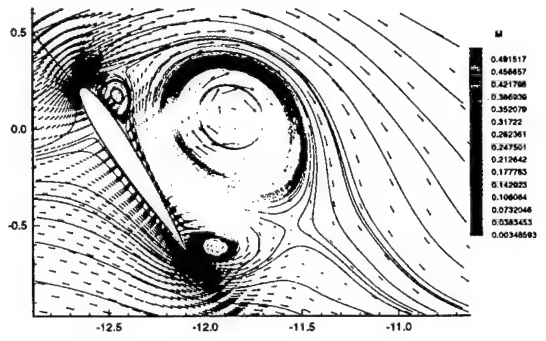


**Figure 6.** Streamlines and velocity vectors colored by Mach contour for pitching NACA 0012 at Mach number, M=0.2, and Reynolds number 1000.

# SECTION 3

# REFERENCES


Beltz, S., Ghia, K.N. and Osswald, G.,(1995), "Validation of Unsteady Incompressible Navier-Stokes Analysis in Generalized coordinates using Flow Past a circular cylinder," *AIAA Paper No.* 95-2183, June.

Blodgett, K., Ghia, K.N., Ghia, U. and Streett, C.L.,(1994), "An Examination of Leading-edge Receptivity on a Parabolic Cylinder using the Navier-Stokes Equations," *Advances in computational methods in Fluid Dynamics,* FED Vol.196, ASME Press, pp. 53-57, June.

Blodgett, K., Ghia, K.N., and Streett C.L.(1994), " Towards Simulation of Leading Edge Receptivity using a Spectral Multidomain Method in Generalized curvilinear coordinates," *AIAA Paper No.* 94-0063, January.

Brandes-Duncan, B., Noll, C., and Ghia, K.,(1996), "An Object-Oriented Class Library for High-Performance Computing," presented at *AIAA Science and Technology Mini-symposium*, Holiday Inn, Dayton, Ohio, March

Chandrasekhara, M.S., Carr,L.W. and Wilder,M.C.,(1993),"Interferometric Investigation of Compressible Dynamic Stall over a Transiently Pitching Airfoil," *AIAA Paper No.*93-0211, January; also in *AIAA J,* vol 32, No. 3. 586-593.

Davis, R.T.,(1972), "Numerical Solution of the Navier-Stokes Equations for Symmetric Laminar Incompressible Flow Past a Parabola," *Journal of Fluid Mechanics*, Vol. 51, pp. 417-433.

Douglas, J., and Gunn, J.E., (1964), "A General Formulation of Altenating Direction Methods Part I-Parabolic and Hyperbolic problems," *Numerische Mathematic,* Vol 6,pp. 426-453.

Duncan, B.D., and Ghia, K.N., "An Iterative Approach for Solving the Incompressible Navier-Stokes Equations for Simulation of Transition and Turbulence in Complex Geometries," *Proceedings of First AFOSR Conference on DNS/LES*, Editors: C. Liu and Z. Liu, Louisiana Tech University, Ruston, Louisiana, August, pp.185-187.1997.

Duncan, B.D., and Ghia, K.N., "Direct Numerical Simulation of Transition to Turbulence in a Curved Channel Flow with Wall Foughness," *Bull. Am. Phy. Soc.*, Vol.42, No.11, p 2175, November 1997.

Lin, M., Reid, H.L., and Saric, W.S.,(1992), "Effect of Leading-Edge Geometry on Boundary-Layer Receptivity to Free Stream Sound" *Instability, Transition and Turbulence,* Editors: Hussaini, M.Y., Kumar, A., and Streett, C.L., Springer-Vertag,pp. 421-440.

Noll, C., and Ghia, K., 1996, "A Generalized Time-Dependent Analysis for Studying Compressibility Effects on Dynamic Stall Implemented on a Parallel Computer", *Proceedings of the First AFOSR Conference on Dynamic Motion CFD*, Editors: L. Sakell and D.D. Knight, Rutgers University, New Brunswick, NJ, June 3-5, pp. 307-316.

Noll, C., Brandes-Duncan, B., and Ghia, K., 1996, "Object-Oriented Programming Applied to Computational Fluid Dynamics," presented at *AIAA Science and Technology Mini-symposium*, Holiday Inn, Dayton, Ohio, March.

Noll. C., 1997, Development and Application of an Object-Oriented Fluid Dynamics Analysis for Compressible Flow About Maneuvering Bodies, to appear in *Ph.D., Dissertation,* University of Cincinnati

**APPENDIX A**

# AIAA 95-2183
# Validation of Unsteady Incompressible Navier-Stokes Analysis in Generalized Coordinates Using Flow Past a Circular Cylinder

S. Beltz, K. N. Ghia and G. A. Osswald
Computational Fluid Dynamics Research Laboratory
University of Cincinnati
Cincinnati, OH

**26th AIAA Fluid Dynamics Conference**
**June 19-22, 1995/San Diego, CA**

# VALIDATION OF UNSTEADY INCOMPRESSIBLE NAVIER-STOKES ANALYSIS IN GENERALIZED COORDINATES USING FLOW PAST A CIRCULAR CYLINDER*

by

S. Beltz**, K. N. Ghia+, and G. A. Osswald++

**Computational Fluid Dynamics Research Laboratory**
**Department of Aerospace Engineering and Engineering Mechanics**
University of Cincinnati
Cincinnati, OH 45221

## ABSTRACT

A vorticity-stream function circulation $(\omega,\psi,\Gamma_\infty)$ formulation is explored as an extension of the earlier work of the authors to focus upon the accurate implementation of the far-field boundary condition for the study of two-dimensional incompressible unsteady flows past Joukowski airfoils. The distinction in the implementation of the formulation is achieved through the incorporation of the viscous circulation $\Gamma_\infty$. The resulting system of governing equations is solved numerically using the Block Gaussian Elimination (BGE) procedure to solve the integral form of the curl equation, and the Alternating Direction Implicit (ADI) technique of Douglas and Gunn to solve the vorticity transport equation, with an iterative procedure used to solve the coupled governing equations and boundary conditions as well as ensure pressure continuity along the airfoil surface. Due to a lack of available data pertaining to Joukowski airfoils, the validation study is performed using the circular cylinder geometry, considering the wake development at early time for two different values of the Reynolds *Re* number. Additionally, the grid independence of the solutions obtained is established using the Grid Convergence Index (*GCI*). Additional parallel studies are currently being conducted by the authors at Computational fluid Dynamics Research Laboratory (CFDRL) to examine the wall vorticity boundary condition and compare the force coefficient data obtained with the available experimental data.

## 1. INTRODUCTION

The understanding of the flow mechanisms inherent in unsteady high-*Re* flows past lifting airfoils lends valuable information towards the aerodynamic design of these devices. However, these flows have been found to exhibit a variety of complex flow phenomena. Much effort has been expended by researchers in attempting to investigate these flows. However, experiments involving high-*Re* flows are, in general, very costly and are often unable to provide the detailed quantitative information concerning the temporal behavior of the flow field. Additionally, even with the advent of large-memory high-speed supercomputers, the task of numerically simulating high-*Re* separated flows over the complex configurations which are of practical interest remains formidable, due to the widely disparate length scales present in these flows.

An alternative to the prohibitive costs associated with high-*Re* flow simulations lies in the direct numerical simulation of low- and moderate-*Re* flows using the Navier-Stokes equations. The presently-available supercomputer resources have made the calculation of these flow solutions practical, since they typically require considerably less memory and CPU resources than their higher-*Re* counterparts.

---

* This research is supported, in part, by the AFOSR Grant Nos. F49620-93-1-0393 and F49620-92-J-0292 and by the Ohio Supercomputer Center Grant No. PES070-5.

** Graduate Research Assistant, Permanent Address: Integrated Research, 2716 Erie Ave., Suite 2W, Cincinnati, OH 45208.

+ Herman Schneider Professor of Engineering, Associate Fellow AIAA.

++ Research Assistant Professor, Member AIAA.

Since these lower-*Re* systems often exhibit locally the nonlinearities characteristic of high-*Re* separated flows, detailed examination of these flow solutions may provide the insight which is needed for understanding of high-Re flow systems. Towards this end, it is the purpose of the present study to implement an alternative far-field boundary condition and examine its effect on the overall flow. To achieve this, a newly-developed formulation, presented in the Section 2, is implemented for application to low-speed flows.

Although the current study focuses on the development and subsequent validation of a vorticity-stream function-circulation $(\omega,\psi,\Gamma_\infty)$ formulation for application to Joukowski airfoils, the ability of the formulation, which uses generalized orthogonal coordinates, to incorporate an arbitrary sequence of conformal mappings enables a range of flow configurations to be studied. The versatility of the formulation makes it advantageous to consider a validation study using the circular cylinder geometry due to the lack of available data pertaining to Joukowski airfoils. This approach was used previously by Rohling (1991) to validate the vorticity-stream function formulation, which was subsequently applied to conduct a detailed analysis of the flow past a symmetric Joukowski airfoil at various angles of attack; for certain combinations of flow parameters, the flow exhibited a chaotic behavior.

The value of the Reynolds number, *Re*, has been shown to be of considerable importance in determining the characteristics of the flow past a circular cylinder. Morkovin (1964) and Marris (1964) have presented detailed reviews of the behavior of the flow past a circular cylinder as a function of *Re*. They have noted that, for subcritical values of *Re*, i.e., $Re < 100{,}000 - 130{,}000$, the flow is characterized by a laminar near wake consisting of coherent vortex structures which remain symmetric for a period of time and subsequently shed alternately from the rear of the cylinder. This periodic vortex shedding phenomenon has also been noted in the computational investigations of Liu (1987), K. Ghia et. al. (1987) and Blodgett (1990), but at very low *Re* values. Additionally Braza, Chassaing and Ha Minh (1986) have noted the presence of periodic vortex shedding for relatively low values of *Re* and believe this to be an intrinsic flow phenomenon which is contained in the Navier-Stokes equations.

Of particular relevance to the current study is the experimental investigation of Bouard and Coutanceau (1980), which considered the early wake development of the flow past an impulsively-started circular cylinder at low-, moderate- and high-Reynolds numbers. Their study utilized a flow visualization technique, which permits detailed observation of the temporal behavior of the flow structures, to successfully examine both quantitatively and qualitatively, the evolving flow structures and vortex interactions. Their investigations of the flow at moderate *Re* demonstrated a strong qualitative agreement with the results of Honji and Taneda (1969), Taneda (1972) and Thoman and Szewczyk (1969). Quantitatively, their consideration of separation bubble lengths at early times were in close agreement with the results of Collins and Dennis (1973) and Panikker and Lavan (1975), among others. It is therefore chosen to utilize the experimental results of Bouard and Coutanceau (1980) to validate the results of the present study.

## 2. MATHEMATICAL FORMULATION

### 2.1 Governing Equations

The earlier analysis of Osswald, K. Ghia and U. Ghia (1985), which considered the numerical solution of the Navier-Stokes (NS) equations in terms of the derived variables of vorticity $\omega$ and stream function $\psi$, has been modified to incorporate an alternative far-field boundary condition, which results in the coupling of the viscous circulation $\Gamma_\infty$ with the disturbance stream function $\psi^D$. Additionally, in an on-going study at CFDRL, Osswald has investigated the advantages of obtaining the stream function $\psi$ from an integral, rather than differential, relation, which facilitates proper treatment of the weak singularity existing at the body surface. Then, the governing equations take the form of the temporally-parabolic vorticity transport equation and the spatially-elliptic integral form of the curl equation for velocity, also known as Stokes Theorem. These are given in terms of generalized orthogonal coordinates as:

**Vorticity Transport Equation:**

$$\frac{\partial\omega}{\partial t}+\frac{1}{\sqrt{g}}\left\{\frac{\partial}{\partial\xi^1}\left(\frac{g_{22}}{\sqrt{g}}\omega V_1\right)+\frac{\partial}{\partial\xi^2}\left(\frac{g_{11}}{\sqrt{g}}\omega V_2\right)\right\}$$
$$=\frac{1}{Re}\frac{1}{\sqrt{g}}\left\{\frac{\partial}{\partial\xi^1}\left(\frac{g_{22}}{\sqrt{g}}\frac{\partial\omega}{\partial\xi^1}\right)+\frac{\partial}{\partial\xi^2}\left(\frac{g_{11}}{\sqrt{g}}\frac{\partial\omega}{\partial\xi^2}\right)\right\} \qquad (1)$$

**Integral form of Curl Equation:**

$$\iint_{dA} \sqrt{g}\omega \, d\xi^1 d\xi^2 = \oint_C \left( \frac{1}{\sqrt{g}} \frac{\partial \psi}{\partial \xi^2} \bar{e}_1 - \frac{1}{\sqrt{g}} \frac{\partial \psi}{\partial \xi^1} \bar{e}_2 \right) \cdot d\bar{l} \quad (2)$$

with $\nabla \cdot \bar{V} = 0$ being automatically satisfied by the stream function formulation.

Since the stream function does not appear explicitly in Eq. (1), it is necessary to incorporate the relation between stream function and velocity into the formulation, given as

$$\bar{V} = \nabla \psi \times \hat{k} \ , \quad (3)$$

where $\hat{k}$ denotes the unit vector normal to the two-dimensional flow domain. Osswald has show that when Eqs. (2-3) are discretized using a conservative central-difference scheme, the resulting set of algebraic equations is, for points which lie in the interior of the flow domain, exactly the same as that obtained previously by Osswald et al. (1985), while having considered the discretized form of the spatially-elliptic stream function equation, given as

$$\nabla^2 \psi = -\omega \ . \quad (4)$$

**2.2 Boundary and Initial Conditions**

The numerical solution of the temporally-parabolic vorticity transport equation and the spatially-elliptic integral form of the curl equation necessitates the specification of appropriate boundary conditions, both at the far-field boundaries of the flow domain and at the airfoil surface, as well as an appropriate initial condition. Previous experience with maneuvering simulations has revealed the critical role of the boundary conditions in determining the flow evolution. The present formulation represents an exploratory study where boundary conditions are re-examined to achieve continuity in the surface pressure distribution.

Previously, Rohling (1991), in his analysis of the unsteady incompressible flow past a 12% thick symmetric Joukowski airfoil using the $(\omega,\psi)$ formulation, implemented boundary conditions which consisted of the no-slip condition along the body surface and free-stream conditions at the far-field boundaries. However, recently, Osswald, while developing an analysis to study the three-dimensional flow past a finite wing using the incompressible unsteady NS equations, found the Cauchy-Riemann operator to be singular for multiply connected domains, regardless of whether a C-grid or an O-grid is employed. This results in a single degree of degeneracy which needs to be accounted for. Since the no-slip condition, applied at the airfoil surface, is well-behaved, and, since the vorticity at infinity is identically zero, and hence, clearly well-behaved, the asymptotic behavior of the far-field stream function was carefully examined in hopes of resolving the singularity in the Cauchy-Riemann operator. The study of Yang (1992), which included an asymptotic analysis of the far-field behavior of the stream function obtained using a Laurent series expansion, revealed that the viscous circulation exhibits a similar behavior at infinity. In light of this behavior, the original $(\omega,\psi)$ formulation has been modified to include an alternative far-field boundary condition for the stream function, which results in the coupling of the viscous circulation at infinity with the vorticity transport and integral form of the curl equations. The resulting $(\omega,\psi,\Gamma_\infty)$ formulation necessitates that additional conditions be used to (*i*) provide the value of $\Gamma_\infty(t)$ at each time step, and (*ii*) uniquely specify its relationship to the disturbance stream function at infinity.

To remove the numerical difficulties associated with the unbounded behavior of the stream function at infinity, the stream function is decomposed as:

$$\psi = \psi^0 + \Gamma_\infty \psi^G + \psi^D \ , \quad (5)$$

where $\psi^0$ denotes the stream function corresponding to the zero-lift, i.e., zero-circulation inviscid flow solution, $\psi^G$ represents the stream function corresponding to a unit circulation potential slip solution, with the viscous circulation $\Gamma_\infty$ which remains nonzero at infinity, and $\psi^D$ represents the disturbance stream function, which is chosen as the dependent variable in the numerical solution of the integral form of the curl equation. The use of the zero-lift inviscid stream function $\psi^0$, rather than the inviscid stream function $\psi^I$, which, in general, possesses a non-zero circulation, serves to account for the inviscid behavior except for that due to the circulation in the decomposition of the stream function. It should be noted that, since the unbounded behavior at infinity associated with the zero-lift inviscid stream function and the viscous circulation have been removed

from $\psi^D$, the numerical solution of the disturbance stream function constitutes a well-posed problem, since $\psi^D$ and its boundary conditions are nonsingular over the entire flow domain.

Therefore, boundary conditions are needed on $\psi^D$. The examination of the far-field behavior of the stream function by Osswald revealed that the disturbance stream function, $\psi^D$, does not, as was previously believed, approach zero at infinity, but rather, it approaches an unknown constant. Therefore, the Dirichlet boundary condition on the disturbance stream function used in the study of Yang (1992), namely, the enforcement of $\psi^D = 0$ at infinity, was modified in the current study to reflect this. Then, the boundary conditions employed in the present study are given as:

**At the airfoil surface:**

$$\vec{V} = 0 \quad \text{(No-slip condition)}, \tag{6}$$

**At infinity:**

$$\psi^D = \psi^D_\infty \quad \text{(Dirichlet Boundary Condition)}, \tag{7}$$

where $\psi^D_\infty$ denotes the constant value of the stream function at infinity. These boundary conditions are shown graphically in Fig. 1. The no-slip condition is implemented via the integral form of the curl equation applied over the domain consisting of the half cell surrounding the body.

Previously, in the study of Rohling (1991), the inviscid potential flow solution at the flow angle of attack $\alpha_f$ was considered as the initial condition. However, it was later discovered by Osswald that, for the $(\omega, \psi, \Gamma_\infty)$ formulation considered in the present study, the use of an inviscid solution as the initial condition fails to provide the correct initial value of the viscous circulation, and hence cannot be applied. Therefore, the initial condition considered in the present study is the viscous flow solution at time $t = 0^+$, corresponding to an impulsive start from rest of the airfoil.

The system of equations consisting of Eqs. (1) and (2), combined with their respective boundary and initial conditions, cannot be solved uniquely unless the value of $\psi^D_\infty$ is given at each time step. As mentioned previously, specification of $\psi^D_\infty$ requires knowledge of the viscous circulation remaining at infinity. Therefore, an additional condition is needed which gives the appropriate value of $\Gamma_\infty(t)$ at each time step. Mathematically, this condition may be written as

$$\Gamma_\infty = \Gamma_B - \iint_D \omega \, dA \,, \tag{8}$$

where $\Gamma_B$ denotes the circulation at the body surface and $D$ denotes the entire flow domain. Note that the boundary condition $\omega = 0$ at infinity makes it possible to impose the far-field limit of integration on the $\iint_D \omega \, dA$ term at the half-cell location, rather than at the actual boundary of D, which lies at true infinity. The difficulties associated with numerical integration over the semi-infinite cells at the far-field boundary are thus avoided. Also, with regards to the present study, the relation

$$\Gamma_B(t) = 0 \,, \tag{9}$$

holds for all time, since (*i*) the angular acceleration of the airfoil is identically zero, and (*ii*) no suction or injection is applied. While Eq. (8) provides the value of $\Gamma_\infty(t)$ at each time step, its relationship to the far-field stream function must be specified in order to ensure a well-posed problem. This is achieved by

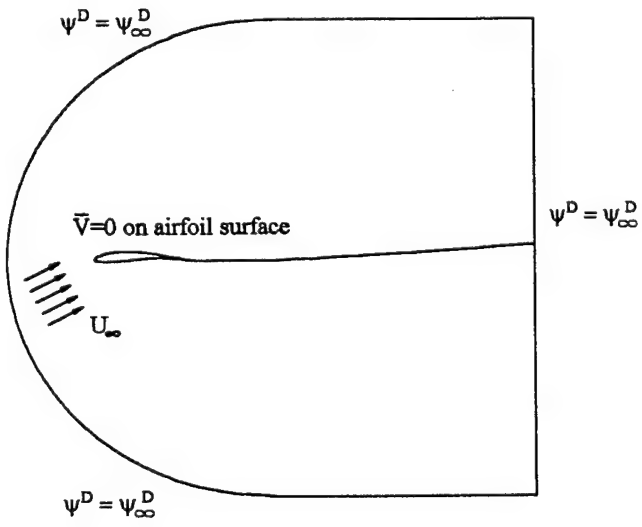


**Figure 1** Boundary Conditions for the Joukowski Airfoil

invoking the integral form of the curl equation along the body surface as

$$\oint_{\tilde{B}} \bar{V} \cdot d\bar{l} = -\Gamma_\infty - \iint_{\bar{B}} \omega dA \ , \qquad (10)$$

where the subscript $\tilde{B}$ denotes the path one half cell off of the body surface and $\bar{B}$ denotes the domain between the body and the path denoted by $\tilde{B}$. The above Eq. (10), when discretized is a linear combination of the discretized form of the no-slip conditions and thus there is still a degree of freedom to be accounted for. Following the method of Yang (1992), this difficulty is resolved by eliminating one of the discrete no-slip conditions and imposing the condition that the pressure be single-valued and continuous along the airfoil surface. Mathematically, this condition is given as

$$\oint_B dp = 0 \ , \qquad (11)$$

where the subscript $B$ denotes the body surface, and represents the Kutta condition for unsteady viscous flow, i.e., Eq. (11) necessitates that the pressure at the infinitely-sharp trailing-edge of the airfoil must be single-valued and continuous.

Equation (11) may be evaluated mathematically by considering the linear momentum equation as

$$\nabla p = \bar{V} \times \bar{\omega} - \frac{1}{Re}\left(\nabla \times \bar{\omega}\right) - \frac{\partial \bar{V}}{\partial t} - \nabla\left(\frac{\bar{V} \cdot \bar{V}}{2}\right) \qquad (12)$$

and recalling that, at the body surface, the boundary condition $\bar{V} = 0$ must be satisfied. Then, at the airfoil surface, Eq. (12) is reduced to a statement that the variation of pressure along the body surface depends only upon the normal variation of the vorticity. Mathematically, this statement is given as

$$\oint_B dp = -\oint_B \frac{\partial \omega}{\partial n} dl = 0 \ , \qquad (13)$$

where $n$ denotes the direction normal to the body surface, and $dl$ is taken along the body surface. In the solution procedure, Eq. (13) is combined with the no-slip condition to provide a unique distribution of the body surface vorticity, with pressure closure enforced at the leading stagnation point (LSP). An advantage of enforcing pressure closure at the LSP is that this is a point of symmetry for the cases of (i) flow past a symmetric airfoil at zero angle of attack, and (ii) flow over a non-rotating circular cylinder. Therefore, for these symmetric cases, the enforcement of pressure closure at the LSP results in the inherent flow symmetry being retained throughout the calculation.

## 3. GRID GENERATION PROCEDURE

The present study utilizes the grid generation procedure of Osswald et al. (1985), which uses a series of analytical transformations to map a unit square computational domain into a C-grid topology in the physical plane, with cubic spline transformations [see Rohling (1991)] to provide precise grid point control. This approach has been shown by Rohling (1991) to result in a robust and efficient grid generation procedure which is capable of yielding nearly optimal grids for Joukowski airfoils at various angles of incidence; details of this grid generation procedure may be found in Rohling (1991).

The grid generation procedure uses a total of four separate transformations, as shown in Fig. 2, to achieve the desired mapping between the physical plane and the computational plane. The first two transformations, which constitute a mapping of the physical plane (Fig. 2 (a)) to the complex-potential plane (Fig. 2 (c)), are conformal and are representative of the inviscid flow solution, which, for Joukowski airfoils, is known in analytical form. Subsequently, a parabolic conformal mapping is used to "unfold" the complex-potential plane about the leading-edge stagnation point, thus enabling a C-grid topology to be generated in the physical plane. The final transformation is merely orthogonal, i.e., nonconformal, and uses a contraction mapping in the far field to transform the doubly-infinite $\eta$-plane (Fig. 2 (d)) into a unit square computational domain (Fig. 2 (e)), which makes it possible to impose the far-field boundary conditions at true infinity, rather than at some finite distance away from the body. This transformation also uses one-dimensional cubic spline functions of Rohling (1991) in the interior region to provide the necessary control over the grid point distribution by allowing the number of cells in specified streamwise and normal zones as well as the positions of the zonal boundaries to be completely arbitrary and specified by the analyst.

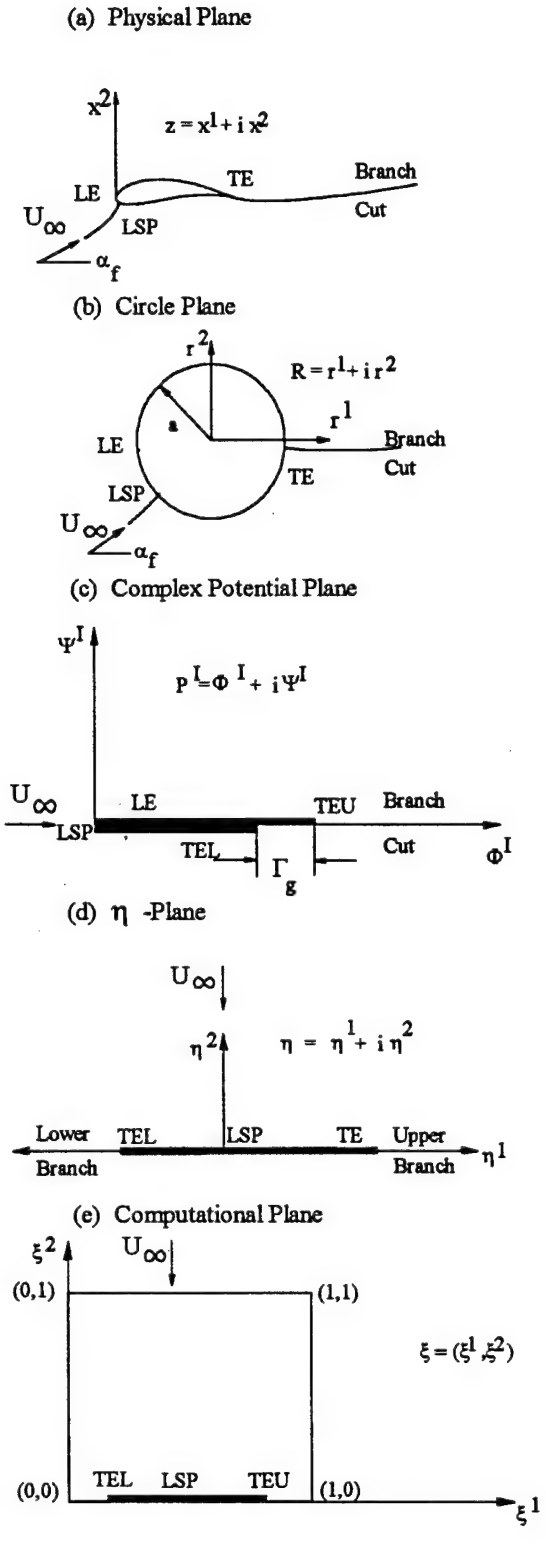


**Figure 2** Transformations employed in the grid generation procedure.

## 4. NUMERICAL PROCEDURE

The numerical solution procedure utilized in the present study follows the original fully-implicit time-marching solution method for unsteady flows developed by Osswald, K. Ghia and U. Ghia (1985). Modifications to this method have been made in order to incorporate the recent advances of Yang (1992) and unpublished work of Osswald towards the correct implementation of the boundary and initial conditions. A detailed description of the solution procedure is contained in Beltz (1994).

Although the set of governing equations presented in Section 2 clearly demonstrates the coupling of the vorticity and stream function fields, the present $(\omega, \psi, \Gamma_\infty)$ formulation contains a natural separation of the spin dynamics of a fluid particle, governed by the vorticity transport equation, and its translational kinematics, governed by the integral form of the curl equation. This permits the vorticity and stream function fields to be solved separately. Additionally, the disturbance stream function, viscous circulation and surface vorticity are predicted and corrected via an iteration procedure, which involves updating the surface vorticity via the no-slip condition and the pressure closure constraint. This procedure is repeated until convergence of the surface vorticity is obtained to within a specified tolerance. The use of the iterative procedure in obtaining the surface vorticity at the $n+1$ time level results in a formal accuracy of the overall numerical solution procedure of $O\left[(\Delta t)^2, (\Delta\xi^1)^2, (\Delta\xi^2)^2\right]$.

In providing the discretization of the vorticity transport equation, the original procedure of Osswald, K. Ghia and U. Ghia (1985) considered the use of the second-order accurate central difference scheme (CDS) to approximate all spatial derivatives. However, it was later shown by Yang (1992) that the flow solution obtained using this differencing technique showed spurious oscillations in the vorticity field for the $Re = 10{,}000$ flow past a NACA 0015 airfoil undergoing a constant pitch-up motion. This was attributed by Yang (1992) to a shortcoming of the central differencing technique, which retains second-order accuracy but is limited by the cell Reynolds number criterion.

The effectiveness of artificial dissipation in eliminating the numerically-induced oscillations associated with the CDS has been well-established by

researchers. However, the amount of artificial dissipation required differs for each specific case, making its application difficult. An alternative to this approach is the use of a third-order accurate biased upwind difference scheme (UDS), which has a natural tendency to provide dissipation, to approximate the convective terms in the vorticity transport equation. This approach was demonstrated by Yang (1992) to successfully eliminate the spurious oscillations previously observed, resulting in a more accurate physical solution. Additionally, Blodgett, K. Ghia, Osswald and U. Ghia (1990) successfully obtained results for the high-*Re* flow past an elliptic cylinder using the UDS. Therefore, in the present study, the diffusion terms appearing in the vorticity transport equation are discretized using a second-order accurate central difference scheme (CDS), while, for the convective terms, this CDS is applied only in the low-speed regions of the flow. When the apparent flow velocity is relatively large, a third-order biased UDS is applied.

The set of algebraic equations resulting from the discretization of the vorticity transport equation is solved using the alternating-direction implicit (ADI) technique of Douglas and Gunn (1964). This method possesses the advantage of computational efficiency and facilitates easy extension to the three-dimensional case of a finite Joukowski wing. As noted in Douglas and Gunn (1964), application of the ADI technique requires the solution of two implicit pentadiagonal matrix equations, one corresponding to each directional sweep, which are solved sequentially over the entire flow domain. Following the method of Yang (1992), these matrix equations are solved using the generalized Thomas algorithm. The stability of the ADI method is assured provided that the aforementioned matrices are diagonally dominant. The use of directional switching in the UDS serves to consistently augment the diagonal terms of the matrices, thus increasing the stability envelope of the ADI procedure.

The linearity and constant coefficients of the integral form of the curl equation enable it to be solved directly via the Block Gaussian Elimination (BGE) technique, with the value of the viscous circulation $\Gamma_\infty$ used to determine the far-field stream function $\psi_\infty^D$. The matrix vector equation thus obtained contains the block tridiagonal matrix previously obtained by Osswald et al. (1985), with an extra row and column added to this matrix to accommodate the coupling of the integral form of the curl equation with the viscous circulation. As shown by Beltz (1994), the presence of this extra row and column in the matrix does not significantly alter the BGE solution procedure or its computational efficiency. The interior of the matrix is reduced to upper-diagonal form using the Block Gaussian Elimination (BGE) procedure of Osswald et al. (1985); subsequently, the techniques of this method are used to perform the necessary elimination of the last row and column. Since the matrix consists entirely of constant metric coefficients, it is necessary to perform the BGE procedure only once. A computationally-efficient back-substitution procedure is used to compute $\psi^D$ over the entire flow domain at each level of iteration.

## 5. Results and Discussion

The mathematical formulation and numerical solution procedure presented here is validated using flows past the circular cylinder geometry. This is easily accomplished by eliminating the final Joukowski transformation from the sequence of analytical mappings used in the grid generation procedure, which results in the transformation of the unit square computational domain (Fig. 2(e)) to a C-grid topology in the circular cylinder plane (Fig. 2(b)). This minor modification affects only the analytically-calculated metric terms, and hence does not impact the numerical solution procedure, thus allowing easy extension of the current formulation to study the unsteady viscous flow over a circular cylinder.

As mentioned earlier, the numerical simulation results are validated using the experimental study of Bouard and Coutanceau (1980), which considered the early stages of the wake development behind the cylinder using a flow visualization technique fine enough to allow detailed observation of the flow structures. A subsequent analysis of the photographs obtained was used to provide quantitative measurements of the wake properties, as well as qualitative characteristics regarding the time development of the recirculation region which forms behind the cylinder. Although the geometry is simple, complex phenomena have been found to occur at higher Reynolds numbers.

The present study considers flow past the cylinder at two different Reynolds number, namely, the simple test case of $Re_D = 200$ and also the more complex flow case of $Re_D = 9500$, where $Re_D$ denotes

the Reynolds number based on the cylinder diameter, defined as

$$Re_D = \frac{2a\,U_\infty}{\nu}\,, \tag{14}$$

where $U_\infty$ is the free-stream velocity, $a$ is the radius of the cylinder and $\nu$ is the kinematic free-stream viscosity. Also, the nondimensionalized time based on cylinder diameter $t_D$ is taken as

$$t_D = \frac{t^* U_\infty}{2a}\,. \tag{15}$$

### 5.1 Results of $Re_D$=200 Case

The results of the simple test case of $Re_D = 200$ are presented in detail in Beltz (1994), and hence, only a synopsis of these results is contained here. The grid size considered for the $Re_D = 200$ case is $(97 \times 30)$, corresponding to 97 points in the streamwise direction and 30 points in the normal direction, and a time step of $\Delta t_D = 0.001$ is employed. The use of this relatively coarse grid is consistent with the low Reynolds number of the flow, and the results for this case have shown its ability to yield the desired degree of flow resolution.

Examination of the vorticity and stream function fields for this case revealed the presence of a distinct separation bubble behind the cylinder at $t_D = 0.5$, indicating that flow separation has occurred prior to this time. As time progresses, the vorticity generated at the cylinder surface convects downstream into the wake, inducing a recirculating flow region behind the cylinder which grows steadily with time. This recirculation region consists of a single pair of counter-rotating vortices which remain symmetric and attached to the cylinder through $t_D = 3.0$. At this low Reynolds number, the wake development has been shown to occur without any visible distortion or instability.

The above description of the flow evolution closely matches the qualitative description of the wake development given by Bouard and Coutanceau (1980). A quantitative comparison of (*i*) the nondimensionalized wake length $l_W / D$, (*ii*) the nondimensionalized maximum wake width $w_{max} / D$, and (*iii*) the nondimensionalized streamwise location of the maximum wake width $x_{W_{max}} / D$ was made and compared with the experimental results. These quantities are shown schematically in Fig. 3. A graphical comparison of the computed and experimental measurements of $l_W / D$, $w_{max} / D$, and $x_{W_{max}} / D$ for this case is given in Fig. 4, and these results demonstrate a close agreement with the experimental results of Bouard and Coutanceau (1980). Discrepancies between the numerical and experimental results may be attributed to differences in the numerical and experimental techniques used to pinpoint the location of the stagnation streamline. Specifically, experimental investigations allow this contour value to be determined from the flow visualization and velocity measurements, whereas numerical studies rely upon an interpolation of the stream function values at neighboring grid points. Additionally, Bouard and Coutanceau (1980) acknowledge that, despite the high degree of flow resolution attained in their study, a margin of error as great as 10% may be present in their results for the measured wake properties. Therefore, the disagreements observed between the experimental and numerical measurements is considered to lie well within the realm of the uncertainty associated with these data sets.

### 5.2 Results of $Re_D$=9500 Case

The successful validation of the numerical simulation results for the simple test case of $Re_D = 200$ led to the consideration of the more complex case of $Re_D = 9500$. A grid size of $(705 \times 91)$, corresponding to the higher Reynolds number of the flow, was utilized for this case, and the time step considered was $t_D = 0.0001$. The corresponding grid distribution is shown in Fig. 5, and the time evolution of the vorticity and stream function fields is shown in Fig. 6. While the wake development is similar to the $Re_D = 200$ case in that the flow is mainly characterized by a symmetric pair of counter-rotating vortices which form behind the cylinder, the flow at $Re_D = 9500$ is considerably more complex. As shown in Fig. 6, a secondary phenomenon has clearly emerged prior to $t_D = 1.0$ in the stream function field near the wall at about three-quarters of the distance between the rear stagnation point and the separation point. Initially, this secondary phenomenon consists of an isolated secondary eddy, which has a rotation opposite to that of the main eddy. In the study of Bouard and Coutanceau (1980), the formation of the

secondary eddy is attributed to the separation of the back flow from the cylinder wall, which is a direct result of the high flow velocity. As the secondary eddy develops and grows in size, it touches the boundary of the main recirculating zone and splits into two parts, forming another secondary eddy which is equivalent in size and strength to the first. This description of the flow evolution closely matches the behavior described in the study of Bouard and Coutanceau (1980). A qualitative comparison of the numerical and experimental visualization results, which demonstrates the secondary phenomenon at $t_D = 1.0$ and $t_D = 1.5$, is given in Fig. 7. This comparison clearly demonstrates the ability of the numerical simulation to accurately capture the secondary flow structures observed in the experimental study.

A quantitative comparison of the flow at $Re_D = 9500$ is given in terms of (*i*) the nondimensionalized wake length $l_W / D$ and (*ii*) the nondimensionalized circle plane coordinates of the main eddy core $(a_{core} / D, b_{core} / 2D)$. A comparison of the numerical and experimental values of these quantities given in Tables 1 through 3; the corresponding graphical comparison is given in Fig. 8. As for the $Re_D = 200$ case, discrepancies between the numerical and experimental results may be attributed to differences in the techniques used to pinpoint the location of the stagnation streamline. Note that the discrepancy between the numerical and experimental measurements of $l_W / D$ increases with time, which may be expected due to the increasing complexity of the flow. The numerical measurements of the nondimensionalized $r^1$-coordinate of the main eddy core $a_{core} / D$ are, in general, in very close agreement with the experimental results. Although the agreement is not as close for the nondimensionalized $r^2$-coordinate $b_{core} / 2D$, it should be noted that the trend is somewhat duplicated, as shown in Fig. 8(c). In general, the quantitative agreement between the numerical and experimental measurements of the wake properties is satisfactory; this agreement is largely the result of the accurate resolution of the secondary eddy phenomenon realized in the current study.

### 5.3 Grid Independence Study

The validation study described thus far is not complete without an investigation of the grid independence of the solutions obtained. This section serves to resolve this issue by analyzing the numerical simulation results obtained at $Re_D = 9500$ using three different grids. In this analysis, the $(705 \times 91)$ grid considered in the previous section is taken to be the "medium", or "base", grid. A coarse $(353 \times 46)$ grid is obtained via a 50% reduction of the number of grid points in both the streamwise and normal directions

**Table 1** Comparison of numerical and experimental measurements of $l_W / D$ for $Re_D = 9500$.

| Time | Numerical Result | Experimental Result |
|---|---|---|
| 0.50 | 0.025 | 0.028 |
| 0.75 | 0.061 | 0.069 |
| 1.00 | 0.098 | 0.097 |
| 1.25 | 0.135 | 0.167 |
| 1.50 | 0.232 | 0.250 |
| 1.75 | 0.293 | 0.389 |
| 2.00 | 0.440 | 0.528 |

**Table 2** Comparison of numerical and experimental measurements of $a_{core} / D$ for $Re_D = 9500$.

| Time | Numerical Result | Experimental Result |
|---|---|---|
| 0.75 | -0.082 | -0.094 |
| 1.00 | -0.061 | -0.044 |
| 1.25 | 0.013 | 0.013 |
| 1.50 | 0.071 | 0.069 |
| 1.75 | 0.075 | 0.113 |

**Table 3** Comparison of numerical and experimental measurements of $b_{core} / 2D$ for $Re_D = 9500$.

| Time | Numerical Result | Experimental Result |
|---|---|---|
| 0.75 | 0.348 | 0.350 |
| 1.00 | 0.427 | 0.363 |
| 1.25 | 0.348 | 0.300 |
| 1.50 | 0.285 | 0.289 |
| 1.75 | 0.329 | 0.325 |

of the medium grid; a similar 25% increase of the medium grid is used to obtain a fine $(881 \times 113)$ grid. The results obtained on each of the aforementioned grids are quantitatively examined in terms of the nondimensionalized wake length streamwise and normal directions $l_W / D$. Additionally, some discussion is included regarding the qualitative

differences observed in the flow structures obtained using the different grids.

Before presenting the simulation results, it is necessary to give some information pertaining to the standards used to assert grid independence of the solutions, since a vast number of methods have been developed by researchers in the reporting of grid refinement studies. In the current study, the Grid Convergence Index (*GCI*) of Roache (1993) is used in analyzing the simulation results. This technique was developed to provide a uniform method of reporting of grid refinement studies, thus alleviating the difficulties associated with the varied, and sometimes confusing, methods commonly found in the literature. The use of the *GCI* accomplishes this by relating the degree of error realized in considering a $p$-th order accurate solution method and two different grids of grid-size ratio $r$ to the degree of error which would have been obtained via a grid refinement study of the same problem with the same base grid using $p = 2$ and $r = 2$. Details of the method used to compute the *GCI* for the fine and coarse grids is given in Roache (1993).

**Table 4** Comparison of values of $l_W / D$ for base grid, coarse grid and experiment.

| Time | Base Grid Result | Coarse Grid Result | Experimental Result |
|---|---|---|---|
| 0.50 | 0.025 | 0.015 | 0.028 |
| 0.75 | 0.061 | 0.049 | 0.069 |
| 1.00 | 0.098 | 0.095 | 0.097 |
| 1.25 | 0.135 | 0.129 | 0.167 |
| 1.50 | 0.232 | 0.186 | 0.250 |
| 1.75 | 0.293 | 0.287 | 0.389 |
| 2.00 | 0.440 | 0.438 | 0.528 |

**Table 5** Comparison of values of $l_W / D$ for base gird, fine grid and experiment.

| Time | Base Grid Result | Fine Grid Result | Experimental Result |
|---|---|---|---|
| 0.50 | 0.025 | 0.026 | 0.028 |
| 0.75 | 0.061 | 0.064 | 0.069 |
| 1.00 | 0.098 | 1.000 | 0.097 |
| 1.25 | 0.135 | 0.136 | 0.167 |
| 1.50 | 0.232 | 0.232 | 0.250 |
| 1.75 | 0.293 | 0.293 | 0.389 |
| 2.00 | 0.440 | 0.445 | 0.528 |

Examination of the vorticity and stream function results obtained for the coarse grid clearly showed the inability of this grid to adequately resolve the flow characteristics. This is reflected in the quantitative comparison of the measured values of $l_W / D$ obtained for this case with the base grid and experimental results, given in Table 4. For the fine grid, the flow structures were found to appear very similar to those obtained previously using the medium grid, indicating that the medium grid yields sufficient resolution of the flow structures. A comparison of values of $l_W / D$ obtained for this case with the both the medium grid and experimental results is shown in Table 5, and a very close agreement is shown in the results.

To quantitatively compare the grid independence study results thus obtained, the Grid Convergence Index (*GCI*) is computed for both the coarse and fine grids. These results are shown in Table 6. It is thus shown that the coarse grid yields insufficient resolution of the flow structures and hence does not yield a grid independent result. However, the fine grid *GCI* shows a great improvement and thus demonstrates the grid independence of the results obtained using the base and fine grids. Note that both the fine and coarse grid values of the *GCI* generally show improvement at later times. This may be attributed to the fact that the initial condition is not grid independent, since the calculation of body surface vorticity values at time $t = 0^+$ depends on the distance of the first normal grid point from the body surface.

**Table 6** Comparison of values of $l_W / D$ for base grid, fine grid and experiment.

| Time | Coarse Grid GCI | Fine Grid GCI |
|---|---|---|
| 0.50 | 2.213 | 0.213 |
| 0.75 | 1.002 | 0.267 |
| 1.00 | 0.202 | 0.107 |
| 1.25 | 0.180 | 0.040 |
| 1.50 | 0.741 | 0.000 |
| 1.75 | 0.021 | 0.000 |
| 2.00 | 0.075 | 0.061 |

## 6. CONCLUSIONS AND RECOMMENDATIONS

The self-consistent formulation, using circulation as a means to arrive at the correct far-field boundary condition for the stream function, is presented. The unsteady Navier-Stokes analysis presented for the study of incompressible viscous flows over Joukowski airfoils has been validated utilizing the

circular cylinder geometry, due to the wealth of experimental and numerical data which exists for this flow configuration. Therefore, flow past a circular cylinder was simulated for flow configurations for which Bouard and Coutanceau (1980) have given satisfactory experimental data. A high degree of agreement is found between the numerical simulation results and the experimental results for both the simple test case of $Re_D = 200$ and also for the more complex flow case of $Re_D = 9500$. Thus, the self-consistent formulation utilized here permits an alternative implementation of the far-field boundary condition for the disturbance stream function, while still retaining the original surface boundary condition for the vorticity. Indeed, the results obtained for early time integration show a remarkably high degree of conformity with the experimental data in the resolution of the secondary-eddy phenomenon for this case. Following the method of Yang (1992), the use of upwind-differencing has been successful in averting the difficulties associated with the stability restrictions of the central difference scheme. No spurious oscillations in the vorticity field were observed when necessary grid sizes were used, even for the higher-Re flow case of $Re_D = 9500$.

The new formulation was also implemented in an unsteady analysis for flow past a maneuvering body by Osswald at CFDRL. His observations were that, although the force field results are considerably improved over the existing $(\omega,\psi)$ formulation, the numerical results nevertheless do not conform to the experimental results in the highly nonlinear unsteady flow regime. Further examination of the current formulation suggests that the vorticity boundary condition at the surface may need re-examination. In the meantime, until further improvements in the surface boundary condition are obtained, the successful validation thus realized for the current formulation makes it desirable to extend the present work to study more complex flow cases, including flows over Joukowski airfoils at various angles of attack.

## ACKNOWLEDGMENT

The authors sincerely appreciate the help of Keith E. Blodgett in the preparation of the final manuscript.

## BIBLIOGRAPHY

Beltz, S., (1992), "Simulation of Open System Flows Exhibiting Nonlinear Behavior," presented at the Fluids Engineering Spring Conference, Los Angeles, CA, June 21-26, 1992.

Beltz, S., (1994), "Validation of Unsteady Incompressible Navier-Stokes Analysis for Flows Past Joukowski Airfoils," *Masters Thesis,* University of Cincinnati, Cincinnati, Ohio.

Blodgett, K., (1990), "Unsteady Separated Flow Past and Elliptic Cylinder Using the Two-Dimensional Navier-Stokes Equations,:" *Masters Thesis,* University of Cincinnati, Cincinnati, Ohio.

Blodgett, K.E., Ghia, K.N., Osswald, G.A., and Ghia, U., (1990), "Analysis of Unsteady Separated Flow Past an Elliptic Cylinder," *Bull. Am. Phys. Soc.*, Vol. 35, No. 10, pp. 2244.

Bouard, R. and Coutanceau, M., (1980), "The Early Stage Development of the Wake Behind an Impulsively Started Cylinder for $40 \le Re \le 10^4$," *Journal of Fluid Mechanics*, Vol. 101, pp. 583-607.

Braza, M., Chassaing, P. and Ha Minh, H., (1986), "Numerical Study and Physical Analysis of the Pressure and Velocity Fields in the Near Wake of a Circular Cylinder," *Journal of Fluid Mechanics,* Vol. 165, pp. 79-130.

Collins, W. M. and Dennis, S. C. R., (1973), "The Initial Flow Past an Impulsively Started Circular Cylinder," *Quarterly Journal of Mechanics and Applied Mathematics*," Vol. 26, p. 53.

Douglas, J. and Gunn, J. E., (1964), "A General Formulation of Alternating Direction Methods. Part i - Parabolic and Hyperbolic Problems," *Numerische Mathematik*, Vol. 6, pp. 428-453.

Ghia, K. N., Liu, C. A., Ghia, U. and Osswald, G. A., (1987), "Analysis of Unsteady Wake of a Circular Cylinder Using Navier-Stokes Equations," *Unsteady Flow Separation,* FED Vol. 52, pp. 187-190.

Honji, H. and Taneda, S., (1969), "Unsteady Flow Past a Circular Cylinder," *Journal of Physical Society, Japan,* Vol. 27, p. 1628.

Izumi, K. and Kuwahara, K., (1983), "Unsteady Flow Field, Lift and Drag Measurements of Impulsively Started Elliptic Cylinder and Circular-Arc Airfoil," *AIAA Paper* 83-1711.

Kourta, A., Boisson, H. C., Chassaing, P. and Ha Minh, H., (1987), "Nonlinear Interaction and the Transition to Turbulence in the Wake of a Circular Cylinder," *Journal of Fluid Mechanics*, Vol. 181, pp. 141-161.

Liu, T., (1987), "Study of Two-Dimensional Viscous Flow Past a Circular Cylinder Using Unsteady Navier-Stokes Equations", *Masters Thesis*, University of Cincinnati, Cincinnati, Ohio.

Marris, A. W., (1964), "A Review on Vortex Streets, Periodic Wakes, and Induced Vibration Phenomena," *Transactions of the ASME, Journal of Basic Engineering*, pp. 185-196.

Morkovin, M. V., (1964), "Flow Around a Circular Cylinder - A Kaleidoscope of Challenging Fluid Phenomena," In *ASME Symposium on Fully Separated Flows*, pp. 102-118.

Osswald, G. A., (1983), "A Direct Numerical Method for the Solution of Unsteady Navier-Stokes Equations in Generalized Orthogonal Coordinates", *PhD Thesis*, University of Cincinnati, Cincinnati, Ohio.

Osswald, G. A., Ghia, K. N. and Ghia, U., (1987), "A Direct Algorithm for Solution of Incompressible Three-Dimensional Unsteady Navier-Stokes Equations," *AIAA CP* 874, pp. 408-421.

Osswald, G. A., Ghia, K. N. and Ghia, U., (1985), "A Clustered Conformal Grid Generation Technique for Symmetric Joukowski Airfoils at Arbitrary Angle of Attack," *AFL Report* 85-1-69, University of Cincinnati, Cincinnati, Ohio.

Osswald, G. A., Ghia, K. N. and Ghia, U., (1985), "An Implicit Time-Marching Method for Studying Unsteady Flow With Massive Separation," *AIAA CP*-854.

Panikker, P. K. G. and Lavan, Z., (1975), "Flow Past Impulsively Started Bodies Using Green's Functions," *Journal of Computational Physics*, Vol. 18, p. 46.

Roache, P. J., "A Method for Uniform Reporting of Grid Refinement Studies," presented at *Symposium on Quantification of Uncertainty in Computational Fluid Dynamics*, ASME Fluids Engineering Summer Meeting, Washington, DC, June 20-24, 1993.

Rohling, T., (1991), "Simulation of Chaotic Flows Past Airfoils at High Incidence Using the Unsteady Navier-Stokes Equations," *Masters Thesis*, University of Cincinnati, Cincinnati, Ohio.

Taneda, S., (1972), "Visualization Experiments on Unsteady Viscous Flows Around Cylinders and Plates," In *Recentes recherches sur les couches limetes instationnaires*, Vol. 2, Editor: E. A. Eichelbrenner, Laval University Press, Quebec, p. 1165.

Thoman, D. C. and Szewczyk, A. A., (1969), "Time-Dependent Viscous Flow Over a Circular Cylinder," *In Physics of Fluids Suppl.*, Vol. 12 (II), p. 76.

Yang, J., (1992), "Study of Dynamic Stall Phenomenon and its Control Using Vorticity, Stream Function and Circulation Form of the Unsteady Navier-Stokes Equations," *PhD Thesis*, University of Cincinnati, Cincinnati, Ohio.

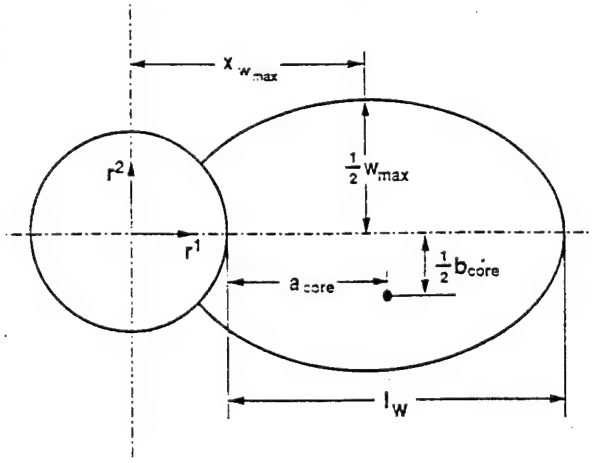


**Figure 3.** Schematic representation of measured wake properties.

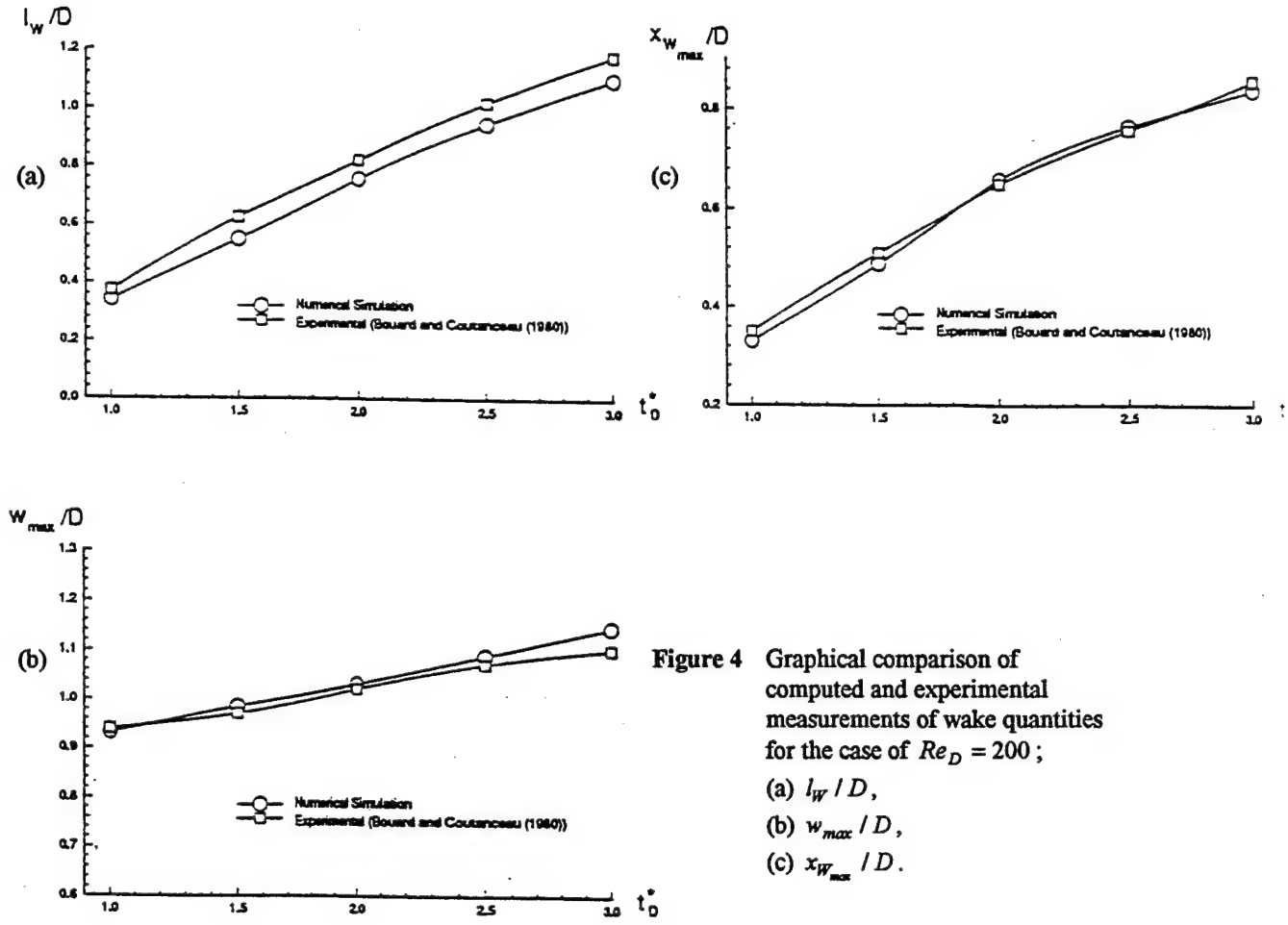


**Figure 4** Graphical comparison of computed and experimental measurements of wake quantities for the case of $Re_D = 200$;
(a) $l_W / D$,
(b) $w_{max} / D$,
(c) $x_{W_{max}} / D$.

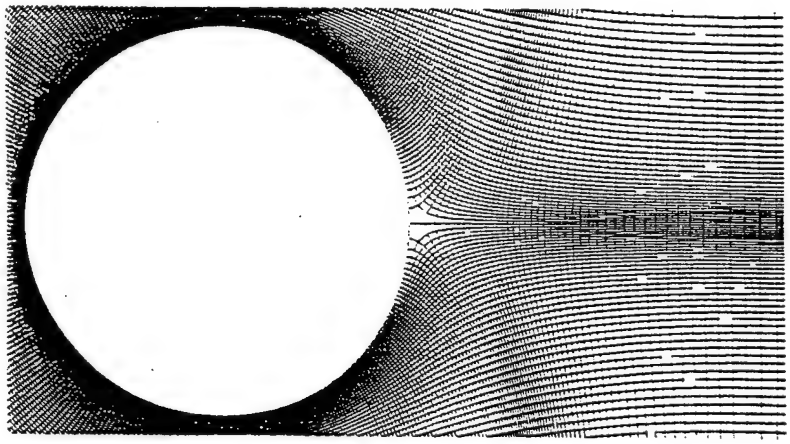

**Figure 5** Grid distribution for the case of $Re_D = 9500$.

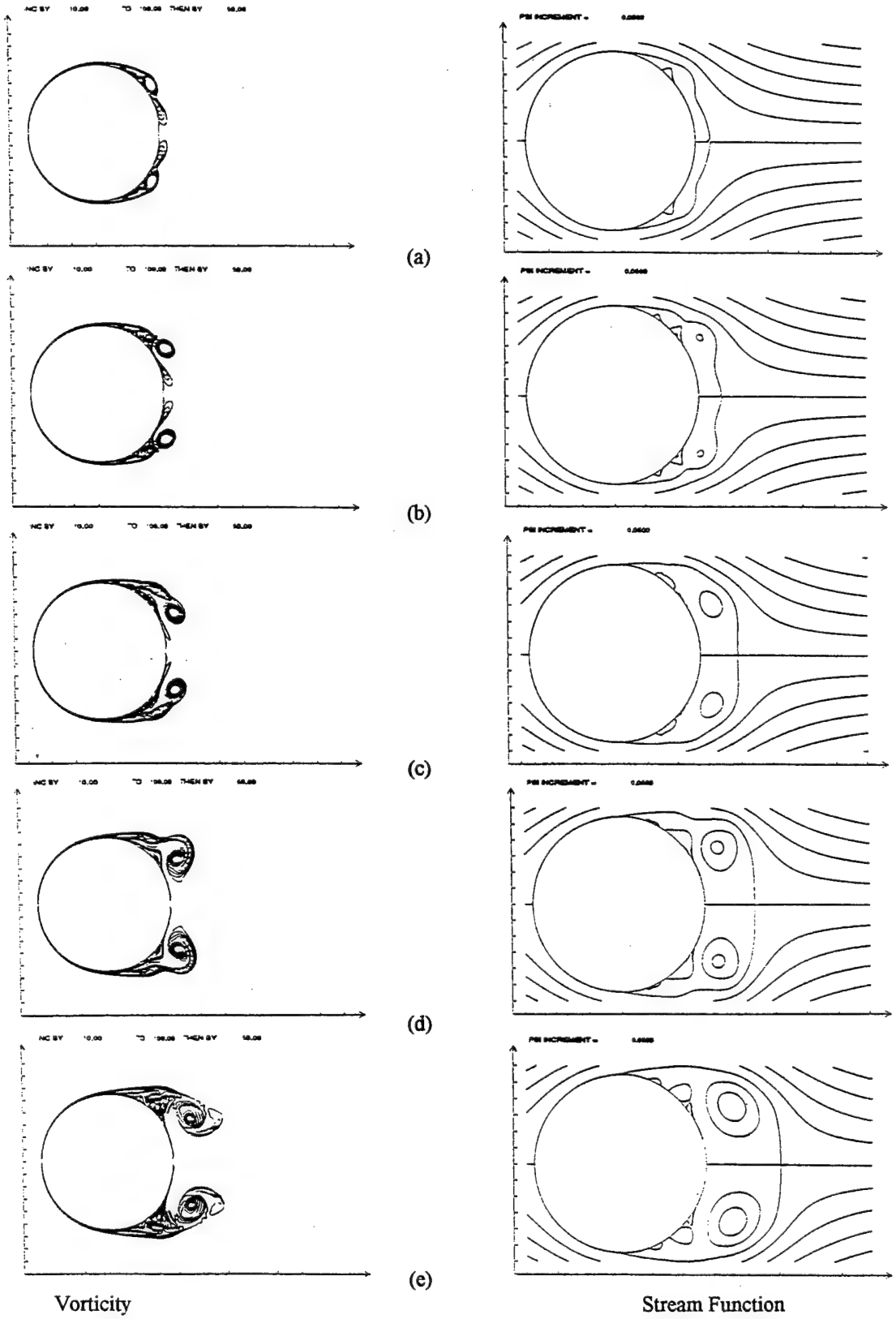


**Figure 6** Vorticity and stream function fields for the case of $Re_D = 9500$; (a) $t_D = 1.0$, (b) $t_D = 1.25$, (c) $t_D = 1.5$, (d) $t_D = 1.75$, and (e) $t_D = 2.0$.

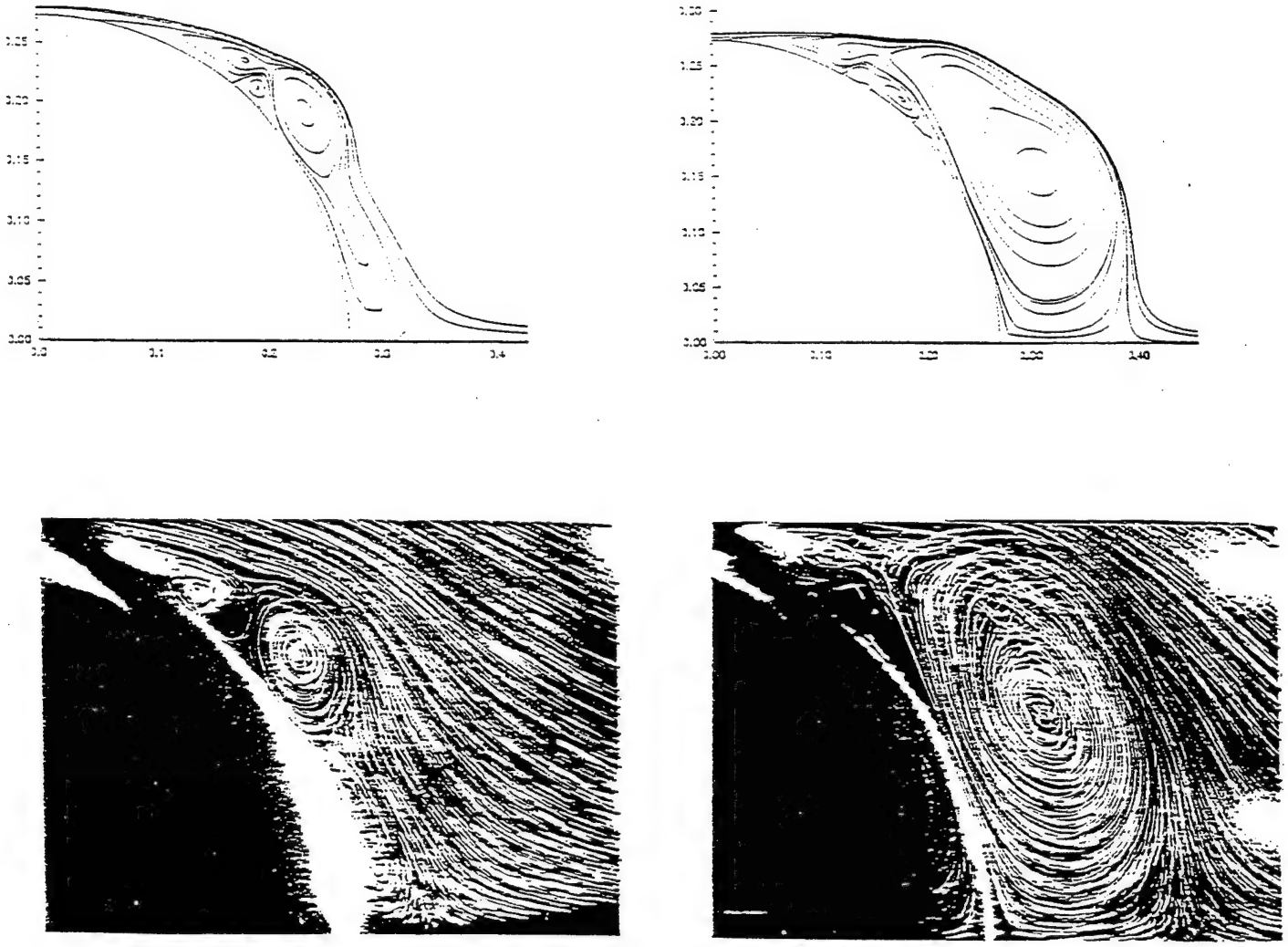

(a) (b)

**Figure 7** Comparison of experimental and numerical flow visualization results; (a) $t_D = 1.0$, and (b) $t_D = 1.5$.

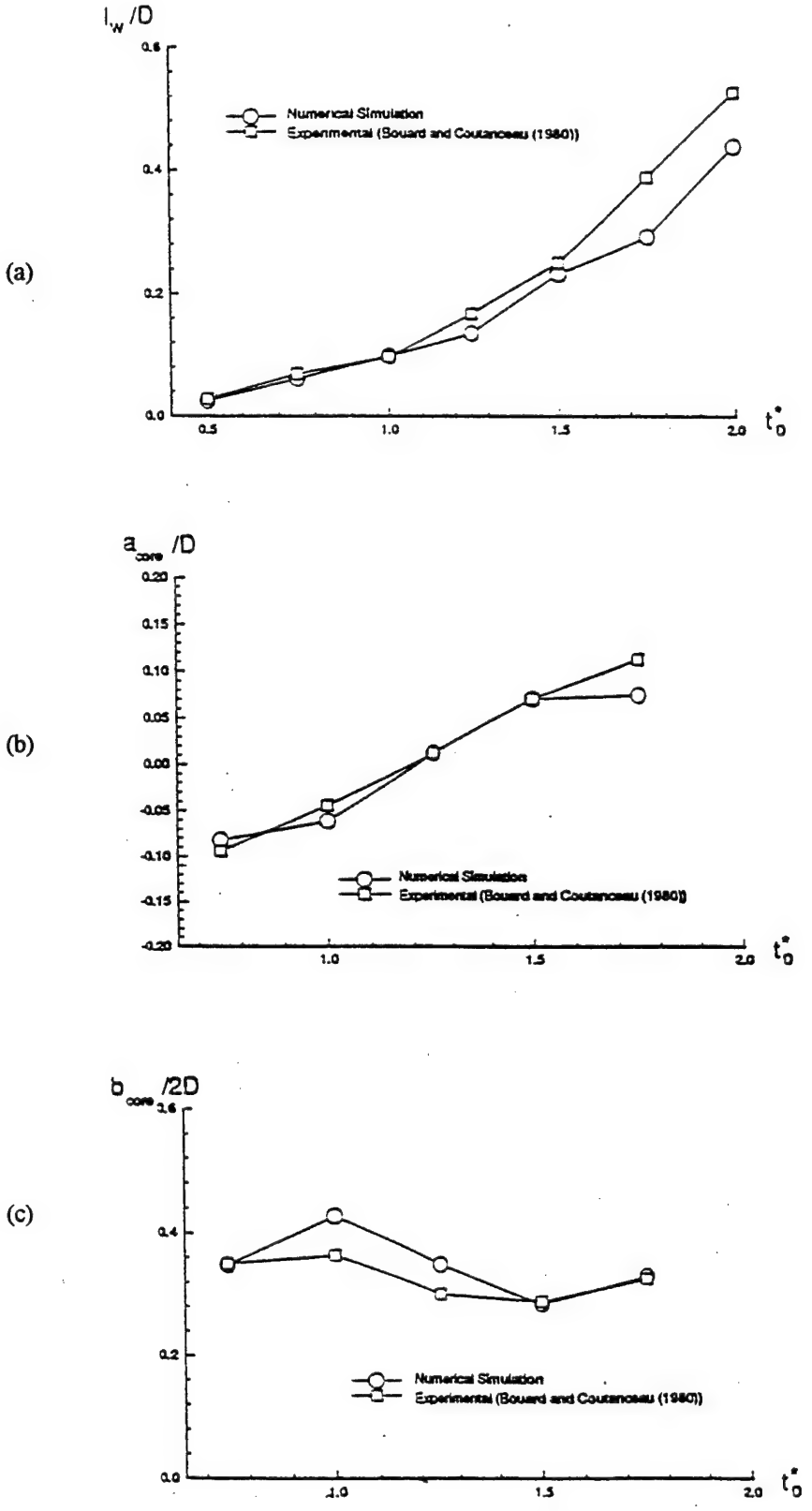


**Figure 8** Graphical comparison of computed and experimental measurements of wake quantities for the case of $Re_D = 9500$; (a) $l_W / D$, (b) $a_{core} / D$, and (c) $b_{core} / 2D$.

APPENDIX B1

AIAA 94-0063

# Towards Simulation of Leading-Edge Receptivity Using A Spectral Multidomain Method in Generalized Curvilinear Coordinates

K. Blodgett and K.N. Ghia,
University of Cincinnati,
Cincinnati, OH,
and C.L. Streett,
NASA Langley Research Center,
Hampton, VA

**32nd Aerospace Sciences Meeting & Exhibit**
January 10-13, 1994 / Reno, NV

# Towards Simulation of Leading-Edge Receptivity Using A Spectral Multidomain Method in Generalized Curvilinear Coordinates*

Keith Blodgett† and K.N. Ghia‡
*Computational Fluid Dynamics Research Lab,*
*University of Cincinnati, Cincinnati, OH 45221-0070*
and
Craig L. Streett§
*NASA Langley Research Center, Hampton, VA 23665*

## Abstract

A 2-D unsteady analysis is developed using the Navier-Stokes equations in generalized coordinates. The use of generalized curvilinear coordinates permits flexibility in geometry. A spectral method is employed to achieve the desired higher-order accuracy. Further, the utilization of the multidomain technique facilitates the resolution of the disparate length scales associated with Navier-Stokes solutions. The analysis is validated for a model geometry and base flow results are obtained for the parabolic cylinder geometry. The ultimate goal of this work is to investigate the leading-edge receptivity to free-stream acoustic disturbances on a parabolic cylinder.

## 1 Introduction

Transition to turbulence plays a critical role in many engineering problems ranging from heat transfer to drag reduction on such applications as the National Aerospace Plane and the High-Speed Civil Transport (HSCT) vehicle. Drag-reduction technologies are especially important, considering the saving that can be obtained for the commercial airline industry by achieving laminar flow on some or all exterior surfaces through Laminar Flow Control (LFC) [1]. LFC seeks to delay/eliminate transition by attenuating the growth of instability modes. Additionally, in conjunction with wave- and vortex-drag reduction techniques, LFC can radically alter both the economic and ecological viability issues associated with the HSCT [2].

Receptivity, the earliest stage of transition to turbulence, is the process by which free-stream disturbances get internalized inside of a boundary layer in the form of instability waves, e.g., Tollmien-Schlichting waves. Receptivity complements linear stability theory in that it provides what has been lacking from the theory, mainly the initial amplitude of the instability wave. The initial amplitude would make the results obtained from empirical methods such as the $e^N$ method of Smith and Gamberoni [3] and Van Ingen [4] more reliable. Currently, receptivity is the least understood phase of the transition process. Of primary concern is how the long-wavelength disturbance wave is able to transfer energy to the much shorter-wavelength instability wave. The high-Reynolds number asymptotic studies of Goldstein [5, 6] and Kerschen [7] indicate that rapid adjustments in the streamwise direction of the mean flow provide a wavelength conversion mechanism. A region where such streamwise adjustments occur is the leading-edge region, where the boundary layer grows rapidly.

Theory and experiments have revealed three possible mechanisms for the problem of leading-edge receptivity in the absence of roughness. In the first, Goldstein's leading-edge receptivity mechanism [5], the wavelength is shortened by the nonparallel effects of the rapidly growing boundary layer. Goldstein [5] developed this theory by examining the receptivity of an infinitely-thin flat plate to a plane acoustic wave. Heinrich et al. [8] later refined this analysis to include oblique acoustic waves and convected gusts. It was found that oblique acoustic waves provide a much higher receptivity level

*This Research is Supported, in part, by NASA Grant No. NGT-50416, AFOSR Research Grant No. F-49620-92-J-0292, and Ohio Supercomputer Center Grant No. PES070.

†Graduate Research Asst., Student member AIAA.

‡Professor, Associate Fellow AIAA.

§Senior Research Scientist, Member AIAA.

than the plane acoustic wave, due to an unsteady flow around the leading-edge. In both theories, substantial decay of the instability waves occurs prior to their reaching the neutral stability point where they could begin to grow. The infinitely-thin flat plate might be the only model suitable for isolating this non-parallel receptivity mechanism, thus possibly excluding experimental investigation of this receptivity mechanism. The numerical studies of Murdock [9] and Gatski and Grosch [10] on the infinitely-thin flat plate have been inconclusive due to the exclusion of the leading-edge region (Murdock) and the receptivity results being preliminary in nature (Gatski), i.e., early-time results. Irregardless, this non-parallel boundary-layer receptivity mechanism can be considered of higher order as compared to the other two mechanisms described in the following paragraphs.

The second receptivity mechanism, also formulated by Goldstein [6], corresponds to the scattering of the disturbance's long wavelength on some short-scale streamwise variation. With respect to the leading-edge receptivity problem, the surface variation could occur in the form of a surface curvature discontinuity somewhere in the leading-edge geometry. Strong evidence of this receptivity mechanism is provided by the experiments of Wlezien et al. [11–13] and the computations of Reed et al. [14, 15] on a semi-infinite flat plate with an elliptical leading edge.

The third and final leading-edge receptivity mechanism present is given by Nishioka and Morkovin [16] and relies on the pressure gradient field to provide the needed wavelength conversion mechanism. In essence, this mechanism operates in a manner similar to that of the surface-variation receptivity mechanism, with the important distinction that the short-scale streamwise variations are provided by the pressure field rather than by the surface. This receptivity mechanism should be active to some degree for all blunt-body geometries. Evidence of this mechanism in leading-edge geometries is provided by the numerical results of Reed et al. [14, 15] and Buter et al. [17, 18] for vortical disturbances.

Lastly, it should be noted that the inherent favorable or adverse pressure gradients associated with the leading-edge receptivity problem also lead to a retardation or acceleration, respectively, of the entire transition process by shifting the neutral stability curve towards or away from the leading edge, respectively.

In the present study, the analysis and numerical procedure are developed for studying the leading-edge receptivity on a parabolic cylinder. The analysis is validated using the shear-driven cavity geometry. Subsequently, it is extended to the parabolic cylinder, and steady-state base flows are obtained and compared with the work of Davis [19]. In addition, the resolution requirements for the receptivity problem are examined.

# 2 Mathematical Formulation

The flow past a semi-infinite parabolic cylinder is simulated by employing the 2-D, unsteady vorticity/stream function $(\omega, \psi)$ form of the Navier-Stokes equations in generalized curvilinear coordinates:

**Vorticity Transport Equation:**

$$\sqrt{g}\frac{\partial \omega}{\partial t} + \frac{\partial}{\partial \xi^1}\left(\omega\frac{\partial \psi}{\partial \xi^2}\right) - \frac{\partial}{\partial \xi^2}\left(\omega\frac{\partial \psi}{\partial \xi^1}\right) = \frac{1}{Re}\left\{\frac{\partial}{\partial \xi^1}\left(\frac{g_{22}}{\sqrt{g}}\frac{\partial \omega}{\partial \xi^1}\right) + \frac{\partial}{\partial \xi^2}\left(\frac{g_{11}}{\sqrt{g}}\frac{\partial \omega}{\partial \xi^2}\right)\right\} \qquad (1)$$

**Stream Function Equation:**

$$\frac{\partial}{\partial \xi^1}\left(\frac{g_{22}}{\sqrt{g}}\frac{\partial \psi_v}{\partial \xi^1}\right) + \frac{\partial}{\partial \xi^2}\left(\frac{g_{11}}{\sqrt{g}}\frac{\partial \psi_v}{\partial \xi^2}\right) = -\sqrt{g}\,\omega\,, \qquad (2)$$

where $\psi$ is the total stream function and $\psi_v$ is the viscous deviation from the inviscid stream function, $\psi_{inv}$, i.e., $\psi = \psi_{inv} + \psi_v$. The viscous deviational stream function has been introduced to alleviate the unboundedness of $\psi$ by analytically containing it in $\psi_{inv}$. In addition, $(\xi^1, \xi^2)$ are the generalized orthogonal curvilinear coordinates, with metrics, $\sqrt{g}$, $g_{11}$, $g_{22}$, determined by the transformation between the physical coordinates and the generalized coordinates. The equations have been nondimensionalized using the kinematic viscosity, $\nu$, the free-stream velocity, $U_\infty$, and the frequency of the free-stream disturbance, $\Omega$, to produce the Reynolds number $Re = \frac{U_\infty^2}{\nu\Omega}$. This nondimensionalization is consistent with that used by Goldstein [5, 6].

## 2.1 Boundary Conditions

The appropriate boundary conditions consist of the no-slip and no-penetration conditions on the body surface, free-stream conditions in the far-field, symmetry conditions along the stagnation line, and outflow conditions corresponding to the Blasius boundary-layer solution at downstream infinity. Mathematically, the boundary conditions can be stated as follows

$$\omega = \psi_v = 0 \quad \text{along symmetry line,}$$
$$\omega = \frac{\partial \psi_v}{\partial \xi^2} = 0 \quad \text{at far-field infinity,}$$

$$\psi_v = \frac{\partial \psi}{\partial \xi^2} = 0 \quad \text{on the body surface.} \tag{3}$$

## 2.2 Solution Procedure

The overall solution procedure is subdivided into two phases: the determination of the base flow and the simulation of its receptivity. For the base flow, the work of Davis [19] has served as a guide. The domain of interest was reduced by exploiting the symmetry of the flow about the stagnation line. Davis' nondimesionalization was also adopted for this phase of the analysis. The Reynolds number, $Re_r = \frac{U_\infty r_n}{\nu}$, is based on the nose radius $r_n$, and the independent spatial coordinates are scaled according to $Re_r$. In addition, the similarity variables introduced by Davis were utilized to aid in the application of the outflow boundary conditions. Specifically, the similarity variables were used in the farthest downstream domain to allow the Blasius solution to be applied accurately. The similarity variables were not used in the domain around the leading edge as the similarity-variable form of the governing equations contain terms which are singular at the stagnation line. Spectral methods are notorious for being sensitive to singularities and this singularity was no exception. Since a steady-state base solution is desired, a fictitious time-derivative was added to Eq. (2) to accelerate the convergence to the steady-state solution.

For the receptivity simulation, the base flow is renondimensionalized to be consistent with Eqs. (1–2). The plane acoustic wave is simulated by pulsating the free-stream flow, i.e.,

$$U_\infty(t) = 1 + \epsilon \sin t\,, \tag{4}$$

where $\epsilon$ is a small quantity.

# 3 Numerical Method

The algebraic equations are obtained by discretizing spectrally in space and using a finite-difference approximation in time [20]. A spectral collocation method has been chosen over other numerical differencing schemes due to its high accuracy and negligible phase errors. Both of these characteristics will be needed to simulate the small amplitude waves. The dependent variables are expanded using Chebyshev polynomials in both space dimensions, and the governing equations are enforced at the Gauss-Lobatto collocation points. All diffusive terms are treated implicitly using a Crank-Nicolson scheme, while the nonlinear convective terms are advanced using a second-order Adams-Bashforth scheme.

The resulting set of semi-implicit algebraic equations is solved iteratively at each time step using a Preconditioned Truncated Conjugate Residual (PTCR) method [21]. Finite-difference and finite-element preconditioners are employed for the time-dependent and time-independent equations, respectively. The finite-difference preconditioners are inverted by an Alternating-Direction Implicit method, while the finite-element preconditioner uses an efficient block gaussian elimination scheme.

Since spectral methods are extremely sensitive to the boundary conditions used, care has been exercized in the implementation of the boundary conditions so as to not degrade the accuracy of the method. Particular attention has been paid to the no-slip condition which was implemented via an integral constraint condition [22].

In addition, the spectral method is supplemented by a patched multidomain technique which ensures $C^1$-continuity on the interface. Unfortunately, the better global-integral-flux interface conditions of Macaraeg et al. [23] could not be used due to the similarity-variable form of the equations employed in the last subdomain. The interface conditions and the surface boundary conditions have been implemented using the influence-coefficient-matrix technique [23]. Three subdomains were employed in the streamwise direction. The first two allow adequate resolution of the region of interest, while the remaining domain served as a buffer domain for the receptivity calculations.

The grid is generated using parabolic coordinates in conjunction with 1-D clustering transformations. The clustering transformations, along with the multiple domains, allow the disparate length scales of the Navier-Stokes solutions to be resolved. For the parabolic cylinder, the use of multiple domains in the streamwise direction also facilitates the implementation of the buffer domain technique [24] in which the small disturbances are passed out of the buffer domain without reflection. This takes the place of the outflow boundary condition for the case in which the acoustic disturbance has been introduced. The far-field boundary is located at a large, but finite normal distance from the body surface. Care has been exercized to ensure that this location is sufficiently far away so as to not influence the solution. In the streamwise direction, the grid generation has employed the logarithmic stretching, used by Davis [19], in the last domain to stretch to downstream infinity. This allows for the accurate implementation of the Blasius solution as the outflow boundary condition for the base flow. The spectral method experienced no adverse effects since the similarity variables were used in this last domain. In addition, the parameters of the normal

stretching transformation were set such that half of the total number of grid points in the normal direction lay within the boundary layer.

# 4 Results

The overall analysis and the numerical technique developed were first validated using the results obtained for a shear-driven square cavity for various Reynolds numbers and compared successfully with the available benchmark solutions of Ghia et al. [25] and Nishida et al. [26]. Table 1 shows a comparison of the primary vortex properties for $Re = 100$ as obtained by the present method for various discretizations with both Ghia et al.'s [25] 2nd-order accurate results and Nishida et al.'s [26] 10th-order accurate results on $129 \times 129$ grids. The results for the present method have been obtained on three grid discretizations using both Chebyshev and Legendre polynomials as expansion bases. Excellent agreement is achieved despite the coarse discretization used in the present method. Figure 1 depicts some typical plots of the grid, stream function, vorticity, and vorticity for $Re = 100$.

Subsequently, results are obtained for flow past a parabolic cylinder.

## 4.1 Base Flow

Computations on a single domain were performed to ascertain the effects of the placement of the normal far-field boundary on the solution, as well as determine the grid size necessary for accurate resolution of the problem. It was found that the placement of the far-field boundary had little effect on the solution for a range of values of the distance of this boundary from the body surface. In addition, essentially similar results are obtained with discretizations as small as $17 \times 25$ points.

Figure 2 depicts the wall vorticity function for various Reynolds numbers for the three-domain configuration. The results were obtained using a total of 53 points in the streamwise direction for all three domains and 33 points in the normal direction. There is no discernable indication in the solution as to the presence of the interfaces between the domains. The results shown in Fig. 2 conform to those obtained by Davis [19] which are reproduced here in Fig. 3 (The reader is asked to ignore the symbols which correspond to the parabolized Navier-Stokes solutions). Davis used a finite-difference method with a $40 \times 125$ grid. In each of the present calculations, the interface between the last two domains lies in the region where the wall vorticity function has essentially attained the Blasius value (See Fig. 2). This is so that, in the receptivity calculations, the instability wave will have a chance to grow, i.e., the flow will pass branch I of the linear stability curve prior to entering the buffer domain.

To show that the flow variables are continuous across the multidomain interfaces, Fig. 4 depicts the computational plane for the three-domain configuration, along with the contours of the similarity viscous-deviational stream function, similarity vorticity and physical vorticity for $Re_r = 100$. As can be clearly seen, there is no discontinuity in the flow variables across the interfaces, despite the discontinuity in grid metrics. Figure 5 shows some physical-plane results for $Re_r = 100$; the contours here are of the total stream function and vorticity. The extent of the physical domain shown in this figure is contained solely in the first subdomain.

## 4.2 Receptivity Requirements

Before embarking on the simulation of the receptivity, it is prudent to examine what has been done previously and what the grid requirements will be for accurately resolving the Tollmien-Schlichting wavelength.

Murdock [27] first examined this geometry's response to free-stream acoustic disturbances using the Parabolized Navier-Stokes equations. His results indicated a declining receptivity level with increasing nose radius. Unfortunately, he had difficulties with his downstream boundary condition [28]. More recently, Kerschen and co-workers [28, 29] and Gatski and Kerschen [30] have collaborated to study this geometry using theoretical and computational tools, respectively. The theoretical work of Hammerton et al. [29], based on a matched-asymptotic expansion analysis, has also indicated that the effect of nose bluntness is to decrease the receptivity. They introduced a Strouhal number, $S = \frac{\Omega r_{\blacktriangle}}{U_\infty} = \frac{Re_r}{Re}$, which is a measure of the nose bluntness. The receptivity was found to decrease by an order of magnitude when $S$ increased to a value of 0.3. Gatski et al. [30] presented some preliminary results for one receptivity case. His disturbance quantities compare qualitatively with the Stokes-shear-wave response to acoustic forcing.

As a further validation of the present method, it is planned to simulate the same receptivity case that Gatski et al. [30] examined. The parameters for this case are as follows: $Re = 10^4$ and $Re_r = 10$. The nose radius for this case is smaller than the Tollmien-Schlichting wavelength and the favourable pressure gradient is not as strong as for larger nose radii. Therefore, based on

the theory [29], the receptivity can be expected to be nearly optimal for the configuration. The Tollmien-Schlichting wavelength in the current nondimensionalization will be approximately 2 [30]. Spectral methods need at least three points per wavelength, thus requiring approximately 100 points or more in the streamwise direction distributed in the first two subdomains.

Of the three basic receptivity mechanisms discussed in the introduction, only Goldstein's [5] leading-edge and Nishioka et al.'s [16] receptivity mechanisms can be considered active for the parabolic cylinder receptivity problem since the parabolic cylinder geometry is free of surface variation discontinuities. In addition, the nose bluntness produces a favourable pressure gradient over a portion of the nose region, further retarding the receptivity process. Hence, any receptivity can be expected to be small compared to that of other receptivity mechanisms. This places a severe strain on any numerical method used to simulate this receptivity problem. These results are presently being generated.

# 5 Conclusion

An analysis and a spectral multidomain method are developed for examining receptivity problems. The analysis and method are validated using a model geometry, and thereafter, extended to the parabolic cylinder geometry. Steady-state base flows are obtained and conform to previous numerical results. Lastly, the requirements for simulating receptivity to plane acoustic waves are examined.

# Acknowledgement

K.B. and K.G. would like to thank Professors Urmila Ghia and Gary Osswald for many technical discussions during the course of this study. K.B. would also like to thank Brad Brandes-Duncan, a fellow graduate student, for many mutually benefitial technical discussions during this study and for his time and help in the preparation of the paper.

# References

[1] Hefner, J.N., "Dragging Down Fuel Costs," *Aerospace America*, 26(1), pp. 14–16, (1988).

[2] Bushnell, D.M., "Aircraft Drag Reduction," AGARD-R-786, *Special Course on Skin Friction Drag Reduction*, NATO, (1992).

[3] Smith, A.M.O. and Gamberoni, N., "Transition, Pressure Gradient, and Stability Theory," *Proceesings of the International Congress on Applied Mechanics*, 234, Brussells, (1956).

[4] Van Ingen, J.L., "A Suggested Semi-Empirical Method for the Calculation of the Boundary-Layer Transition Region," Report UTHL–74, University of Technology, Delft Holland, (1956).

[5] Goldstein, M.E., "The Evolution of Tollmien-Schlichting Waves Near a Leading Edge," *Journal of Fluid Mechanics*, **127**, pp. 59–81, (1983).

[6] Goldstein, M.E., "Scattering of Acoustic Waves into Tollmien-Schlichting Waves by Small Streamwise Variations in Surface Geometry," *Journal of Fluid Mechanics*, **154**, pp. 509–529, (1983).

[7] Kerschen, E., "Boundary Layer Receptivity," AIAA paper 89–1109, (1989).

[8] Heinrich, R.A., Choudhari, M. and Kerschen, E., "A Comparison of Boundary Layer Receptivity Mechanisms," AIAA paper 88–3758, (1988).

[9] Murdock, J.W., "The Generation of a Tollmien Schlichting Wave by a Sound Wave," *Proceedings of the Royal Society of London A*, **372**, pp. 517–534, (1980).

[10] Gatski, T.B. and Grosch, C.E., "Numerical Experiments on Boundary Layer Receptivity," *Stability of Time Dependent and Spatially Varying Flows*, Springer-Verlag, pp. 82–96, (1987).

[11] Wlezien, R.W., "Measurement of Boundary Layer Receptivity at Suction Surfaces," AIAA paper 89–1006, (1989).

[12] Wlezien, R.W., Parekh, D.E. and Island, T.C., "Measurement of Acoustic Receptivity at Leading Edges and Porous Strips," *Applied Mechanics Review*, **43**(5), pp. S167–S174, (1990).

[13] Parekh, D.E., Pulvin, P. and Wlezien, R.W., "Boundary Layer Receptivity to Convected Gusts and Sound," *FED–Vol. 114, Boundary Layer Stability and Transition to Turbulence*, Reda, D.C., Reed, H.L. and Kobayashi, R., Eds., ASME, pp. 69–75, (1991).

[14] Reed, H.L., Lin, N. and Saric, W.S., "Boundary Layer Receptivity to Sound: Navier-Stokes Computations," *Applied Mechanics Review*, **43**(5), pp. S175–S180, (1990).

[15] Lin, N., Reed, H.L. and Saric, W.S., "Effect of Leading-Edge Geometry on Boundary-Layer Receptivity to Freestream Sound," **Instability, Transition, and Turbulence**, Hussaini, M.Y., Kumar, A. and Streett, C.L., Eds., Springer-Verlag, pp. 421–440, (1992).

[16] Nishioka, M. and Morkovin, M.V., "Boundary-Layer Receptivity to Unsteady Pressure Gradients: Experiments and Overview," *Journal of Fluid Mechanics*, **171**, pp. 219–261, (1986).

[17] Buter, T.A. and Reed, H.L., "Leading-Edge Receptivity to a Vortical Freestream Disturbance: A Numerical Analysis," **Instability, Transition, and Turbulence**, Hussaini, M.Y., Kumar, A. and Streett, C.L., Eds., Springer-Verlag, pp. 452–469, (1992).

[18] Buter, T.A. and Reed, H.L., "Numerical Investigation of Receptivity to Freestream Vorticty," AIAA paper 93–0073, (1993).

[19] Davis, R.T., "Numerical Solution of the Navier-Stokes Equations for Symmetric Laminar Incompressible Flow Past a Parabola," *Journal of Fluid Mechanics*, **51**, pp. 417–433, (1972).

[20] Canuto, C., Hussaini, M.Y., Quarteroni, A., and Zang, T.A., *Spectral Methods in Fluid Mechanics*, Springer-Verlag, New York, (1987).

[21] Wong, Y.S., Zang, T.A., and Hussaini, M.Y., "Preconditioned Conjugate Residual Methods for the Solution of Spectral Equations," *Computers in Fluids*, **14**(2), pp. 85–95, (1986).

[22] Dennis, S.C.R. and Quartapelle, L., "Some Uses of Green's Theorem in Solving the Navier-Stokes Equations," *International Journal for Numerical Methods in Fluids*, **9**, pp. 871–890, (1989).

[23] Macaraeg, M.G. and Streett, C.L., "Improvements in Spectral Collocation Discretizations Through a Multiple Domain Technique," *Applied Numerical Mathematics*, **2**, pp. 95–108, (1986).

[24] Danabasoglu, D., Biringen, S., and Streett, C.L., "Spatial Simulation of Instability Control by Periodic Suction Blowing," *Physics of Fluids A*, **3**, pp. 2138–2147, (1991).

[25] Ghia, U., Ghia, K.N., and Shin, C., "High-Re Solutions for Incompressible Flow Using the Navier-Stokes Equations and a Multigrid Method," *Journal of Computational Physics*, **48**, pp. 397–411, (1982).

[26] Nishida, H. and Satofuka, N., "Higher-Order Solutions of Square Driven Cavity Flow Using a Variable-Order Multi-Grid Method," *International Journal for Numerical Methods in Engineering*, **34**, pp. 637–653, (1991).

[27] Murdock, J.W., "Tollmein-Schlichting Waves Generated by Unsteady Flow Over Parabolic Cylinders", AIAA paper 81–0199, (1981).

[28] Kerschen, E., "Leading-Edge Receptivity for Blunt-Nose Bodies, Annual Progress Report," *NASA CR*–188063, (1991).

[29] Hammerton P.W. and Kerschen E.J., "Effect of Nose Bluntness on Leading-Edge Receptivity," **Instability, Transition, and Turbulence**, Hussaini, M.Y., Kumar, A. and Streett, C.L., Eds., Springer-Verlag, pp. 441–451, (1992).

[30] Gatski, T.B. and Kerschen, E.J., "Leading Edge Effects on Boundary Layer Receptivity," *Twelfth International Conference on Numerical Methods in Fluid Dynamics*, Morton, K.W., Ed., Springer-Verlag, pp. 157–161, (1990).

| Primary Vortex, $Re = 100$<br>Location $(x, y) = (0.6172, 0.7344)$ | | | |
|---|---|---|---|
| | $\psi_{vc}$ | $\omega_{vc}$ | Grid Points |
| Ghia et al. | -0.103423 | -3.16646 | $129 \times 129$ |
| Nishida et al. (10th) | -0.103512 | -3.168725 | $129 \times 129$ |
| Chebyshev Spectral | -0.103531 | -3.245310 | $17 \times 17$ |
| Chebyshev Spectral | -0.103511 | -3.145170 | $21 \times 21$ |
| Chebyshev Spectral | -0.103510 | -3.115730 | $25 \times 25$ |
| Legendre Spectral | -0.103544 | -3.191216 | $17 \times 17$ |
| Legendre Spectral | -0.103514 | -3.162267 | $21 \times 21$ |
| Legendre Spectral | -0.103511 | -3.163334 | $25 \times 25$ |

Table 1: Comparison of Primary Vortex Properties obtained form Present Spectral Method and previous Finite-Difference Methods; $Re = 100$.

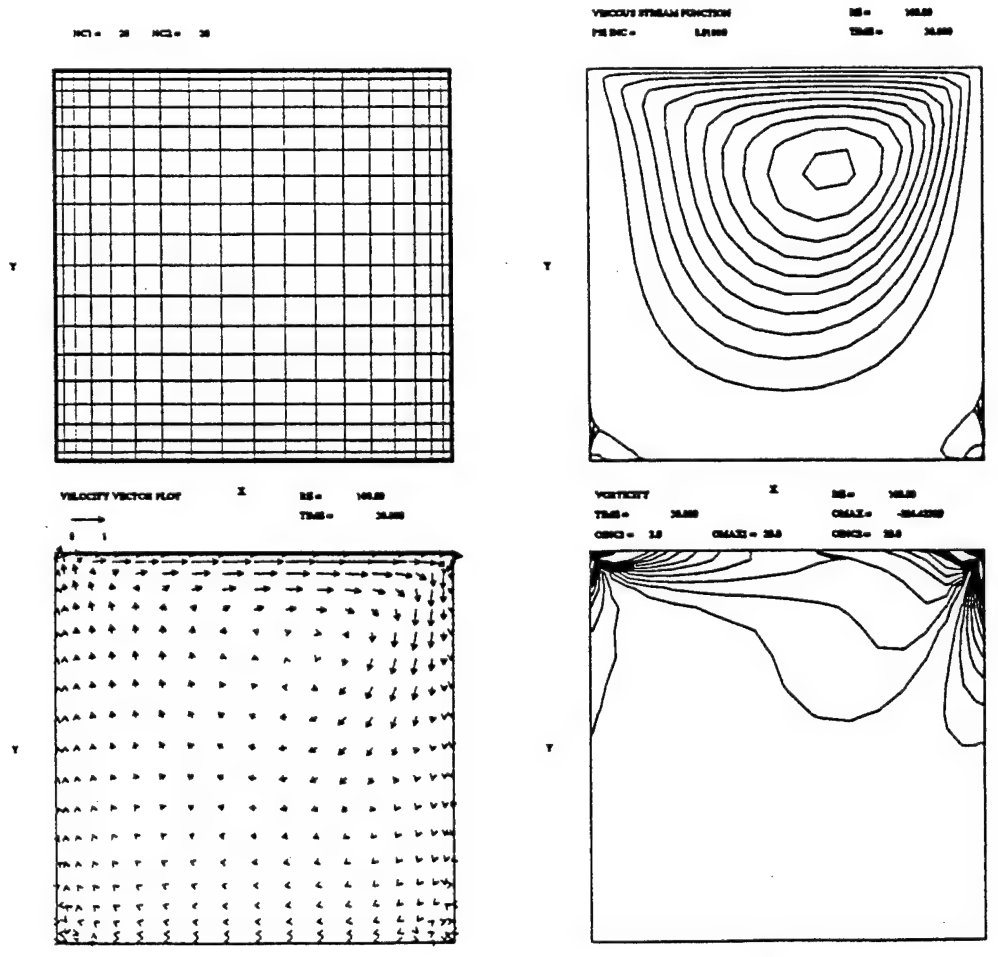

Figure 1: Chebyshev Spectral Results on a $21 \times 21$ Grid for the Shear Driven Cavity, $Re = 100$.

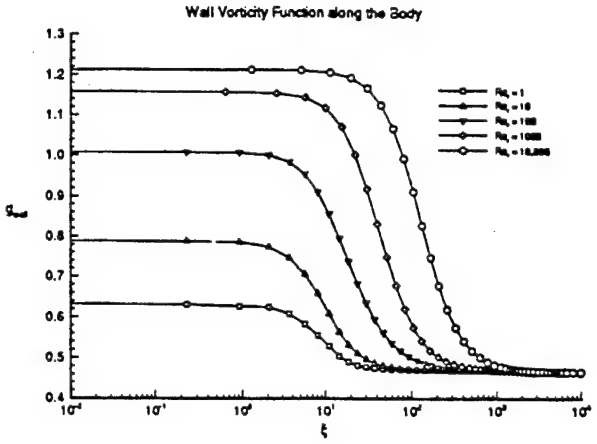


Figure 2: Navier-Stokes Solutions for Wall Vorticity Function using Single Domain.

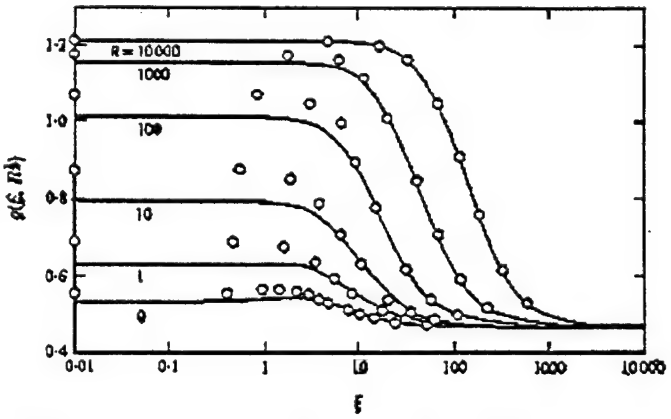


Figure 3. Skin friction distribution on a parabolic cylinder. O, parabolic approximation.

Figure 3: Solutions for Wall Vorticity Function by Davis [19].

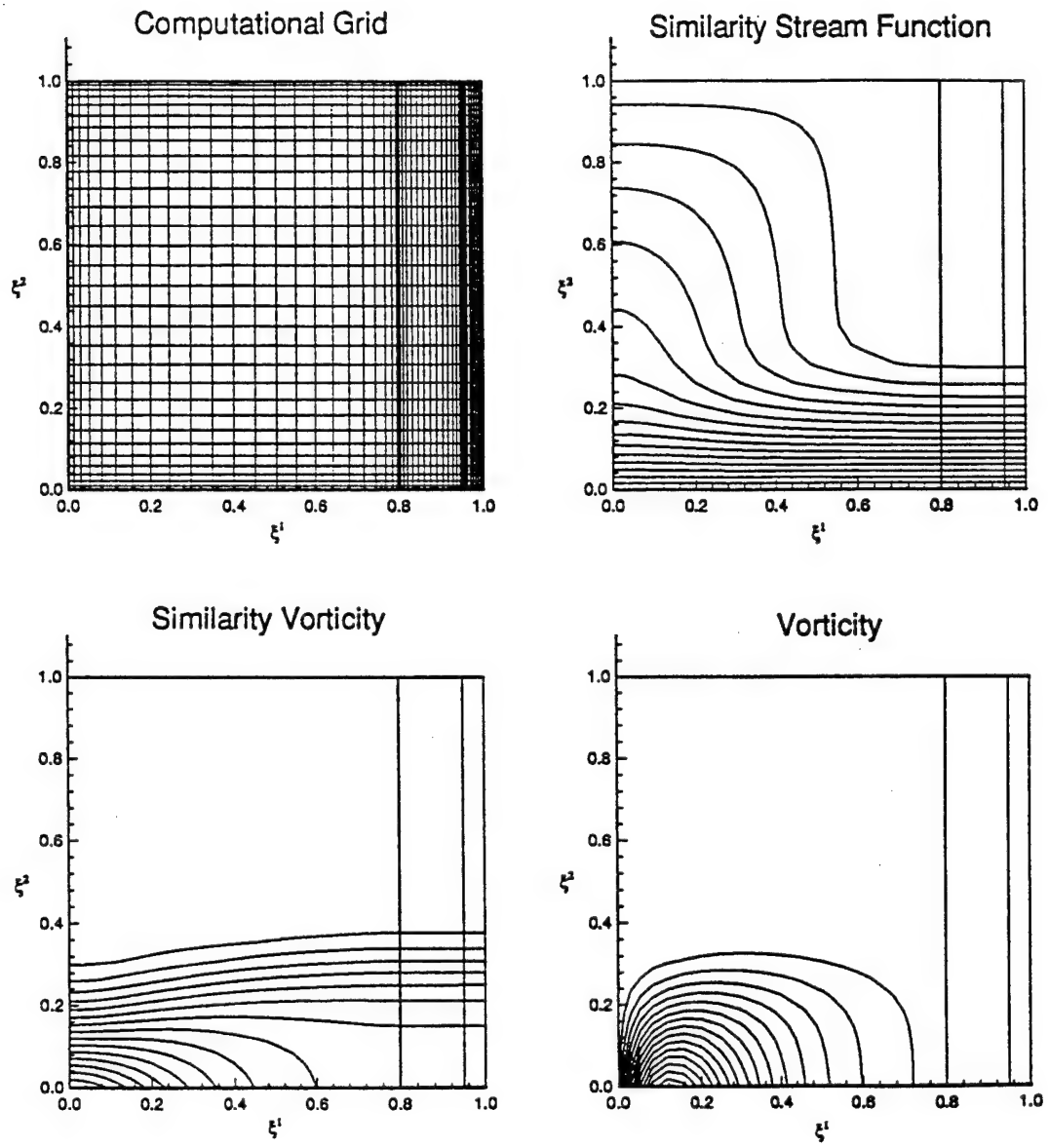


Figure 4: Parabolic Cylinder Results Plotted in Computational Plane: $Re_r = 100$.

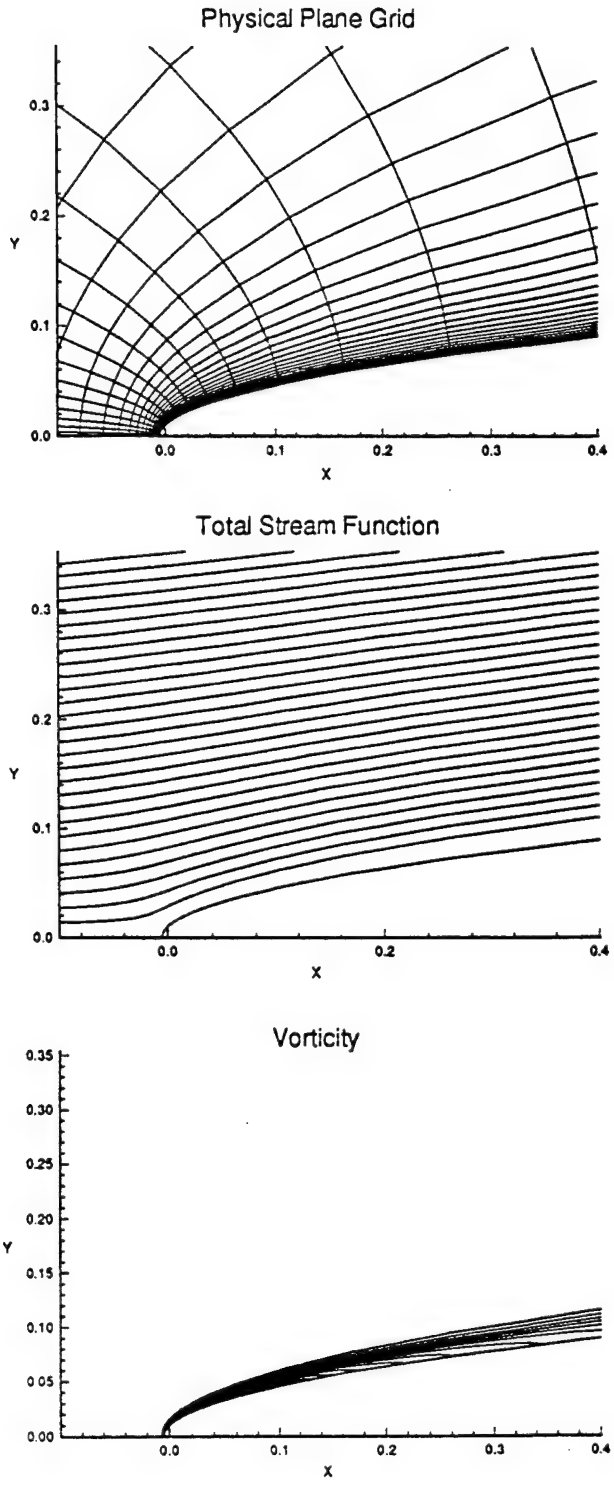


Figure 5: Physical Plane Results for $Re_r = 100$.

FED-Vol. 196

APPENDIX B2

# ADVANCES IN COMPUTATIONAL METHODS IN FLUID DYNAMICS

Edited By
K. N. Ghia
U. Ghia
D. Goldstein

# An Examination of Leading-Edge Receptivity on a Parabolic Cylinder Using the Navier-Stokes Equations*

**K. Blodgett, K.N. Ghia and U. Ghia**
CFDRL, University of Cincinnati, Cincinnati, OH 45221

**Craig L. Streett**
NASA Langley Research Center, Hampton, VA 23665

## ABSTRACT

Leading-edge receptivity to free-stream acoustic disturbances is studied. A semi-infinite geometry, i.e., the parabolic cylinder, is employed to isolate the effects of nose-bluntness on the receptivity process. The receptivity process is simulated using the 2-D unsteady Navier-Stokes equations in generalized curvilinear coordinates. In addition to the generalized coordinates, a multidomain technique is utilized to help resolve the disparate length scales of the problem. A spectral collocation method has been selected for the spatial discretization since the receptivity mechanisms active in this geometry are weak and the resulting instability wave can be expected to undergo substantial decay prior to reaching the neutral stability location. The overall method is validated by comparing the steady-state base flow results with previously published numerical results. Results for Reynolds numbers of 10, 100, and 1000 are obtained where the Reynolds number is based on the nose radius of the parabola. This allows assessment of the effects of nose-bluntness on the receptivity mechanism. Forcing is introduced by pulsating the free-stream velocity to simulate an acoustic wave. Both plane and oblique acoustic waves can be simulated in this manner. The forcing frequency has been selected such that the Reynolds number based on the forcing frequency is 10,000.

## 1. INTRODUCTION

Transition to turbulence continues to be of critical importance to a variety of current technologies such as drag reduction and heat transfer. Several conceptual models of the many routes to transition exist [1], but the most prevalent model is one in which the transition process is divided into three phases: receptivity, linear stability, and nonlinear breakdown. The linear stability phase has been well established for many years and has provided the current tools used in transition prediction, namely, the $e^N$ method [2]. Similarly, the nonlinear breakdown phase, while not completely understood, is represented fairly well in the early stages by secondary instability theory [3]. The first phase, receptivity, is the process by which small disturbances in the free stream enter the boundary layer and excite the instability modes of the boundary layer. This phase of transition has been the least understood; however, in recent years, significant progress has been made towards its theoretical understanding. What has been lacking is an understanding of how free stream disturbances, typically of much longer wavelength than instability waves, are able to transfer energy into instability wave in the presence of a wavelength mismatch. Theories by Goldstein [4] and Kerschen [5] indicate that rapid adjustments in the streamwise direction provide the necessary wavelength conversion mechanism resulting in the required wavelength match-up. Regions where such rapid adjustments occur include the leading-edge region where the boundary layer is growing rapidly.

In the present study, leading-edge receptivity to a free-stream acoustic wave is examined for a blunt leading-edge geometry consisting of a parabolic cylinder. The primary goals of this work are to provide verification of some recent theoretical results obtained by Hammerton et al. [6] for the effects of nose bluntness on receptivity and to provide a numerical tool for studying receptivity for flows in non-simple geometries.

## 2. MATHEMATICAL AND NUMERICAL METHODS

In the present analysis, the 2-D unsteady Navier-Stokes equations are utilized in the vorticity/stream function formulation. In addition, the equations have been developed in generalized curvilinear coordinates to better represent arbitrary geometries and to achieve improved resolution of the disparate length scales of the flow physics. Following the theory on

* This research is supported, in part, by NASA Grant No. NGT-50416, AFOSR Research Grant No. F-49620-92-J-0292, and Ohio Supercomputer Center Grant No. PES080.

receptivity, the equations have been nondimensionalized using the free-stream velocity, the free-stream kinematic viscosity and the forcing frequency of the free-stream disturbance. This provides the appropriate scaling of the variables for the receptivity study. The necessary boundary conditions are provided by the free-stream conditions far from the body, the no-slip and no-penetration conditions at the surface, and an appropriate outflow boundary condition. Additionally, the symmetry of the problem is exploited to reduce the physical domain of interest; hence, symmetry boundary conditions are also used. More details about the analysis have been described by Blodgett et al. [7].

A spectral collocation method [8] has been selected for the spatial discretization because of its low phase error and superior accuracy properties. The equations are advanced in time using a semi-implicit time stepping method. The resulting set of algebraic equations are solved iteratively using a preconditioned conjugate residual method [9] with a finite-difference preconditioner.

In addition to the spectral method, a multidomain method has been added to allow a zonal approach to the problem. The utilization of the multidomain method allows better use of grid points, different grid clustering transformations in different subdomains, and even the use of different equations in different subdomains. The subdomains are connected by a patched grid, and $C^1$-continuity of the dependent variables is enforced across the interfaces between the subdomains.

The numerical implementation of the boundary conditions is straightforward, with the exception of the no-slip condition. For this boundary condition, an integral constraint condition [10] has been employed. In essence, this integral constraint condition allows the surface vorticity to be determined so as to be consistent with the no-slip condition. The remaining boundary conditions consist of symmetry conditions along the stagnation line, free-stream conditions at the outer normal boundary, and an outflow boundary condition downstream. The outflow boundary condition will be addressed further in the next paragraph. Lastly, since spectral methods are sensitive to any errors in boundary conditions, care has been taken in the implementation of the boundary conditions.

For the parabolic cylinder geometry, the benchmark work of Davis [11] has been used to guide the current analysis. His asymptotic analysis of the problem indicates that similarity-type variables are the preferred dependent variables for this semi-infinite geometry. Unfortunately, the resulting governing equations are singular at the stagnation line, and spectral methods are extremely sensitive to singularities. However, the use of the similarity variables provides an accurate outflow boundary condition, namely, the Blasius boundary-layer solution. Hence, a unique feature of the current analysis is the use of different dependent variables in different subdomains. In particular, the similarity variables are utilized in the farthest downstream subdomain in the streamwise direction. This allows the asymptotically correct outflow boundary condition to be applied. No difficulty is experienced in the solution process in this subdomain since the similarity variables are well behaved as they approach downstream infinity.

The grid is generated by the conformal parabolic coordinates as described by Davis [11]. For the present analysis, the grid in the physical plane is stretched to downstream infinity in the streamwise direction, but only to a far but finite location in the normal direction. A three subdomain set-up is used in the streamwise direction, with different clustering transformations possible in each subdomain. In particular, the streamwise clustering transformation used by Davis [11] is utilized in the last subdomain, while algebraic clustering transformations are used in the first two subdomains. In the normal direction, a clustering transformation similar to that used by Davis [11] is employed, and allows the stretching parameters to be chosen such that half of the grid points in the normal direction lie within the boundary layer. The location of the outer boundary in the normal direction has been selected carefully so that its location does not influence the solution significantly.

The receptivity simulation is done in two parts. In the first part, a base flow is obtained in the absence of any free-stream disturbances. A typical base flow might consist of a steady-state solution to the problem. Once this base flow is obtained, the actual receptivity simulation can commence by the introduction of the free-stream disturbance.

In obtaining the base flow, a fictitious time derivative has been added to the stream function equation, and local time stepping is employed to accelerate the convergence of the flow field towards a steady state base flow. Despite the convergence acceleration techniques, the relaxation time to reach a steady state is prohibitively large for the current numerical method. Therefore, once the convergence to steady-state reaches a certain specified level, the solution is stopped, and this result is used as the base flow.

For the receptivity simulation, the time-accurate form of the equations is employed. The free-stream acoustic disturbance is introduced in the far field by pulsating the free-stream velocity. The introduction of the disturbance poses an additional difficulty for implementing the outflow boundary condition. To circumvent this, the buffer domain technique [12] is utilized in the last domain, so as to attenuate any disturbances to zero in the last domain without causing any reflection of waves.

The present numerical method has been validated on the shear-driven cavity geometry as well as via the base flow results obtained [7].

## 3. BASE FLOW RESULTS

Base flow results are obtained for several parabolas with different nose radii. The amount of nose bluntness of the different parabolas is distinguished by the Reynolds number

based on the nose radius, i.e., $Re_r$. Figure 1 depicts the similarity vorticity function along the wall as a function of the streamwise similarity coordinate, for various $Re_r$. These results compare very well with those obtained by Davis [11] using a finite-difference method with a $40 \times 125$ grid, and reproduced here in Figure 2. The current results were obtained with a total of 53 and 33 points in the streamwise and normal directions, respectively. The results shown in Fig. 1 have not been completely converged to a steady-state solution, but are sufficiently close.

Figure 3 shows the computational grid, the similarity vorticity, the similarity viscous-deviational stream function, and the physical vorticity in the computational plane for $Re_r = 100$. It is clear from this figure that the flow variables are continuous across the interfaces which are shown in the contour plots as vertical lines.

## 4. RECEPTIVITY SIMULATION

Receptivity results for three different nose radii, e.g., $Re_r = 10$, 100 and 1000 are currently being obtained and analyzed. The forcing frequency has been selected to yield a Reynolds number of 10,000, based on the frequency. The amplitude of the free-stream acoustic wave has been set at $10^{-3}$ of the free-stream velocity. This should be sufficiently small to avoid nonlinear responses. Gatski and Kerschen [13] have also considered these same parameters and have estimated that the resulting Tollmien-Schlichting instability wave should have a wavelength around 2.3 units in the current nondimensionalization. In order to resolve the Tollmien-Schlichting wavelength, roughly three grid points are required per wavelength for the current spectral method. To meet this requirement, the streamwise grid distribution has been increased to slightly more that 150 grid points distributed to the first two subdomains. In addition, the normal distribution has been increased to 49 points. Since, a spectral method is being used, the base flow results from a coarser grid can be interpolated onto the finer grid without loss of accuracy.

Obtaining results for three different nose radii should allow the qualitative reproduction of the trend predicted by theory in Hammerton et al.'s [6] work. They show that, as the Strouhal number, $S = \frac{Re_r}{Re}$, is increased, the receptivity coefficient decreases.

## REFERENCES


[1] Reshotko. E., 1994, "Boundary Layer Instability, Transition and Control," *AIAA Paper* 94--0001.

[2] Smith, A.M.O. and Gamberoni, N., 1956, "Transition, Pressure Gradient, and Stability Theory," *Proceedings of the International Congress on Applied Mechanics*, 234, Brussells.

[3] Herbert, T., 1988, "Secondary Instability of Boundary Layers," *Annual Review of Fluid Mechanics*, **20**, pp. 487--526.

[4] Goldstein, M.E., 1983, "The Evolution of Tollmien-Schlichting Waves Near a Leading Edge," *Journal of Fluid Mechanics*, **127**, pp. 59--81.

[5] Kerschen, E., 1989, "Boundary Layer Receptivity," *AIAA Paper* 89--1109.

[6] Hammerton P.W. and Kerschen E.J., 1992, "Effect of Nose Bluntness on Leading-Edge Receptivity," *Instability, Transition, and Turbulence*, Hussaini, M.Y. and Kumar, A. and Streett, C.L., Eds., Springer-Verlag, pp. 441--451.

[7] Blodgett, K., Ghia, K.N., and Streett, C.L., 1994, "Towards Simulation of Leading-Edge Receptivity Using A Spectral Multidomain Method in Generalized Curvilinear Coordinates," AIAA paper 94--0063.

[8] Canuto, C., Hussaini, M.Y., Quarteroni, A., and Zang, T.A., 1987, *Spectral Methods in Fluid Mechanics*, Springer-Verlag, New York.

[9] Wong, Y.S., Zang, T.A., and Hussaini, M.Y., 1986, "Preconditioned Conjugate Residual Methods for the Solution of Spectral Equations," *Computers in Fluids*, **14** (2), pp. 85--95.

[10] Dennis, S.C.R. and Quartapelle, L., 1989, "Some Uses of Green's Theorem in Solving the Navier-Stokes Equations," *International Journal for Numerical Methods in Fluids*, **9**, pp. 871--890.

[11] Davis, R.T., 1972, "Numerical Solution of the Navier-Stokes Equations for Symmetric Laminar Incompressible Flow Past a Parabola," *Journal of Fluid Mechanics*, **51**, pp. 417--433.

[12] Danabasoglu, D., Birigen, S., and Streett, C.L., 1991, "Spatial Simulation of Instability Control by Periodic Suction Blowing," *Physics of Fluids A*, **3**, pp. 2138--2147.

[13] Gatski, T.B. and Kerschen, E.J., 1990, "Leading Edge Effects on Boundary Layer Receptivity," *Twelfth International Conference on Numerical Methods in Fluid Dynamics*}, Morton, K.W., Ed., Springer-Verlag.

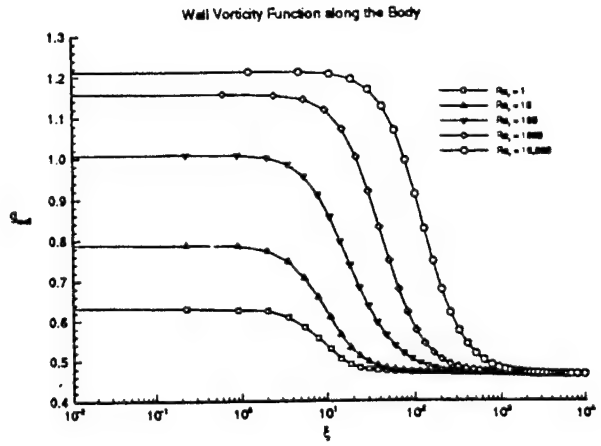


Figure 1: Navier-Stokes Solutions for Wall Vorticity Function using Single Domain.

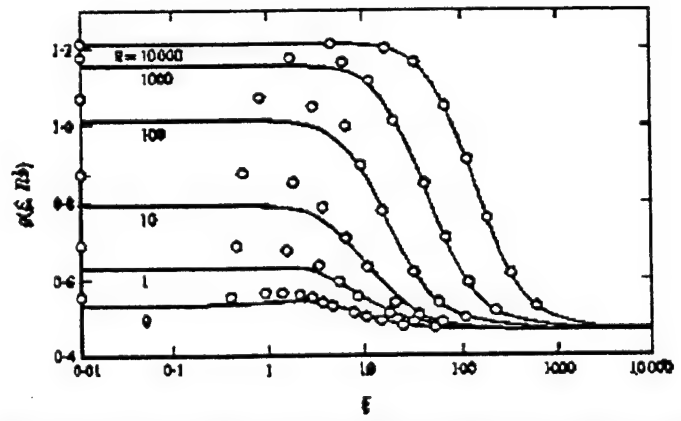


Figure 3. Skin friction distribution on a parabolic cylinder. O, parabolic approximation.

Figure 2: Solutions for Wall Vorticity Function by Davis [11].

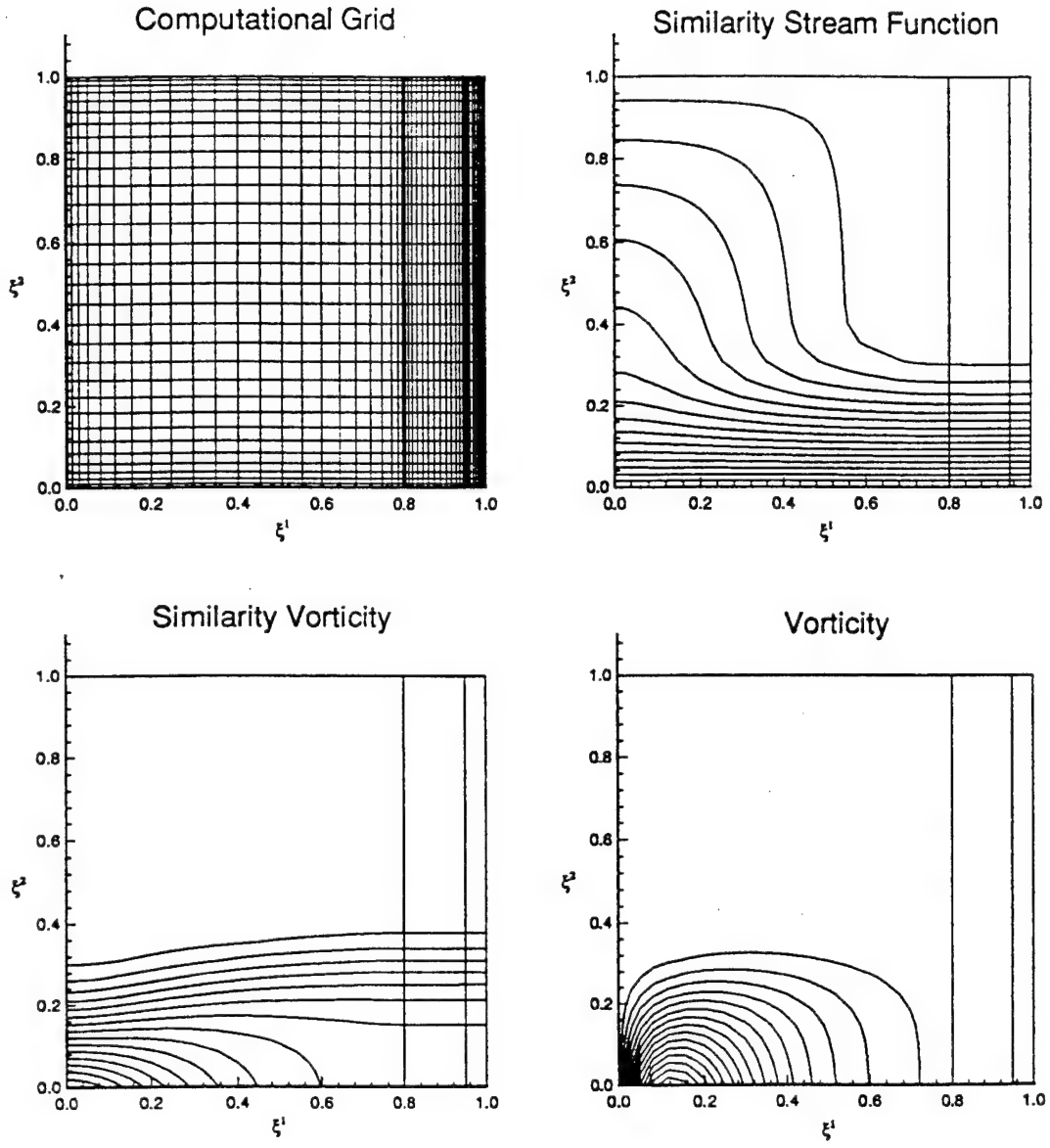


Figure 3: Parabolic Cylinder Results Plotted in Computational Plane: $Re_r = 100$.

APPENDIX C1

# AIAA 96-2018

## Numerical Simulation of Nonlinear Instabilities in Complex Channel Flows

B.D. Brandes-Duncan and K.N. Ghia
University of Cincinnati
Cincinnati, OH

**27th AIAA Fluid Dynamics Conference**
June 17-20, 1996 / New Orleans, LA

# NUMERICAL SIMULATION OF NONLINEAR INSTABILITIES IN COMPLEX CHANNEL FLOWS*

B. D. Brandes-Duncan†
K. N. Ghia‡
*Computational Fluid Dynamics Research Laboratory*
*Department of Aerospace Engineering and Engineering Mechanics*
*University of Cincinnati, Cincinnati, Ohio 45221*

**A tool for the numerical simulation of transition to turbulence in 3D complex channel flows has been developed using a single-domain spectral collocation method. The present study describes results which validate the accuracy of the spectral method and demonstrate the ability of the code to simulate temporal stability problems. Nonlinear stability results for plane and curved channel flows were obtained. In particular, a quasi-saturated Tollmien-Schlichting wave for plane channel flow with Reynolds number 4000 was computed and compares favorably with available results. The nonlinear evolution equations for subcritical plane and curved channel flows were obtained and compared with Landau's equation governing the growth of weakly nonlinear waves.**

## Introduction

THE study of the transition of laminar flow to a turbulent state has, in recent research efforts, focused on the nonlinear growth and interaction of waves which originate as linear eigenmodes of the flow-governing equations. Many experimentally and numerically observed routes to turbulence can be understood theoretically in terms of the nonlinear instability of waves which are excited in the flow. Plane channel flow has been studied extensively[1-8] and has shown many commonalities with plane boundary-layer flow. In plane channel flow, Tollmien-Schlichting waves interact with streamwise vortices to produce three-dimensional hairpin, or Λ vortex, structures which are precursors to a fully-turbulent state. Curved channel flow, that is, azimuthal flow in an annulus, has also been examined and has demonstrated a different instability mechanism due to streamwise curvature[9-13]. Streamwise vortices, called Dean vortices for curved channel flow, grow to a stable equilibrium for a range of Reynolds numbers. Increasing the Reynolds number in time leads to bifurcations to more complex, but stable, states until a critical Reynolds number is reached for which no stable flow exists, and the flow becomes fully turbulent.

Studies of flows in more complex types of channels have shown that the transition mechanisms observed in plane and curved channel flows are also dominant in other types of flows. Examples of complex channel flows include wavy converging-diverging channel[14], constricted channel[15,16], grooved channel[17,18], plane channel with 2D and 3D surface perturbations[19], and channel flow with compliant walls[20]. In complex channel flows, the presence of multiple shear layers at different scales causes the stability properites of the fundamental Tollmien-Schlichting-type modes and streamwise vortex modes to be significantly altered. For example in the 2D

*This work is supported in part by a Department of Defense NDSEG Fellowship, AFOSR Grant No. FH9620-93-1-0393, and the Ohio Supercomputer Center Grant No. PES070-5.

†Graduate Student, Department of Aerospace Engineering and Engineering Mechanics. Member AIAA.

‡Herman Schneider Professor of Engineering, Department of Aerospace Engineering and Engineering Mechanics. Associate Fellow AIAA.

periodic converging-diverging channel, a chaotic state is achieved through bifurcation of the Tollmien-Schlichting wave to a quasi-periodic state as Reynolds number is increased, following the Ruelle-Takens-Newhouse scenario[14].

The purpose of the current work is to develop a numerical simulation tool to study the temporal evolution of instabilities in incompressible channel flows of various types, in order to examine the routes to turbulence, which are dominant in many types of flows of interest to fluid dynamics researchers and the aerospace industry. A numerical approach has been developed for treating 3D flows, forced by a mean streamwise pressure gradient, in arbitrary channel geometries. These flows are assumed to be periodic in the streamwise and spanwise directions; thus, the temporal evolution of disturbances present in the initial flow is studied. Validation of the numerical approach has included error analysis of the discretization and comparison with linear theory and nonlinear stability results from other authors. This paper discusses the first stage of the work, namely, the validation of the numerical approach and a study of the nonlinear evolution of Tollmien-Schlichting waves in plane and curved channel flows. Future work will study the nonlinear stability of other more complex 2D and, subsequently, 3D channel flows.

## Formulation and Numerical Approach

### Governing Equations

The temporal evolution of 3D channel flows is governed by the incompressible Navier-Stokes equations. These equations have been expressed in a general nonorthogonal coordinate system for the purpose of this study. This allows, by appropriate selection of a coordinate transformation, the simulation of channel flows of arbitrary type with the restriction that both the geometry and the flow solution are periodic in the streamwise and spanwise directions. It is also assumed for present purposes that the geometry is 2D, i.e., that there is no curvature in the spanwise direction. The governing equations in general coordinates consist of the contravariant components of the incompressible momentum equation, and the continuity equation. These are derived by Brandes-Duncan[21] and will not be shown here. The dependent variables are the contravariant components of velocity, along with the pressure.

### Discretization and Solution Method

The approach to the spatial discretization of the governing equations is a single-domain spectral collocation method, and uses Fourier discretization in the streamwise and spanwise directions and Chebyshev discretization in the normal direction. Both the pressure and the continuity equation are staggered in the normal direction, and Chebyshev interpolation is used to relate values at the staggered points to values at grid points. The coordinate transformation facilitates the Fourier transform of the governing equations in the spanwise direction, and this decouples the linear parts of the governing equations from each other in the spanwise direction. The equations are integrated in time using a second-order accurate time-centered discretization. A fully-implicit iterative method is used to solve the discrete equations at each time step, to the desired residual convergence level. All of the nonlinear terms are computed directly, using collocation (matrix-multiplication) derivatives and are lagged in the iteration procedure. For details of the formulation, see Brandes-Duncan[21].

### High-Performance Computing

The above formulation has been implemented as part of an object-oriented framework for performing computational fluid dynamics (CFD) simulations, written in C++. The goal of the object-oriented approach is to achieve maximum code re-use between different CFD applications, as well as optimal computing performance across various scalar, vector, and parallel computer platforms. Optimal floating-point performance has been achieved by encapsulating machine-optimized linear algebra routines within the implementation of CFD objects, while retaining a machine-independent interface for using those objects. Details of the object-oriented approach will be presented in a separate paper. The direct impact of the object-oriented approach on the current study is that the spectral discretization method can be easily expressed in terms of lower-level linear algebra operations, allowing changes to the discretization method, or to the linear or nonlinear iteration levels of

the solution method, to be made easily and independently of the rest of the code.

## Validation of Numerical Approach

### Error Analysis

A method was devised for computing the error in the discretization scheme by prescribing a desired solution and analytically computing a forcing function, which could be added to the residual such that the prescribed solution would satisfy the modified governing equations. Prescribed solutions were selected so that the error due to the Fourier, Chebyshev, and temporal discretizations could each be isolated and examined independently. For example, the prescribed solution for examination of the Fourier discretization in the streamwise direction is shown in Fig. 1. Both the residual level and the solution error after 10 time steps with $\Delta t$=0.001 are indications of the convergence of the discretization with increasing number of points, and are shown in Fig. 2. Similar results are shown for the Chebyshev discretization in Fig. 3. For both the Fourier and Chebyshev discretizations, the error was found to decrease almost exponentially with the number of points and machine-zero convergence was achieved with less than 52 points. The error analysis was performed using the residual evaluation and implicit iterative solver in the CFD code, and thus served as the first validation of the accuracy and correctness of the code.

### Linear Stability Results

The second validation of the code was obtained by computing the temporal evolution of small amplitude Tollmien-Schlichting waves in 2D plane and curved channel flows and by comparing the resulting growth rate and wavespeed with linear stability theory. A spatial resolution of 8x48 (streamwise x normal) grid cells was used with $\Delta t$=T/1000, where T is the period of oscillation of the Tollmien-Schlichting wave from linear stability theory. Shown in Table 1, the results of this study demonstrate comparison with linear stability theory with agreement up to 4 or 5 decimal places.

## Nonlinear Stability Results

### Plane Channel Saturated State

The first stage in the transition to turbulence of plane channel flow is the growth of the primary Tollmien-Schlichting wave. Plane channel flow exhibits subcritical instability, in that growth of finite-amplitude instability waves occurs for Reynolds numbers below the critical Reynolds number predicted by linear stability theory. Early-time results for Reynolds number of 4000 and streamwise wavenumber, $\alpha$, of 1.25, are shown in Fig. 4. The initial conditions are Tollmien-Schlichting waves of different amplitudes. For all cases, the primary mode initially follows a linear evolution, while the harmonics of the primary mode experience rapid growth through nonlinear interaction with the primary mode. After the harmonic modes have grown to a sufficiently high amplitude, the growth of the primary mode is modified. For initial amplitudes, $A_1$, above a critical value of approximately 0.08, the primary mode will begin to grow, and will continue to grow over a long period of time, until it reaches a saturated equilibrium amplitude. At this amplitude, at approximately $A_1$ =0.32, the Tollmien-Schilichting wave will persist indefinitely in a 2D simulation as a stable flow solution; however, this wave is highly unstable to 3D disturbances, and will break down into successively complicated states in a physically realistic 3D flow. The 2D state achieved after 20 periods of the Tollmien-Schlichting wave is shown in Figs. 5 and 6. Though the wave is not completely saturated (saturation would require hundreds of Tollmien-Schlichting periods), the growth is sufficiently small, and the solution is representative of the final state. It also compares well with the time-asymptotic solution found for this case by Orszag and Patera[3].

### Evolution Equation for Plane and Curved Channels

Theories of nonlinear stability examine the nonlinear interactions that occur between primary modes active in the flow and their respective harmonics. Weakly nonlinear stability theory uses an asymptotic expansion, with the amplitude of the

primary mode as a small parameter, and considers the higher-order effects of the harmonics on the evolution of the primary mode; for example, see Singer *et al.*[13]. In these approaches, it is often ascertained that the temporal growth of the primary mode is governed by an ordinary differential equation of the form:

$$\frac{1}{A_1}\frac{d}{dt}A_1 = f(A_1) \qquad (1)$$

where $A_1$ is the magnitude of the complex amplitude of the primary mode. For infinitesimal amplitudes, the evolution equation becomes linear:

$$\frac{1}{A_1}\frac{d}{dt}A_1 = \omega_l \qquad (2)$$

with growth rate $\omega_l$. For small but finite amplitudes, the evolution equation is the Landau equation[22]:

$$\frac{1}{A_1}\frac{d}{dt}A_1 = \omega_l - l\,A_1^2 \qquad (3)$$

where the Landau coefficient, $l$, determines the stability of the solution to finite-amplitude disturbances. In particular, if $\omega_l$ and $l$ are negative, the flow exhibits subcritical instability and growth will occur for values of $A_1$ above a critical value.

The evolution equation, Eq. (1), for plane and curved channel flows was investigated numerically by performing multiple simulations with varying amplitudes. After 1 period of the Tollmien-Schlichting wave, the growth rate $(1/A_1)\,dA_1/dt$ and the square of the amplitude were computed. These results were compiled for various cases and are shown in Figs. 7-9. The rate-axis intercept of each curve is the linear growth rate $\omega_l$ , and the initial slope is an estimate of the negative of the Landau coefficient, $-l$ . These results show that the Landau equation is valid only for small amplitudes up to approximaely 0.01. The Landau coefficients for five different cases are shown in Table 2. The results show the trajectory of the primary mode in amplitude squared vs. rate space. This trajectory is indeed determined by an ordinary differential equation of the form of Eq. (1); however, this trajectory is not polynomial in nature and, therefore, cannot be represented with a finite number of polynomial terms.

## Summary

The first stage of development and validation of a numerical tool for simulation of channel flow stability problems was completed. Linear stability results, accurate to at least 4 decimal places, were obtained. Nonlinear stability results were compared with the Landau equation and showed that weakly nonlinear theory applies in the low amplitude range, up to $A_1 = O(0.01)$, and the evolution equations saturate at higher amplitudes. Future work will investigate the nonlinear stability of additional types of channel flows, and will extend the analysis to study the instability of these flows to 3D disturbances.

## Acknowledgements

The authors wish to acknowledge the use of the incompressible stability analysis code Linear.x developed by Thorwald Herbert for obtaining linear stability results. The first author also wishes to thank Christopher Noll of the University of Cincinnati for many valuable discussions.

## References

[1.] Hall, P., and Smith, F.T. 1989. Near-planar TS Waves and Longitudinal Vortices in Channel Flow: Nonlinear Interaction and Focusing. *ICASE Report No. 89-47.*

[2.] Ehrenstein, U., and Koch, W. 1991. Three-Dimensional Wavelike Equilibrium States in Plane Poiseuille Flow. *Journal of Fluid Mechanics* **228**: 111-148.

[3.] Orszag, S. A., and Patera, A. T. 1983. Secondary Instability of Wall-Bounded Shear Flows. *Journal of Fluid Mechanics.* **128**: 347-385.

[4.] Singer, B.A., Reed, H.L., and Ferziger, J.H. 1989. The Effects of Streamwise Vortices on Transition in the Plane Channel. *Physics of Fluids A* **1**: 1960-1971.

[5] Stocker, J. R., and Duck, P. W. 1995. Sationary Perturbations of Couette-Poiseuille Flow: the Flow Development in Long Cavities and Channels. *Journal of Fluid Mechanics* **292**: pp. 153-182.

[6] Zang, T.A., and Hussaini, M.Y. 1985. Numerical Experiments on Subcritical Transition Mechanisms. *AIAA Paper 85-0296.*

[7] Zang, T.A., and Hussaini, M.Y. 1985. A Three-Dimensional Spectral Algorithm for Simulations of Transition and Turbulence. *ICASE Report No. 85-19.*

[8] Zang, T.A., and Hussaini, M.Y. 1987. Numerical Simulation of Nonlinear Interactions in Channel and Boundary-Layer Transition. *Nonlinear Wave Interactions in Fluids.* ASME Press.

[9] Bland, S.B., and Finlay, W.H. 1991. Transitions Toward Turbulence in a Curved Channel. *Physics of Fluids A* **3**(1): 106-114.

[10] Finlay, W.H., Keller, J.B., and Ferziger, J.H. 1988. Instability and Transition in Curved Channel Flow. *Journal of Fluid Mechanics* **194**: 417-456.

[11] Guo, Y., and Finlay, W.H. 1994. Wavenumber Selection and Irregularity of Spatially Developing Nonlinear Dean and Görtler Vortices. *Journal of Fluid Mechanics* **264**: 1-40.

[12] Ligrani, P.M. 1992. Features of Wavy Vortices in a Curved Channel from Experimental and Numerical Studies. *Physics of Fluids A* **4**: 695-709.

[13] Singer, B.A., Erlebacher, G., and Zang, T.A. 1992. A Weakly Nonlinear Theory for Wave-Vortex Interactions in Curved Channel Flow. *NASA TP-3158.*

[14] Guzmán, A.M. and Amon, C.H. 1994. Transition to Chaos in Converging-Diverging Channel Flows: Ruelle-Takens-Newhouse Scenario. *Physics of Fluids A* 6(6): 1994-2002.

[15] Roberts, E.P.L. 1994. A Numerical and Experimental Study of Transition Processes in an Obstructed Channel Flow. *Journal of Fluid Mechanics* **260**:185-209.

[16] Sobey, I.J., and Drazin, P.G. 1986. Bifurcations of Two-Dimensional Channel Flows. *Journal of Fluid Mechanics* **171**: 263-287.

[17] Ghaddar, N.K., Korczak, K.Z., Mikic, B.B., and Patera, A.T. 1986. Numerical Investigation of Incompressible Flow in Grooved Channels: Part 1, Stability and Self-Sustained Oscillations. *Journal of Fluid Mechanics* **163**: 99-127.

[18] Amon, C.H., and Patera, A.T. 1989. Numerical Calculation of Stable Three-Dimensional Tertiary States in Grooved-Channel Flow. *Physics of Fluids A* **1**:2005-2009.

[19] Carlson, H. A., Berkooz, G., and Lumley, J. L. 1995. Direct Numerical Simulation of Flow in a Channel with Complex, Time-Dependent Wall Geometries. *Journal of Computational Physics* **121**(*1*): pp. 155-175.

[20] Ehrenstein, U., and Rossi, M. 1993. Nonlinear Tollmien-Schlichting Waves for Plane Poiseuille Flow with Compliant Walls. *European Journal of Mechanics, B/Fluids* **12**(*6*): pp. 789-810.

[21] Brandes-Duncan, B. D. 1995. *Numerical Simulation of Early Stages of Transition in Channel Flows.* M.S. Thesis. University of Cincinnati.

[22] Drazin, P.G., and Reid, W.H. 1981. *Hydrodynamic Stability.* Cambridge University Press.

| | *Parameters* | | | *Linear Theory* | | *Simulation* | | |
|---|---|---|---|---|---|---|---|---|
| *Case* | *Re* | $R_C$ | $\alpha$ | $\omega_R$ | $\omega_I$ x 1000 | $\omega_R$ | $\omega_I$ x 1000 | *T* |
| 1 | 8000 | -- | 1 | 0.247075 | 2.66417 | 0.247076 | 2.66445 | 25.4 |
| 2 | 4000 | -- | 1.25 | 0.381718 | -10.923 | 0.381718 | -10.923 | 16.5 |
| 3 | 5000 | 100 | 100 | 0.374757 | 3.28679 | 0.374782 | 3.2868 | 16.8 |
| 4 | 4000 | 1000 | 1250 | 0.530779 | -16.573 | 0.530781 | -16.573 | 11.8 |
| 5 | 5772.22 | -- | 1.02 | 0.269215 | 0 | 0.269214 | 0 | 23.3 |

**Table 1.** Comparison of wavespeed, $\omega_R$, and growth rate, $\omega_I$, from simulations on an 8x48 grid, with $\Delta t$=T/1000 for plane and curved channel flow. *Re* is the Reynolds number, $R_C$ is the radius of curvature for the curved channel cases and $\alpha$ is the streamwise wavenumber.

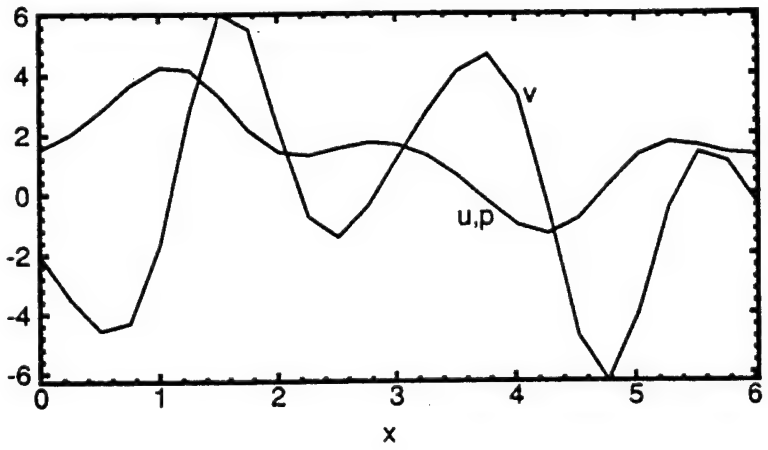


**Figure 1.** Prescribed solution for testing accuracy of the Fourier collocation method for the plane channel. The figure shows u, v, and p along the upper wall of the channel.

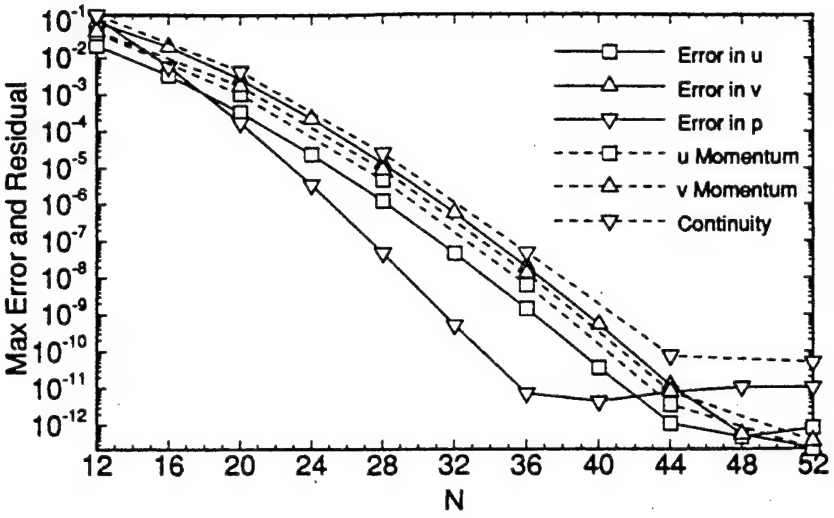


**Figure 2.** Residual and solution error for the Fourier discretization vs. the number of points used

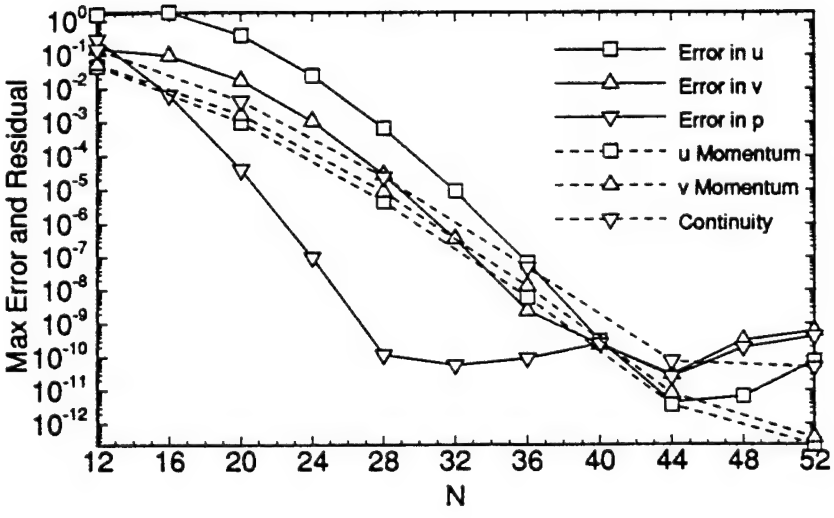


**Figure 3.** Residual and solution error for the Chebyshev discretization vs. the number of points used

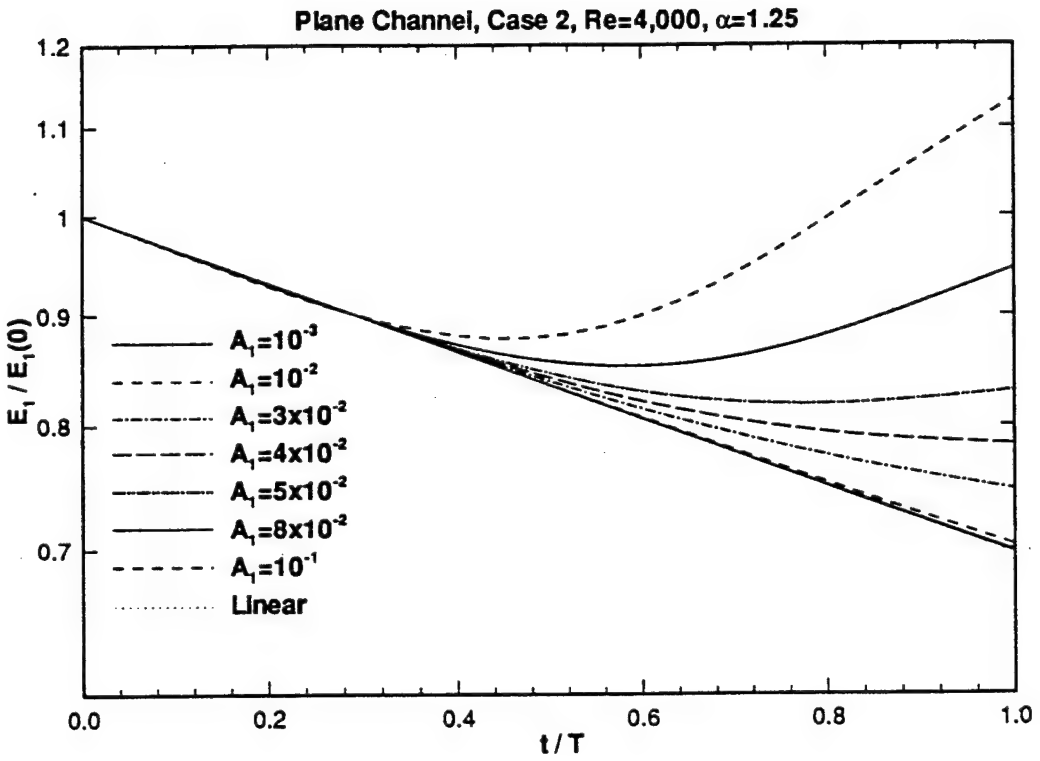


**Figure 4.** Growth of the primary disturbance mode for one period, $T$, for plane channel flow with $Re$=4,000, $\alpha$=1.25 and with varying initial amplitude $A_1$.

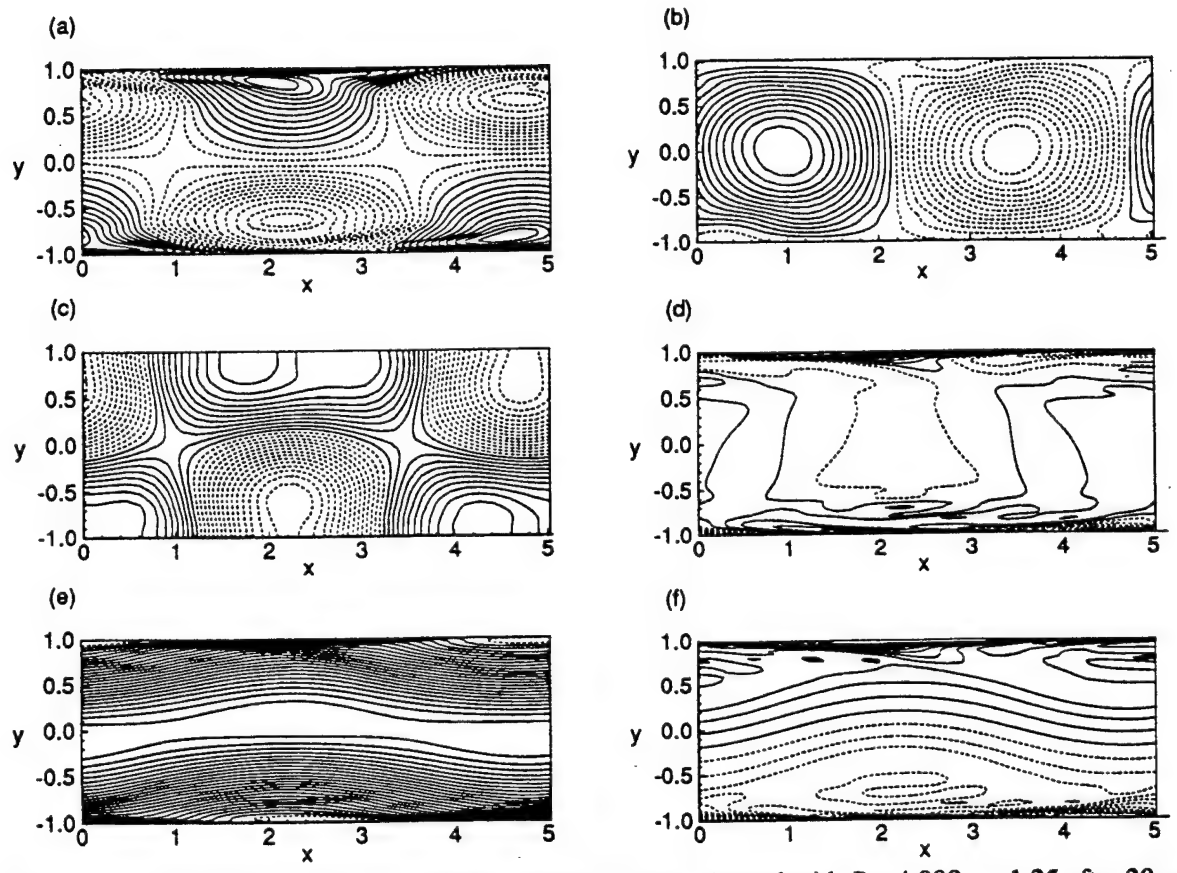


**Figure 5.** Quasi-saturated Tollmien-Schlichting wave in a plane channel with $Re$=4,000, $\alpha$=1.25 after 20 periods of the wave: contours of perturbations in (a) $u$, (b) $v$, (c) $p$, and (d) spanwise vorticity, as well as total flow quantities (e) $u$, and (f) spanwise vorticity.

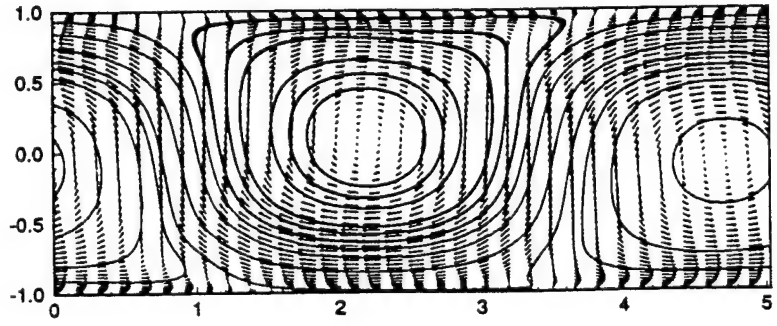


**Figure 6.** Quasi-saturated Tollmien-Schlichting wave. Perturbation velocity vectors and streamlines.

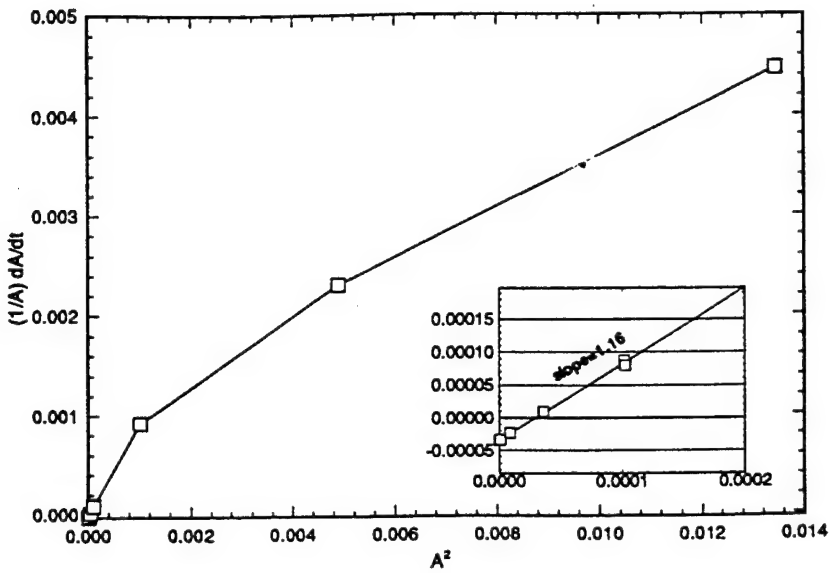


**Figure 7**. Curve showing the numerically-computed evolution equation for plane channel flow at the critical Reynolds number, *Re*=5772, $\alpha$=1.02.

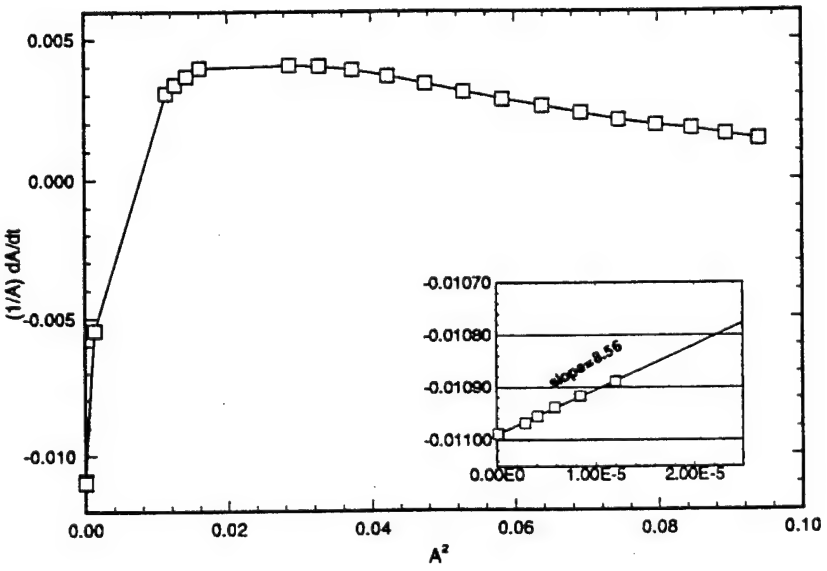


**Figure 8**. Evolution equation for plane channel, *Re*=4,000, $\alpha$=1.25.

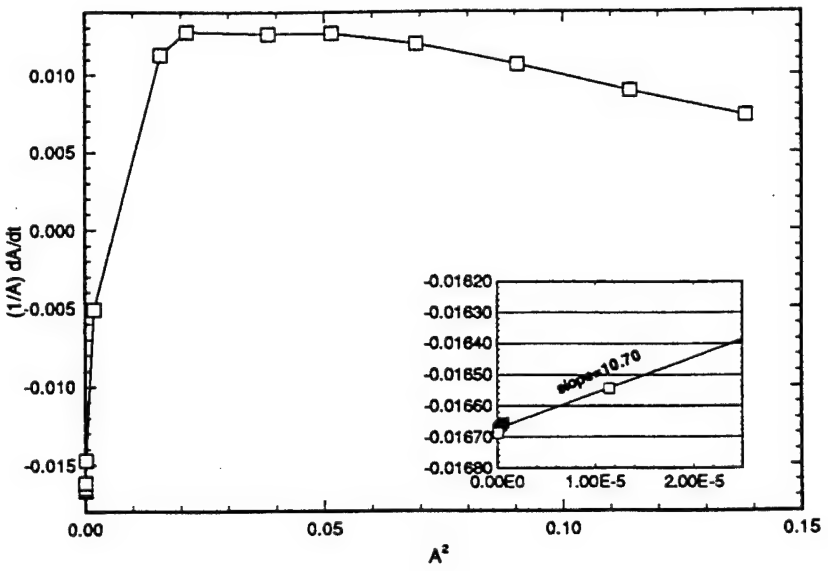


**Figure 9.** Evolution equation for curved channel, $Re$=4,000, $R_c$=1,000, $\alpha$=1250.

| *Case* | *l* | $A_e$ |
|---|---|---|
| 1 | -1.40 | -- |
| 2 | -8.56 | 0.0077 |
| 3 | -1.22 | -- |
| 4 | -10.70 | 0.0063 |
| 5 | -1.16 | -- |

**Table 2.** Nonlinear stability results for the plane and curved channel cases shown in Table 1. The Landau coefficient, $l$, and threshold amplitude, $A_e$, were estimated from the evolution equation results

# FIRST AFOSR INTERNATIONAL CONFERENCE ON DNS/LES

**APPENDIX C2**

## AN ITERATIVE APPROACH FOR SOLVING THE INCOMPRESSIBLE NAVIER-STOKES EQUATIONS FOR SIMULATION OF TRANSITION AND TURBULENCE IN COMPLEX GEOMETRIES*

B.D. Duncan and K.N. Ghia
Computational Fluid Dynamics Research Laboratory
Department of Aerospace Engineering and Engineering Mechanics
University of Cincinnati
Cincinnati, OH 45219

### Abstract

The purpose of this paper is to describe the discrete problem and iterative solution method for spectral simulations of the 3-D Navier-Stokes equations using a general 3-D coordinate mapping. A spectral collocation discretization is proposed along with a multi-level iterative method, and has two unique advantages. First, arbitrary coordinate mappings, which introduce non-constant coefficients into the governing equations, create no additional complication in the spectral collocation approach, but are not feasible for spectral Galerkin and Tau methods. Second, the coupling between velocity and pressure is treated implicitly, allowing either fully- or semi-implicit schemes to be used, and removing the need for the artificial velocity boundary conditions required with fractional-step methods. The performance of the proposed method is competitive with current methods in both memory utilization and operation count. Results were obtained for a canonical case, curved channel flow, to test the suggested approach. Accuracy was examined via the predicted growth rate of a Tollmien-Schlichting wave. Then, simulations for 2-D Dean vortex flow and 3-D breakdown of a saturated Tollmien-Schlichting were obtained.

### Introduction

Direct numerical simulation (DNS) of problems of instability, transition, and turbulence in flows with simple geometric boundaries such as channel, boundary layer, and pipe flows is used extensively to study the complex physical phenomena leading to turbulence. Spectral methods are typically employed for solving the 3-D incompressible Navier-Stokes equations, resulting in an accurate, non-dissipative discretization. For all but the simplest geometry, a coordinate mapping must be used for the computational mesh. The resulting form of the Navier-Stokes equations, however, is not directly amenable to spectral Galerkin or Tau methods, due to the presence of non-constant coefficients, which introduce convolution terms into the wave-number formulation of the governing equations. For this reason, many researchers have turned to spectral element methods which can handle more adequately geometric complexities—see, for example, Guzmán and Amon[1]. Several studies have also been reported in which coordinate mappings have been used along with single- or multi-domain spectral methods. Blodgett[2] has employed a multi-domain spectral collocation method in a 2-D simulation of leading-edge receptivity using a streamfunction-vorticity formulation and a Schwartz-Christoffel (orthogonal) transformation. Carlson *et al.*[3] have used a time-dependent mapping of the wall-normal coordinate in 3-D DNS in a channel with an emerging obstacle on the lower wall. They used a Fourier Galerkin method in both the streamwise and spanwise directions, and a Chebyshev Tau method in the wall-normal direction. They accomplished this by treating only the Cartesian-like constant coefficient terms in the governing equations implicitly and updating the remaining terms iteratively.

The present study proposes an extension to these studies by allowing for an arbitrary 3-D coordinate mapping. The use of collocation, rather than Galerkin or Tau, derivatives allows the implicit part of the algebraic system to include coefficients representing non-constant coordinate metrics. The collocation discretization method is described below. A multi-level iterative approach is then described for solving the resulting nonlinear algebraic system. Finally, 2-D and 3-D simulation results are presented.

---

* This work is supported in part by AFOSR Grant No. F49620-93-1-0393, and Ohio Supercomputer Center Grant No. PES070-5.

## The Discrete Problem

### *Coordinate Mapping*

The 3-D incompressible Navier-Stokes equations in non-dimensional form are solved using the skew-symmetric form of the convective terms[4], and are written:

$$\frac{\partial \mathbf{u}}{\partial t} + \frac{1}{2}\left(\mathbf{u}\cdot\nabla\mathbf{u} + \nabla\cdot(\mathbf{uu})\right) = -\nabla p + \frac{1}{\mathrm{Re}}\nabla^2\mathbf{u} \ , \tag{1}$$

$$\nabla\cdot\mathbf{u} = 0 \ . \tag{2}$$

A non-moving general coordinate mapping is employed, and is described as:

$$\xi_i = \xi_i(x_1, x_2, x_3), \text{ for i = 1,2,3.} \tag{3}$$

The governing equations, Eqs. (1) and (2), are written in generalized coordinates by representing vectors and differential operators in terms of covariant and contravariant base vectors associated with the above transformation. See, for example, Gal-Chen and Somerville[5], for a more thorough discussion of generalized coordinates. The base vectors are defined as:

$$\text{Covariant:} \quad \bar{\mathbf{e}}_i = \frac{\partial x_j}{\partial \xi_i}\hat{\mathbf{i}}_j \ , \quad \text{Contravariant:} \ \bar{\mathbf{e}}^i = \frac{\partial \xi_i}{\partial x_j}\hat{\mathbf{i}}_j \ , \tag{4}$$

for i=1,2,3, and where $\hat{\mathbf{i}}_j$ are the Cartesian base vectors. Automatic summation is assumed for repeating indices. The covariant and contravariant base vectors are related to the covariant and contravariant forms of the metric tensor, respectively, and to the Jacobian of transformation for the generalized mapping of Eq. (3), which will be denoted as $\sqrt{g}$ . These relationships are:

$$\text{Covariant:} \quad g_{ij} = \bar{\mathbf{e}}_i\cdot\bar{\mathbf{e}}_j \ , \ \text{Contravariant:} \ g^{ij} = \bar{\mathbf{e}}^i\cdot\bar{\mathbf{e}}^j \ ,$$

$$\sqrt{g} = +\left[\mathrm{Det}(g_{ij})\right]^{1/2} = +\left[\mathrm{Det}(g^{ij})\right]^{-1/2} = \left|\mathrm{Det}\left(\frac{\partial(x_1, x_2, x_3)}{\partial(\xi_1, \xi_2, \xi_3,)_j}\right)\right| \ . \tag{5}$$

Vectors in transformed space are represented alternatively in terms of Cartesian, covariant, or contravariant components. The notation used is:

$$\text{Cartesian:} \ \mathbf{u} = \hat{u}_i\hat{\mathbf{i}}_i \ , \ \text{Covariant:} \ \mathbf{u} = u_i\bar{\mathbf{e}}^i \ , \ \text{Contravariant:} \ \mathbf{u} = u^i\bar{\mathbf{e}}_i \ . \tag{6}$$

Derivatives of the covariant base vectors are also needed. These are written as:

$$\frac{\partial \bar{\mathbf{e}}_i}{\partial \xi_j} = \Gamma_{ij}^m\bar{\mathbf{e}}_m \ , \tag{7}$$

where $\Gamma_{ij}^m$ are Christoffel symbols of the second kind. Contravariant components of the velocity vector are used in both the momentum and continuity equation, and contravariant components of the momentum equation are used to represent it as three scalar equations. Appropriate wall boundary conditions on velocity, along with the specification of the mean pressure, complete the continuous problem. See Brandes-Duncan[6] for a more complete derivation.

### *Spatial Discretization*

Following Canuto *et al.*[7], the continuous system is spatially discretized using a spectral collocation method by selecting for each coordinate direction a sequence of orthogonal basis functions. For a staggered grid arrangement, the velocity is represented at different points than the pressure, and sets of collocation points are selected for both variables in each coordinate direction. The momentum equation is solved at the velocity points, and the continuity equation is solved at the pressure points. Interpolation on the spectral basis is performed to transfer needed quantities between the two grids. A concise notation for the spatially discrete system is to denote the spectral collocation derivative along the $\xi_i$ coordinate as the matrix operator $D^i$, interpolation from the velocity grid to the pressure grid as the matrix operator $A^-$, and interpolation from the pressure grid onto the velocity grid as $A^+$. Using upper-case letters to represent the discrete values of the velocity and pressure, the spatially discrete momentum equation is written as:

$$\frac{\partial U^i}{\partial t} + N^i(\mathbf{U}) = -G^i(P) + \frac{1}{\mathrm{Re}} L^i(\mathbf{U}) \quad , \text{ where}$$

$$N^i(\mathbf{U}) = \frac{1}{2\sqrt{g}} \mathbf{D}^j\left(\sqrt{g} U^j U^i\right) + \frac{1}{2} U^j \mathbf{D}^j U^i + \Gamma^i_{jk} U^j U^k \quad ,$$

$$G^i(P) = g^{ij} \mathbf{D}^j\left(\mathbf{A}^o P\right) \quad , \text{ and} \tag{8}$$

$$L^i(\mathbf{U}) = \frac{1}{\sqrt{g}} \mathbf{D}^j\left(\sqrt{g}\, g^{jk} \mathbf{D}^k U^i\right) + \left(\frac{1}{\sqrt{g}} \mathbf{D}^j\left(\sqrt{g}\, g^{jk} U^\ell\right) + g^{jk} \mathbf{D}^j U^\ell\right) \Gamma^i_{k\ell}$$
$$+ g^{jk} U^\ell \left(\frac{\partial \Gamma^i_{k\ell}}{\partial \xi^j} + \Gamma^m_{k\ell} \Gamma^i_{jm}\right) \quad .$$

The spatially discrete continuity equation is:

$$D(\mathbf{U}) = 0 \quad , \text{ where} \tag{9}$$

$$D(\mathbf{U}) = \mathbf{A}^+ \left[\frac{1}{\sqrt{g}} \mathbf{D}^i\left(\sqrt{g} U^i\right)\right] \quad .$$

***Temporal Discretization***

In this study, both fully-implicit (FI) and semi-implicit (SI) second-order time integration schemes are considered. For both schemes, Crank-Nicolson time-centered integration is used for the linear terms. For the FI scheme, Crank-Nicolson is also used for the convective term. For the SI method, a second-order Adams-Bashforth method is used for the convective term, which results in a linear algebraic system at each time step. The final discrete form of the momentum equation is then given as:

$$U^{i,n+1} - U^{i,n} + \Delta t\, N^{i,n+1/2}(\mathbf{U}) - \frac{\Delta t}{2} \frac{1}{\mathrm{Re}} \left[L^i(\mathbf{U}^{n+1}) + L^i(\mathbf{U}^n)\right]$$
$$+ \frac{\Delta t}{2} \left[G^i(P^{n+1}) + G^i(P^n)\right] = 0 \quad , \tag{10}$$

where for the FI scheme:

$$N^{i,n+1/2}(\mathbf{U}) = \frac{1}{2}\left[N^i(\mathbf{U}^{n+1}) + N^i(\mathbf{U}^n)\right] \quad , \tag{11}$$

and for the SI scheme:

$$N^{i,n+1/2}(\mathbf{U}) = \frac{1}{2}\left[3N^i(\mathbf{U}^n) - N^i(\mathbf{U}^{n-1})\right] \quad . \tag{12}$$

The continuity equation is satisfied by the velocity at every time step:

$$D(\mathbf{U}^{n+1}) = 0 \quad . \tag{13}$$

Initial and boundary conditions complete the specification of the discrete problem. Since velocity points are located on the walls, wall boundary conditions on velocity are implemented by replacing the discrete equation on the wall with the required boundary conditions. Since pressure points are not located on the wall, no extraneous wall boundary conditions on pressure are needed. To specifiy the mean value of pressure, a continuity equation is removed at an arbitrary location and replaced with the condition that the mean value of pressure be zero.

## Iterative Approach

***Outer Iteration***

Low-memory solution strategies for solving the 3-D discrete system, Eqs. (10)-(13), require the use of multi-level iterative methods. First, the nonlinear algebraic system for the solution at the $n+1$ time level in the FI

method is solved using quasi-Newton's method; where the Jacobian matrix is obtained by linearizing the nonlinear terms and evaluating them at the prescribed base velocity. The quasi-Newton iteration level is written as:

$$\begin{bmatrix} \mathbf{A} & \mathbf{G} \\ \mathbf{D} & \mathbf{B} \end{bmatrix} \begin{Bmatrix} \delta \mathbf{U} \\ \delta P \end{Bmatrix} = \begin{Bmatrix} -\mathbf{R}_1^m \\ -R_2^m \end{Bmatrix}, \qquad \begin{Bmatrix} \mathbf{U}^{n+1,m+1} \\ P^{n+1,m+1} \end{Bmatrix} = \begin{Bmatrix} \mathbf{U}^{n+1,m} \\ P^{n+1,m} \end{Bmatrix} + \begin{Bmatrix} \delta \mathbf{U} \\ \delta P \end{Bmatrix}, \tag{14}$$

where the matrices **A**, **D**, **G**, and **B** represent contributions to the Jacobian matrix from various terms in Eqs. (10)-(13). Note that **B** is null with the exception of a single row which enforces the mean-pressure condition. Also, **A** contains contributions from the linearization of the convective term, evaluated at some base velocity solution. The right-hand-side vectors $\mathbf{R}_1$ and $R_2$ represent the value of the residual of the momentum equation and continuity equation, respectively. The iterative procedure begins (at $m$=0) with the specification of an initial guess for the solution at the $n$+1 time level, and continues until some norm of the right-hand-side is below the convergence criterion. For the SI method, the above method is also used, but produces a converged solution in one iteration, since the algebraic system is linear.

***Inner Iteration***

An inner iteration strategy is used to solve the linear algebra problem resulting from the quasi-Newton scheme. With the linear algebra problem abbreviated as:

$$\mathbf{LX} = \mathbf{F}, \quad \text{where } \mathbf{X} = \begin{Bmatrix} \mathbf{X}_1 \\ X_2 \end{Bmatrix}, \ \mathbf{F} = \begin{Bmatrix} \mathbf{F}_1 \\ F_2 \end{Bmatrix}, \tag{15}$$

a straight-forward iteration technique for solving this system is written as

$$\begin{aligned} \mathbf{M}\delta\mathbf{X} &= \mathbf{F} - \mathbf{L}\mathbf{X}^m, \\ \mathbf{X}^{m+1} &= \mathbf{X}^m + \delta\mathbf{X}, \end{aligned} \tag{16}$$

where **M** is a preconditioner for, or rather, the some easily invertible approximation to, the coefficient matrix **L**. The above iterative method is known as Richardson iteration, or residual correction. Note that the iterative scheme requires the inversion of **M**, rather than **L**, and that **L** is only needed as a multiplicative operator. Other more complicated iterative procedures such as minimum residual methods have the same requirements for the operators **M** and **L**. For the inner iteration method, the preconditioner **M** is chosen as an approximate lower-upper factorization of **L**, of the form:

$$\mathbf{M} = \begin{bmatrix} \mathbf{A} & \mathbf{0} \\ \mathbf{D} & \mathbf{B} - \mathbf{DG} \end{bmatrix} \begin{bmatrix} \mathbf{I} & \mathbf{G} \\ \mathbf{0} & \mathbf{I} \end{bmatrix} = \begin{bmatrix} \mathbf{A} & \mathbf{AG} \\ \mathbf{D} & \mathbf{B} \end{bmatrix}, \text{ where} \tag{17}$$

**M** differs from **L** only in the momentum equation pressure coefficient. The following procedure is used to solve the linear system **MY**=**C**:

$$\begin{aligned} \mathbf{A}\mathbf{Y}_1^* &= \mathbf{C}_1, \\ (\mathbf{B} - \mathbf{DG})Y_2 &= C_2 - \mathbf{D}\mathbf{Y}_1^*, \\ \mathbf{Y}_1 &= \mathbf{Y}_1^* - \mathbf{G}Y_2. \end{aligned} \tag{18}$$

The approximate factorization Eq. (17), produces a solution procedure, Eq. (18), identical to that used in the fractional step method, as shown in Perot[8] and Dukowicz and Dvinsky[9]. In the fractional step method, however, **M** replaces the original linear operator **L**, and the original linear system, Eq. (15), is not satisfied. Modified velocity boundary conditions are used to improve the accuracy of the fractional step method and to make the procedure stable in time[10]. These can be implemented directly in the above linear system. Thus, the outer-inner iteration method proposed here can be reduced to the fractional step method with modifications to the linear system, and using the SI method with one quasi-Newton iteration.

***Velocity and Pressure Solution Methods***

In order to solve the first two steps of Eq. (18) for the velocity correction $\mathbf{Y}^*$ and pressure correction, $Y_2$, respectively, iterative methods are again utilized. The velocity system is well-conditioned, and therefore converges rapidly with any reasonable iterative method. A preconditioned residual correction method as in Eq. (16) is used, with a low-memory, line-implicit, preconditioner.

The pressure system, on the other hand, is ill-conditioned, and constitutes the majority of the computational effort in any simulation. A preconditioned GMRES method with a low-memory line- or plane-implicit preconditioner was implemented, and was effective for 2-D and small 3-D problems. However, the number of iterations required was prohibitive for large 3-D problems, and was not competitive with Galerkin or Tau methods

which have very sparse matrix structures. It was found that the transformation to wave-number space could be performed on the linear pressure system prior to solution with GMRES, with the inverse transformation applied to the result. The transformed pressure system, with a line-implicit preconditioner, converged much more quickly than the original one. This transformed preconditioned solver for pressure allows the performance of the present scheme to compare reasonably well with schemes designed for simple geometries and based on a Galerkin or Tau spectral formulation.

## Curved Channel Results

### *Spectral Discretization*

Solutions using the 3-D spectral collocation formulation with the outer-inner iterative method are shown for a periodic curved channel problem. Fourier collocation is used in the streamwise ($\xi_1$) and spanwise ($\xi_2$) directions. Chebyshev collocation is used in the wall-normal ($\xi_3$) direction, with the pressure and continuity equation staggered. The computational domain is then defined as:

$$\xi_1 \in [0,2\pi] \ , \ \xi_2 \in [0,2\pi] \ , \ \xi_3 \in [-1,1] \ . \tag{19}$$

The metric transformation represents the curved channel geometry using scaled polar coordinates. The lengths $L_1$, $L_2$, and $L_3$ are the scaled lengths of the physical domain, where $L_1$ is the arc length of the channel centerline. The radius of curvature of the channel centerline is referred to as $R_C$, and the physical domain is defined as:

$$\theta \in \left[\frac{\pi}{2}-\frac{L_1}{2R_C},\frac{\pi}{2}+\frac{L_1}{2R_C}\right] \ , \ y \in [0,L_2] \ , \ r \in \left[R_C-\frac{L_3}{2},R_C+\frac{L_3}{2}\right] . \tag{20}$$

The typically-used curvature parameter, $\eta$, is related to $R_C$ through:

$$\eta = \frac{R_C-\frac{L_3}{2}}{R_C+\frac{L_3}{2}} \ , \ R_C = \frac{L_3}{2}\frac{1+\eta}{1-\eta} \ . \tag{21}$$

The resulting metrics and Christoffel symbols are shown in Table 1.

| Symbol | Formula | | |
|---|---|---|---|
| $\sqrt{g}$ | $r\,(L_1/2\pi R_C)\,(L_2/2\pi)\,(L_3/2)$ | $\Gamma^3_{11}$ | $-r\,(L_1/2\pi R_C)^2/(L_3/2)$ |
| $g_{11}$ | $r^2\,(L_1/2\pi R_C)^2$ | $\Gamma^1_{13}$ | $r^{-1}(L_3/2)$ |
| $g_{22}$ | $(L_2/2\pi)^2$ | $\Lambda^1_{111}=\left(\frac{\partial\Gamma^1_{11}}{\partial\xi^1}+\Gamma^m_{11}\Gamma^1_{1m}\right)$ | $-(L_1/2\pi R_C)^2$ |
| $g_{33}$ | $(L_3/2)^2$ | $\Lambda^1_{113}=\left(\frac{\partial\Gamma^1_{13}}{\partial\xi^1}+\Gamma^m_{13}\Gamma^1_{1m}\right)$ | $-(L_1/2\pi R_C)^2$ |
| $g^{11}$ | $r^{-2}\,(L_1/2\pi R_C)^{-2}$ | | |
| $g^{22}$ | $(L_2/2\pi)^{-2}$ | | |
| $g^{33}$ | $(L_3/2)^{-2}$ | | |

**Table 1. Non-zero metrics for the curved channel mapping, where *r* is the polar coordinate radius.**

### *Accuracy and Stability Issues*

The nonlinear algebraic system, Eqs. (10)-(13), was solved using both the FI and SI second-order time integration methods. The accuracy of these two methods was confirmed by computing the evolution of a Tollmien-Schlichting (TS) wave in a curved channel, with Re=5000, and $\eta$=0.9802 ($R_C$=100), the streamwise wavenumber of the TS wave was $\alpha$=100. The amplitude of the TS wave was such that its maximum streamwise velocity was 1% of the mean base flow streamwise velocity. At this amplitude the growth rate departs slightly from that predicted by linear stability theory. The frequency and growth rate of the TS wave at $t$=0.1 are shown in Table 2. For each case, the inner iteration was fully converged (to maximum residual < $10^{-12}$), which required approximately 5 subiterations for each outer iterations. The number of outer iterations required for the FI method was examined, and it was

observed that for $\Delta t$=0.01, 3 outer iterations produced a fully-converged residual. Using only 2 outer iterations produced a method which was less accurate in time, but stable. For smaller $\Delta t$, 2 outer iterations were sufficient to converge the nonlinear iteration. The FI method was observed to be unconditionally stable, while the SI method required a time step on the order of $\Delta t$=0.001 to insure stability. Other validations of the FI method are described in [6] and [11].

| $\Delta t$ | Time-Marching Method | $\omega_R$ | $\omega_I$ |
|---|---|---|---|
| **0.01** | FI, 3 iterations | 0.375203 | $3.29148 \times 10^{-3}$ |
| **0.01** | FI, 2 iterations | 0.375210 | $3.29081 \times 10^{-3}$ |
| **0.001** | FI, 2 iterations | 0.375203 | $3.29184 \times 10^{-3}$ |
| **0.001** | SI | 0.375203 | $3.29185 \times 10^{-3}$ |
| **0.0001** | FI, 2 iterations | 0.375203 | $3.29189 \times 10^{-3}$ |

**Table 2. Frequency ($\omega_R$), and growth rate ($\omega_I$) values at $t$=0.1 for a curved channel Tollmien-Schlichting wave, with Re=5000, $\eta$=0.9802 ($R_C$=100), $\alpha$=100. The inner linear iteration was fully-converged for all cases. *FI* is the fully-implicit method, *SI* is the semi-implicit method.**

*Curved Channel Results*

Curved channel flow has been examined in previous studies such as Finlay *et al.*[12], to demonstrate the effect of streamwise curvature on the possible routes to transition to turbulence. In this study, several results were obtained for curved channel flow, and are listed in Table 3. First, 2-D results in the cross-flow plane were obtained for saturated Dean vortex solutions. Curved channel flow for a channel with at least moderate curvature exhibits a streamwise vortex instability called the Dean vortex, which will experience linear and nonlinear growth above the critical Reynolds number, and will saturate at a finite amplitude. For Case 1 a Reynolds number equal to the critical Reynolds number of 114.26 was used, and the simulation confirmed that the Dean vortex mode would not grow. For Case 2, with a higher Reynolds number of 140.5, the Dean vortex grows to a large-amplitude steady-state solution. Results are shown in Fig. 1. For a higher Reynolds number of 249.8 (Case 3), a second pair of vortices is present in the steady-state solution, as is shown in Fig. 2.

| Case | Re | $\eta$, $R_C$ | $\alpha = 2\pi R_C/L_1$ | $\beta=2\pi/L_2$ | Grid nodes ($N_1 \times N_2 \times N_3$) | Maximum $t$ obtained |
|---|---|---|---|---|---|---|
| 1 | 114.26 | 0.975, 79 | 0 | 1.98 | 1 x 9 x 49 | 40 |
| 2 | 140.5 | 0.975, 79 | 0 | 2.5 | 1 x 9 x 49 | 500 |
| 3 | 249.8 | 0.975, 79 | 0 | 2.5 | 1 x 9 x 49 | 268 |
| 4 | 5000 | 0.9802, 100 | 100 | 0 | 9 x 1 x 49 | 447 |
| 5 | 5000 | 0.9802, 100 | 100 | 1.25 | 13 x 13 x 49 | 527 |

**Table 3. Curved channel flow cases. For each case $\Delta t$=0.01. Values of *0* for $\alpha$ and $\beta$ indicate a 2-D simulation in the corresponding plane.**

Secondly, a 2-D solution of the saturated TS for Case 4 was obtained. For this case a higher Reynolds number of 5000 was used, for which the TS wave is linearly unstable, but grows to a finite amplitude time-asymptotic solution. This state was then used as a starting solution for the 3-D simulation of Case 5. This simulation was performed by adding a streamwise vortex disturbance to the saturated TS wave solution. Results obtained for 80 characteristic time after the introduction of the streamwise vortex mode show the breakdown of the TS wave. The energies of the various streamwise, spanwise, and combination modes are shown in Fig. 3, with the typical notation $E(k_1,k_2)$ for each energy representing the $k_1$-th mode in the streamwise direction and the $k_2$-th mode in the spanwise direction. The increase in amplitude of even the highest frequency modes is typical of a 3-D breakdown to turbulence, rather than bifurcation to a 3-D equilibrium state. Further 3-D results were not available at the time of this writing, but will be shown in the conference presentation.

## Conclusion

The present study described a new approach to spectral DNS in generalized coordinates. The key elements to this approach are the collocation discretization and the fully-coupled multi-level iteration scheme. Future work will include further investigation of the routes to turbulence in curved channel flows, including the low Reynolds number phenomena of wavy and twisting Dean vortices, and the higher Reynolds number breakdown of TS waves due to streamwise vortex disturbances. Then, similar phenomena will be investigated in the presence of a periodic array of surface roughness elements, employing a 3-D non-orthogonal grid transformation with the present method.

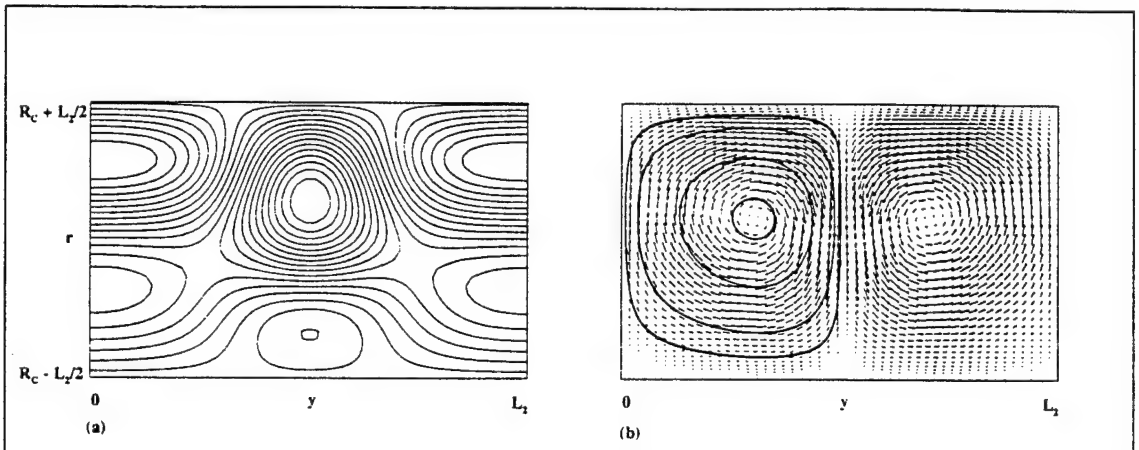


**Figure 1. Cross-section of the velocity field for the Dean vortex, Case 2. a) Contours of the streamwise velocity, b) Vectors and sample streamlines of the cross-section velocity components. The solution was interpolated onto a finer grid for plotting purposes.**

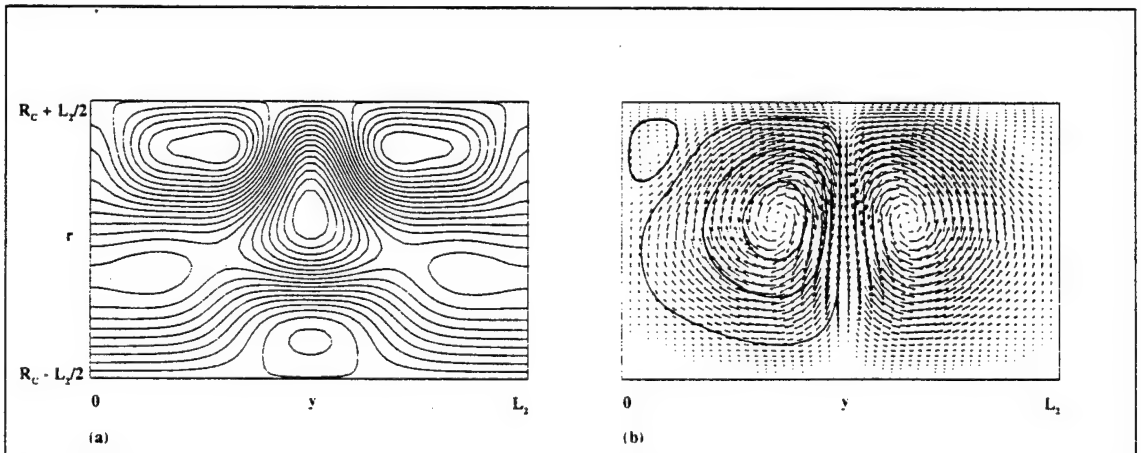


**Figure 2. Cross-section of the velocity field for the Dean vortex, Case 3. a) Contours of the streamwise velocity, b) Vectors and sample streamlines of the cross-section velocity components. The solution was interpolated onto a finer grid for plotting purposes.**

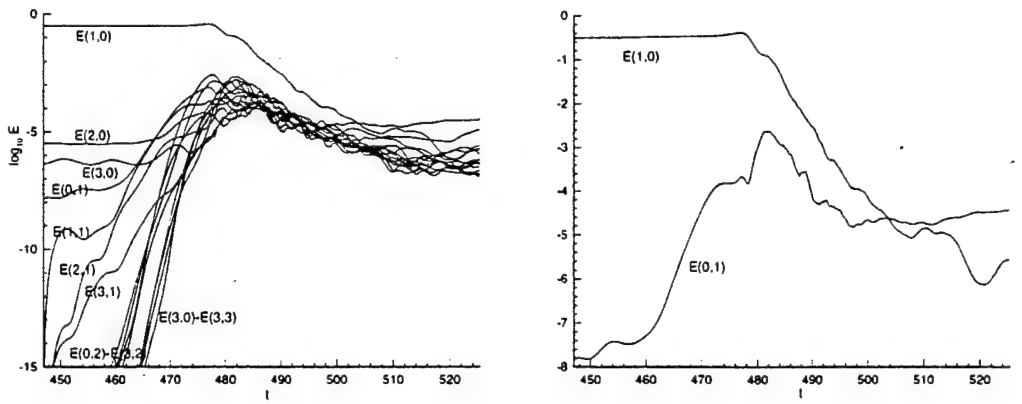


**Figure 3. Time evolution of the energies in various modes for the 3-D TS wave, streamwise vortex interaction simulation, Case 5.**

## References


[1] Guzmán, A.M. and Amon, C.H., "Transition to Chaos in Converging-Diverging Channel Flows: Ruelle-Takens-Newhouse Scenario," *Physics of Fluids A*, Vol. 6, pp. 1994-2002, 1994.

[2] Blodgett, K, *A Spectral Multidomain Method in Generalized Curvilinear Coordinates with Application to Leading-Edge Receptivity*. Ph.D. Dissertation. University of Cincinnati, 1995.

[3] Carlson, H.A., G. Berkooz, and J.L. Lumley, "Direct Numerical Simulation of Flow in a Channel with Complex, Time-Dependent Wall Geometries: A Pseudospectral Method," *J. Comp. Phy.*, Vol. 121, pp. 155-175, 1995.

[4] Zang, T.A. "On the Rotation and Skew-Symmetric Forms for Incompressible Flow Simulations," Appl. Numer. Math., Vol. 6, 1990.

[5] Gal-Chen, T., and R.C.J. Somerville, "On the Use of a Coordinate Transformation for the Solution of the Navier-Stokes Equations," *J. Comp. Phy.*, Vol. 17, pp. 209-228, 1975.

[6] Brandes-Duncan, B.D., "Numerical Simulation of Early Stages of Transition in Channel Flows," M.S. Thesis, Univ. of Cincinnati, 1995.

[7] Canuto, C., M.Y. Hussaini, A. Quarteroni, and T.A. Zang, *Spectral Methods in Fluid Dynamics*, Springer-Verlag, 1988.

[8] Perot, J.B., "Analysis of the Fractional Step Method," *J. Comp. Phy.*, Vol. 108, pp. 51-58., 1993.

[9] Dukowicz, J.K., and A.S. Dvinsky, "Approximate Factorization as a High Order Splitting for the Implicit Incompressible Flow Equations," *J. Comp. Phy.*, Vol. 102, pp. 336-347, 1992.

[10] Karniadakis, G.E., M. Isreali, and S.A. Orszag, "High-Order Splitting Methods in the Incompressible Navier-Stokes Equations," *J. Comp. Phy.*, Vol. 97, pp. 414-443, 1991.

[11] Brandes-Duncan, B.D., and K.N. Ghia, "Numerical Simulation of Nonlinear Instabilities in Complex Channel Flows," *AIAA Paper* No. 96-2018, June 1996.

[12] Finlay, W.H., Keller, J.B., and Ferziger, J.H., "Instability and Transition in Curved Channel Flow," *Journal of Fluid Mechanics*, Vol. 194, pp. 417-456, 1988.

# APPENDIX D

## A Generalized Time-Dependent Analysis Implemented on a Parallel Computer for Studying Compressibility Effects on Dynamic Stall

C. NOLL, K. GHIA

University of Cincinnati

# A Generalized Time-Dependent Analysis Implemented on a Parallel Computer for Studying Compressibility Effects on Dynamic Stall[†]

**C. Noll and K. N. Ghia**

**Computational Fluid Dynamics Research Laboratory**
**Department of Aerospace Engineering and Engineering Mechanics**
**University of Cincinnati, Cincinnati, OH 45221**

## Abstract

This study has been undertaken to analyze the effect of compressibility on the dynamic-stall phenomenon by accurately simulating the prevailing mechanisms of the formation of the stall vortex. Towards this, a generalized analysis is developed in a time-dependent curvilinear coordinate system. It is implemented with flow-adaptive gridding and arbitrarily maneuvering and deforming bodies. One of the major contributions of this analysis is the elimination of the boundary condition of zero normal pressure gradient at solid surfaces, which breaks down in regions where separation occurs and in regions of high surface curvature. The branch cuts are treated properly by solving the complete Navier-Stokes equations at these interior points. The preliminary verification study led to the conclusion that computer resources on the CRAY Y-MP 864 are not adequate for the analysis being undertaken. This resulted in developing an object-oriented linear algebra class library for high-performance computation on parallel machines. At the time of the conference, the verification analysis was not completed, and as such, it was decided to provide some information towards the approach used in this work.

## Introduction

Dynamic stall occurs when an airfoil is pitched rapidly past its static stall angle. The lift as well as the drag continues to increase, to a dramatic extent, past the maximum possible static value. As seen in the experimental results of Jumper et al. (1988) in Fig. 1, as the angle of attack approaches 30° during the pitch-up cycle, there is a dramatic loss in lift, and a corresponding and sudden 'nose-down' moment. This event, termed dynamic stall, is a barrier technology, limiting the operational envelope of supermaneuverable aircraft and helicopters, and the performance of wind turbines and turbomachinery.

As is understood presently, the event of dynamic stall for incompressible flow is dominated by vortex interactions and instabilities. The instability mechanisms observed in two-dimensional flows will be described below. As the airfoil is accelerated from rest in a quiescent flow, the initial instability of this flow occurs when the Reynolds number (Re) exceeds a certain relatively small value and flow separates from the airfoil near the trailing edge. As the Reynolds number is increased further, this initial instability can amplify small asymmetric disturbances in the flow and an asymmetric instability occurs near the trailing edge, eventually developing into a Karman vortex street. This is a stable periodic flow for low enough Re. Due to the periodic nature of this flow, the specific point at which the airfoil is given an initial angular acceleration to begin the pitch-up is extremely important. The development of the resulting flow and the corresponding lift, drag and moment curves are observed to be very dependent on when the pitch-up is begun.

[†] This research is supported, in part, by AFOSR Grant No. F49620-93-1-0393, NASA Grant No. NC22-5096 and by Ohio Supercomputer Center Grant No. PES070-5.

For flows with moderate Re values, an instability occurs during the pitch-up maneuver near the leading edge where the boundary-layer flow separates, eventually intensifying into an attached counter-rotating upper-surface vortex. This vortex is the cause of the increased performance of the airfoil, in terms of its lift. Momentarily, it remains attached over the center of lift, resulting in very little change in moment applied to the airfoil. An underlying paired vortex forms on the airfoil surface. As the maneuver continues, an additional pair of vortices forms below this one. When the second vortex of this new pair is formed, the initial secondary vortex (paired with the dynamic-stall vortex) erupts out into the nearly-inviscid vortex flow, cutting off the feeding shear layer emanating from the leading edge, and the dynamic stall vortex evolves as shown in Fig. 2. The shear layer undergoes a Kelvin-Helmholtz instability, rolling up into the detached vortex which convects downstream over the airfoil, resulting in the large 'nose-down' moment on the airfoil. The dynamic-stall phenomenon in incompressible flow has been simulated very satisfactorily by K. Ghia, Yang, Osswald and U. Ghia (1992) and a suitable modulated suction/injection control law was devised by Yang, K. Ghia, U. Ghia and Osswald (1993).

The presence of compressibility, three-dimensionality, transition and turbulence, as well as a number of other factors, can significantly affect the resulting flow evolution. Compressibility can have significant effects on the sequence of instabilities described above. For flow with a relatively low free-stream Mach number, interaction with a rapidly maneuvering airfoil locally causes the flow to accelerate to a Mach number of two and higher, resulting in significant compressibility effects, specifically the production of additional vorticity. Maneuvers performed in supersonic free-stream flows have even more complex flow physics. In either case, as shown in Fig. 3, shocklets formed from local accelerations of the flow around vortices and wavy unstable shear layers can significantly affect the resulting flow structure according to the results of Chandreshekar et al. (1995). These shocklets exist over only a small range of angles of attack during the maneuver. Small, temporally evolving shocks forming in the presence of vortex interactions and instabilities present challenging flow physics to be simulated by the computational fluid dynamicist.

In order to accurately predict such a flow numerically, the instability mechanisms present in the incompressible flow, and any additional mechanisms present in the compressible flow, must be accurately resolved both spatially and temporally. Compressible phenomena, such as shocklets, must be accurately predicted in order to understand their interaction with vortices and their effect on instability mechanisms. The effects of assumptions made in an analysis on the accuracy of resolving the instability mechanisms must be addressed. Because of the sensitive nature of instabilities to disturbances, errors made in the analysis may be amplified to a point where they affect the resulting flow physics. The standard zero normal pressure gradient boundary condition used on solid surfaces in compressible viscous flow calculations such as those performed by Visbal (1990) and Choudhuri and Knight (1995) may have a significant effect on the resulting flow evolution, because the eruption event described above is characterized by a region of high normal pressure gradient relative to the wall. Since the unsteadiness is of prime interest in dynamic stall flows, time-accuracy of the analysis is of fundamental importance.

The objective of this study is to: i) develop an analysis that is applicable to dynamic motion CFD problems, ii) to use object-oriented programming techniques in the development of the analysis to facilitate the use of complex CFD techniques (such as flow-adaptive grids, Chimera grids, etc.) on ever changing high-performance massively parallel computer platforms, and iii) to develop simulation results for dynamic-stall phenomena under a variety of flow conditions to help in the understanding of the role compressibility plays in the phenomenon of dynamic stall.

Underlying the entire analysis are the physical issues of how to accurately capture instabilities and avoid error growth, as well as the computational issues of optimization and

efficiency. The computational issues should not be allowed to affect the analysis in such a way as to lower confidence in the resulting solutions through the addition of errors.

## Analysis and Discussion

The analysis begins with the first principles of classical field theory applied to a continuum fluid. The integral equations are transformed into a set of non-linear partial differential equations written in terms of an arbitrarily moving coordinate system. Unsteadiness of the coordinate system as well as that of the bodies in the flow are accounted for in this manner. Cross derivatives are retained in the resulting differential equations to ensure accuracy of the solutions of these equations. The equations are neither modified by explicitly adding damping terms nor by using a turbulence model. Both of these are inconsistent with the very equations we are trying to solve. A consistent set of boundary conditions have been developed which removes the requirement for a pressure boundary condition on solid surfaces. Consistent far-field conditions are used, unlike the zero$^{th}$-order extrapolation or characteristics-based boundary conditions commonly used .

The differential equations are discretized, resulting in a non-linear algebraic equation set whose solution approaches the continuum solution at a known rate. Based on the results of a model problem, it can be said that, as the grid is refined, the physics of the discrete equation set does approach that of the continuum equations. *The discrete equations are solved at all points within the flow*, including pseudo-boundaries introduced by computational topologies such as branch cuts and multi-block/Chimera-grid boundaries. Time accuracy is assured by complete convergence of the residual of the non-linear equation set, guaranteeing its solution, and through the use of a fully implicit time discretization. Errors introduced through incomplete convergence of the equations may adversely affect the flow physics of the discrete equation set and, thus, the instability events that are being captured.

Numerical Jacobians are used to efficiently generate the resulting linearized coefficient matrix. A fully direct method is not feasible for solving the resulting very large system of equations, even when the sparse nature of the system is considered. Thus, an iterative method is used to drive the residual of the equation set to zero at each time step.

Computational optimization pervades every aspect of a simulation of a challenging flow problem. To lower memory requirements, the number of operations and numbers of iterations performed, flow-adaptive grid techniques are used to achieve near-optimal grid-point placement and, more importantly, to accurately capture unsteady flow phenomena. Multi-grid techniques have been programmed and will be used, if necessary, to accelerate the convergence of the unsteady equations at each time step. If the problem requires the use of a direct method for convergence-related issues, then a multi-block 'divide and conquer' approach is planned to break the problem into smaller pieces. In addition, underlying all numerical computations is the issue of matching algorithms to the machine architecture in use. The use of massively parallel machines is a necessity for computing dynamic motion CFD problems. Because of the need to change algorithms when switching architectures, code design becomes important, to reduce the time spent porting between various machines.

Object-oriented programming (OOP) techniques have, therefore, been used to address many of these optimization issues. Code complexity increases dramatically as complex CFD techniques, such as flow-adaptive and multi-block grids, are added to an analysis. Advanced programming techniques are necessary to manage such complexity in an organized manner. The interaction between various codes, such as a grid generator and a flow solver, must be expressed in the program itself, in order to allow effective communication. With the use of OOP languages, portability issues are more directly addressed and more adequately resolved. The use of an object-oriented language actually facilitates efficient programming rather than hindering it, since the way an object is used is decoupled from the

particular way it was implemented on a given machine. Specific optimized algorithms can be used where appropriate, without complicating other parts of a code. A good example of this is linear algebra programming, which forms the basis of all CFD codes. A particular efficient implementation of a matrix operation can be used, where one was not before, without changing the way the CFD program loads up its coefficient matrix. An example of the high performance attainable on a CRAY Y-MP with C++ is given in Fig. 4. Because of the design of the linear algebra objects used by the CFD code, this optimized block matrix routine was used without changing a single line of code in the CFD program.

The use of user-defined types allows the program to be written in terms of objects closer to the problem at hand and allows the compiler to know when, for example, a grid was misused and mark the line with an error flag. In a procedural language, such as FORTRAN, the compiler has no way of knowing if a programmer really meant to pass down to a routine the x-coordinates of a grid first, then the y-coordinates, or vice-versa. All it knows is that it was expecting two arrays, and is ignorant of what they were supposed to be representing.

## Summary

The compressible flow past a maneuvering airfoil is being studied. Currently, issues related to boundary conditions, including proper treatment of branch cuts and multi-block/Chimera boundaries are being addressed. Numerical analysis issues for solving large-scale iterative problems are being examined. Finally, object-oriented programming is being used to facilitate the incorporation of complicated CFD techniques into flow codes as well as to address issues of software portability on high-performance supercomputers. Results of this effort, which were not ready at the time of the Conference, will be disseminated shortly in the form of a report.

## References


Chandresekhara, M. S., Carr, L. W., and Wilder, M. C., "Interferometric Investigations of Compressible Dynamic Stall Over a Transiently Pitching Airfoil," ***AIAA Paper*** 93-0211, January, 1993.

Choudhuri, P. G. and Knight, D. D., "Effects of Compressibility, Pitch Rate and Reynolds Number on Unsteady Incipient Boundary Layer Separation Over a Pitching Airfoil," ***AIAA Paper*** 95-0782.

Ghia, K. N., Yang, J., Osswald, G. A., and Ghia, U., "Study of the Role of Unsteady Separation in the Formation of Dynamic Stall Vortex," ***AIAA Paper*** 92-0196.

Visbal, M. R., "Dynamic Stall of a Constant-Rate Pitching Airfoil," ***Journal of Aircraft***, Vol. 27, p. 400, May, 1990.

Yang J., Ghia, K. N., Ghia, U. and Osswald, G. A., "Management of Dynamic Stall Phenomenon Through Active Control of Unsteady Separation," ***AIAA Paper*** 93-3284.

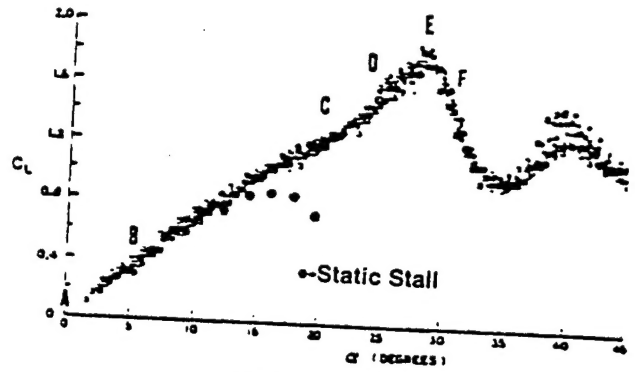


a) Lift History

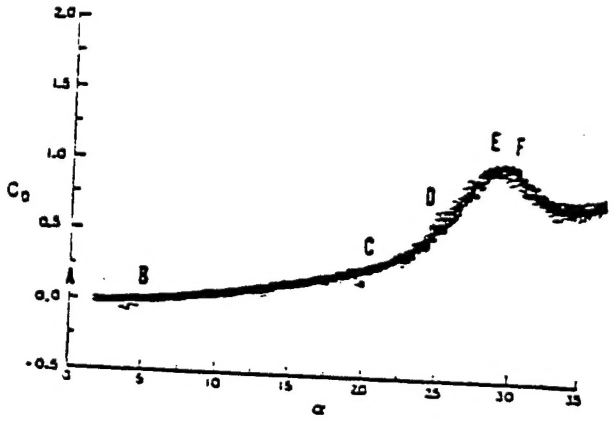


b) Drag History

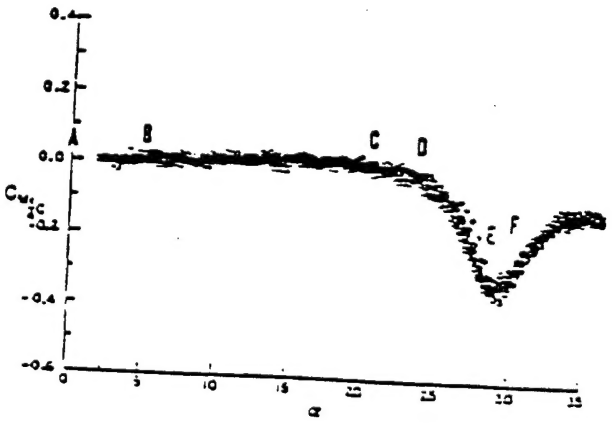


c) Moment History

Figure 1.-Dynamic Stall: Lift, Drag and Moment Curves of Jumper, et al., (1988)

a) Initial leading edge separation

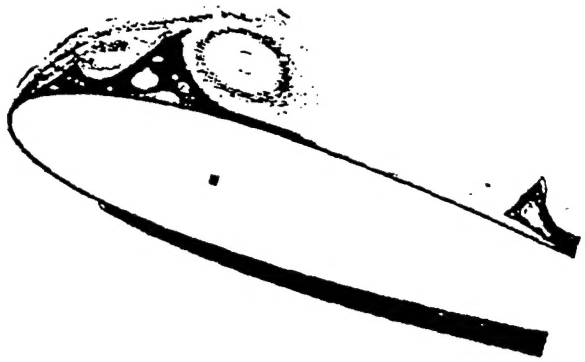

b) Onset of interaction, sharp local pressure change

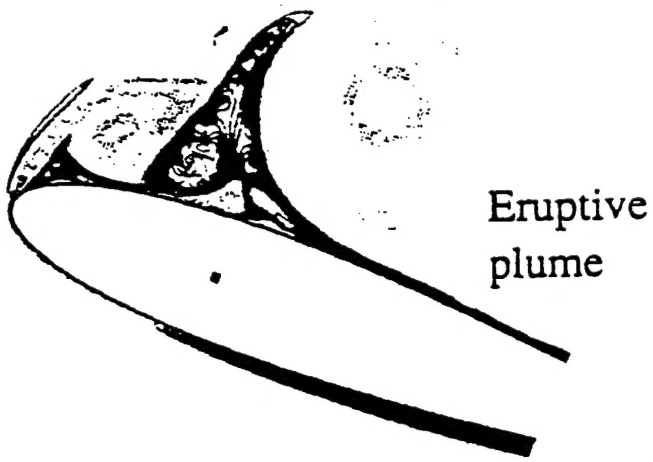


c) Strong interaction

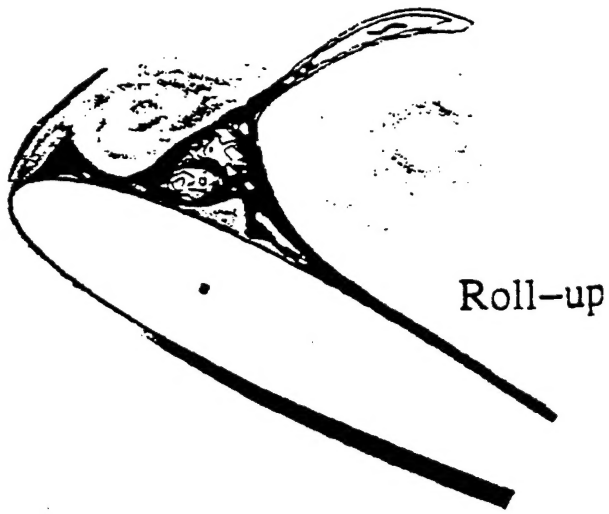


d) Inviscid Interaction

Figure 2.-Vortex Structure in Sequence of Events for Dynamic Stall (K. Ghia, et al., 1992)

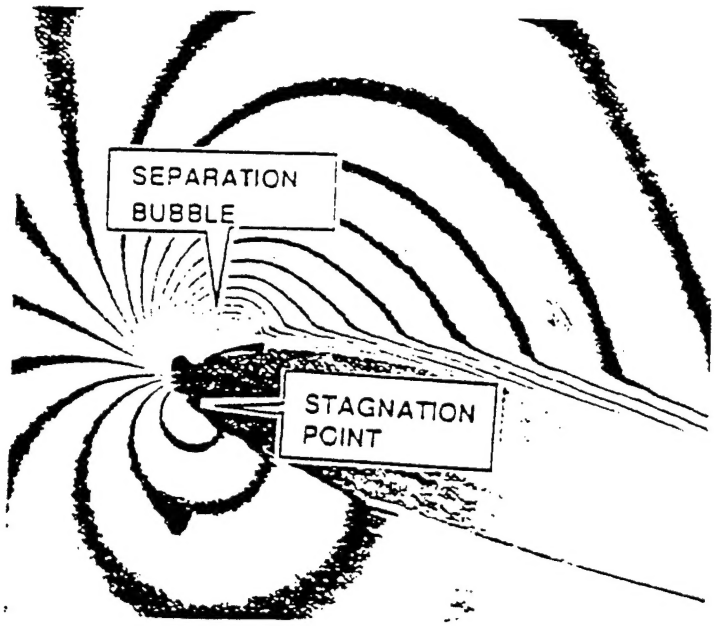


a) M=0.3, $\alpha$=12°, $\bar{\alpha}$=0.03

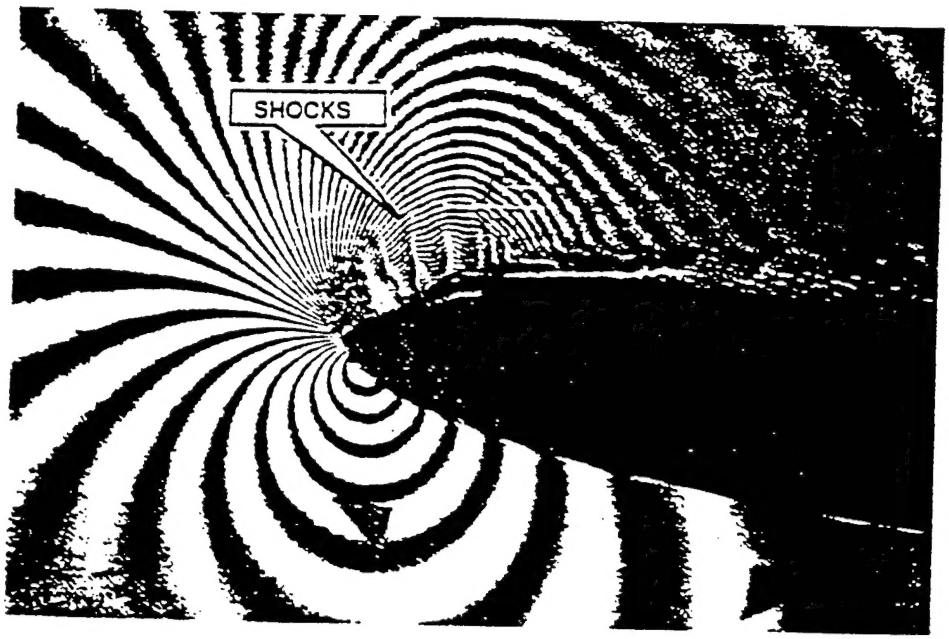


b) M=0.45, $\alpha$=12.6°, $\bar{\alpha}$=0.0313

Figure 3.-Compressibility Effects on Dynamic Stall (Chandresekhara, et al., 1993)

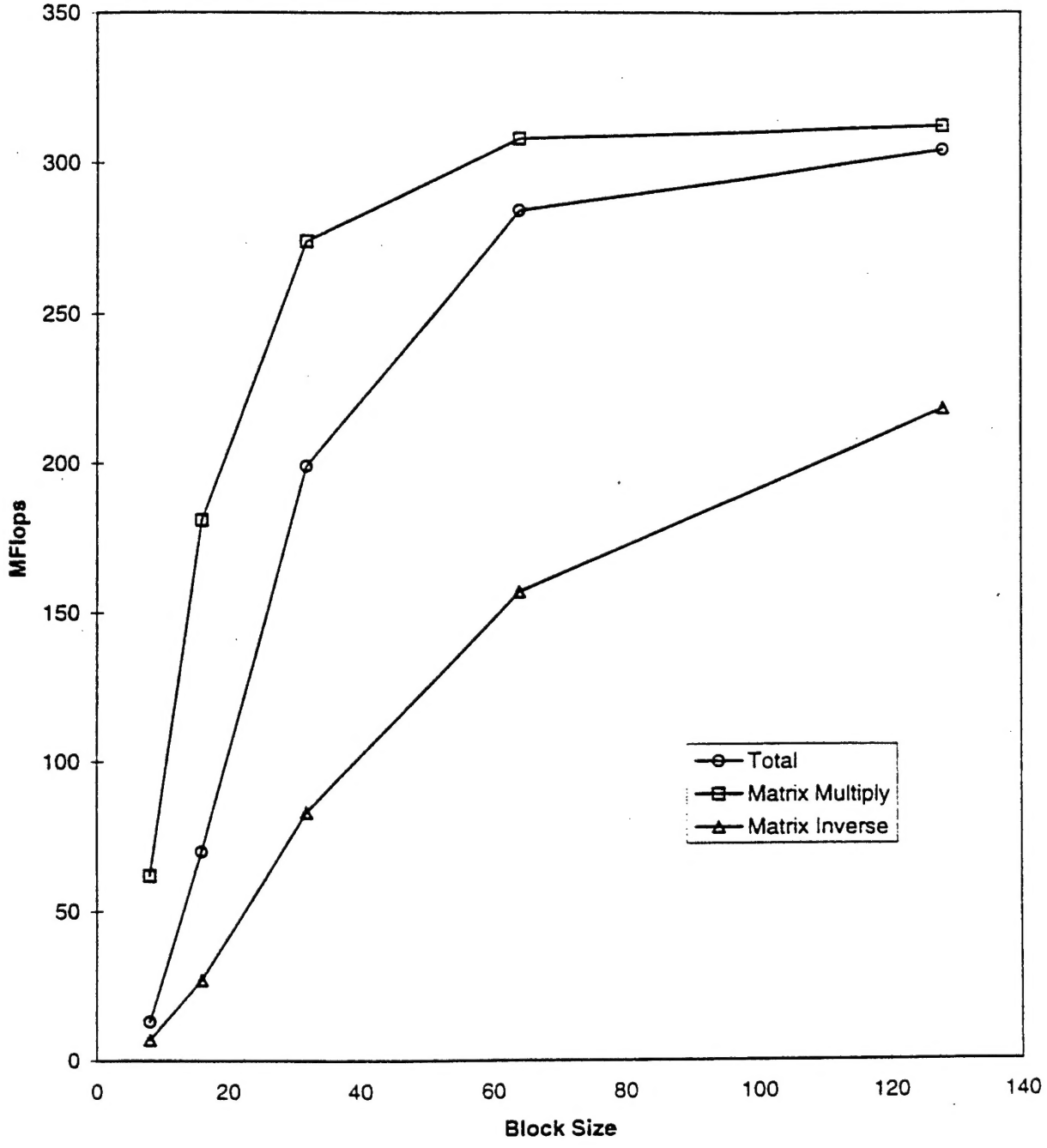


Figure 4.-Cray Y-MP Performance for C++ Block Matrix Inverse